VOLUME 36 OCTOBER 1958 NUMBER 10

Canadian Journal of Chemistry

Published by THE NATIONAL RESEARCH COUNCIL

OTTAWA CANADA

CANADIAN JOURNAL OF CHEMISTRY

(*Formerly Section B, Canadian Journal of Research*)

Under the authority of the Chairman of the Committee of the Privy Council on Scientific and Industrial Research, the National Research Council issues THE CANADIAN JOURNAL OF CHEMISTRY and five other journals devoted to the publication, in English or French, of the results of original scientific research. Matters of general policy concerning these journals are the responsibility of a joint Editorial Board consisting of: members representing the National Research Council of Canada; the Editors of the Journals; and members representing the Royal Society of Canada and four other scientific societies.

The Chemical Institute of Canada has chosen the Canadian Journal of Chemistry as its medium of publication for scientific papers.

Manuscripts for publication should be submitted to Dr. Léo Marion, Editor, Canadian Journal of Chemistry, National Research Council, Ottawa 2, Canada.
(For instructions on preparation of copy, see **Notes to Contributors** (inside back cover).)

Proof, correspondence concerning proof, and orders for reprints should be sent to the Manager, Editorial Office (Research Journals), Division of Administration and Awards, National Research Council, Ottawa 2, Canada.

Subscriptions, renewals, requests for single or back numbers, and all remittances should be sent to Division of Administration and Awards, National Research Council, Ottawa 2, Canada. Remittances should be made payable to the Receiver General of Canada, credit National Research Council.

The journals published, frequency of publication, and prices are:

Canadian Journal of Biochemistry and Physiology	Monthly	$3.00 a year
Canadian Journal of Botany	Bimonthly	$4.00 a year
Canadian Journal of Chemistry	Monthly	$5.00 a year
Canadian Journal of Microbiology	Bimonthly	$3.00 a year
Canadian Journal of Physics	Monthly	$4.00 a year
Canadian Journal of Zoology	Bimonthly	$3.00 a year

The price of regular single numbers of all journals is 75 cents.

Canadian Journal of Chemistry

Issued by THE NATIONAL RESEARCH COUNCIL OF CANADA

VOLUME 36 OCTOBER 1958 NUMBER 10

CONDUCTANCES OF CONCENTRATED AQUEOUS SOLUTIONS OF MIXED ELECTROLYTES[1]

A. N. CAMPBELL, E. M. KARTZMARK, AND A. G. SHERWOOD

ABSTRACT

Equivalent conductances, viscosities, and densities were determined for solutions equimolar in two of the three salts lithium nitrate, ammonium nitrate, and silver nitrate. The three possible combinations of two salts were each studied at 25° C and at 35° C.

The observed conductances and viscosities were compared with those of the single salt solutions at the same total ion concentration. The conductances were lower than the mean of the conductances of the single salt solutions. The viscosities were also lower than the mean viscosities.

INTRODUCTION

Work in this laboratory has, for the past 8 years, been devoted to providing reliable data on the conductances of concentrated solutions of lithium, of silver, and of ammonium nitrates, and of lithium chlorate in aqueous solutions, and also, in the case of lithium nitrate, in alcohol and alcohol–water mixtures. Recently, the accumulated data have assumed an added interest with the appearance of conductance equations which purport to be valid well into the region of finite concentration. These equations are being tested and are showing encouraging results.

It was considered that a study of mixtures of electrolytes in concentrated solution would be interesting as an extension of our general scheme of work. Accordingly the nitrates of lithium, of silver, and of ammonium were investigated in pairs in aqueous solution. The conductances, viscosities, and densities of solutions, equimolar in each salt, were determined at 25° C and at 35° C.

Onsager and Fuoss (1) have extended the calculations of the Debye–Hückel–Onsager limiting law to include a mixture of ions in solution but their treatment cannot be extended, except as a qualitative analogy, to concentrated solutions. It was first observed by Bray and Hunt (2) that the conductance for a given total concentration of ions is not additive. They studied solutions of sodium chloride and hydrogen chloride and attempted to explain their results as due to incomplete dissociation.

Onsager's theory predicts that the faster ion (H^+ in the case mentioned above) will be slowed down, and the slower ion accelerated, in the mixture. This was shown to be true, experimentally, by Longsworth (3) when he determined the transference numbers of the individual ions in mixed aqueous solutions of potassium chloride and hydrogen chloride.

According to Onsager and Fuoss, of the two effects tending to retard the motion of ions in solution, only the relaxation effect will have a different value in mixed solutions from that in a solution of the single salt of the same concentration. Onsager and Fuoss have compared calculated data for solutions of sodium chloride and hydrogen chloride

[1]*Manuscript received June 3, 1958.*
Contribution from the Chemistry Department, University of Manitoba, Winnipeg, Manitoba.

with the experimental values of Bray and Hunt, and the calculated data for mixtures of barium chloride and hydrogen chloride and of potassium chloride and hydrogen chloride (all at 25° C) with the experimental values of Bennewitz, Wagner, and Küchler (4). The comparison indicates that the Onsager–Fuoss treatment is valid as a limiting law, i.e. at extreme dilution. The work of Krieger and Kilpatrick (5) on the conductance of mixed solutions of lithium chloride and potassium chloride in dilute solution also leads to the same conclusion, viz. that the Onsager–Fuoss treatment is valid for very dilute solutions.

Few measurements have been made on concentration solutions. Van Rysselberghe and Nutting (6) measured conductances of mixtures of sodium and potassium halides and nitrates, in solutions whose total concentration was 1.0 molal. They observed that the mixture rule was most nearly correct when the component salts had similar conductances. Van Rysselberghe, Grinnel, and Carson (7) measured conductances of binary mixtures of two–one, two–two, and one–one electrolytes with common anions and with concentrations ranging from 0.5 to 9.0 *N*. They found the departure from the mixture rule to be much larger for higher valence ions.

EXPERIMENTAL PROCEDURE

Our technique has been frequently described and need not be repeated here (8). All solutions were equimolar with respect to the two component salts. A dry box was introduced for the manipulation of the hygroscopic lithium nitrate. The weight concentration was known to within ±0.002%. We have recently found it convenient to adopt the thyratron relay system of temperature control, as described by Swinehart (9), in

TABLE I

DATA FOR SILVER NITRATE – AMMONIUM NITRATE SOLUTIONS

	1		2	3	4	5	6	7	8	9	10
Soln. No.	Weight per cent $AgNO_3$	Weight per cent NH_4NO_3	Total molarity	Density (g/cm³)	Specific conductance (mhos)	Equivalent conductance (Λ, mhos)	Calculated equivalent conductance (Λ (calc.), mhos)	Λ(calc.) − Λ(exp.)	$\frac{\eta - \eta_0}{\eta_0}$ (exp.)	$\frac{\eta - \eta_0}{\eta_0}$ (calc.)	$\frac{\eta - \eta_0}{\eta_0}$ (calc.) − $\frac{\eta - \eta_0}{\eta_0}$ (exp.)
					Temperature, 25° C						
1	0.8524	0.4016	0.1009	1.0058	0.011720	116.11	116.0	0.1	0.0018	0.002	—
2	7.8517	3.6995	1.0008	1.0827	0.08934	89.27	89.7	0.4	0.0184	0.019	0.001
3	14.5182	6.8407	1.9927	1.1659	0.15373	77.15	78.1	0.9	0.0543	0.060	0.006
4	20.6152	9.7134	3.0404	1.2528	0.20680	68.02	69.4	1.3	0.1214	0.140	0.019
5	25.4772	12.0044	3.9912	1.3307	0.24475	61.32	62.6	1.3	0.2033	0.237	0.034
6	30.2011	14.2302	5.0315	1.4152	0.2765	54.96	56.5	1.5	—	—	—
7	31.7256	14.9484	5.3961	1.4448	0.2855	52.91	54.4	1.5	0.3615	0.420	0.058
8	33.9418	15.9927	5.9509	1.4893	0.2971	49.93	51.3	1.4	0.4444	0.506	0.062
9	34.3060	16.1643	6.0452	1.4968	0.2988	49.42	50.7	1.5	0.4583	0.523	0.065
10	37.7817	17.8020	6.9939	1.5724	0.3124	44.67	45.9	1.2	0.6141	0.699	0.085
11	41.1615	19.3945	8.0137	1.6538	0.3196	39.88	40.7	0.8	0.8309	0.944	0.113
12	44.1656	20.8053	9.0029	1.7319	0.3197	35.51	36.1	0.6	1.0973	1.251	0.154
13	46.7859	22.0446	9.9482	1.8062	0.3134	31.50	—	—	1.4137	1.605	0.191
					Temperature, 35° C						
1	0.8524	0.4016	0.1006	1.0027	0.01400	139.13	140.4	1.3	0.0213	0.021	0.000
2	7.8517	3.6995	0.9973	1.0790	0.10587	106.14	107.0	0.9	0.0331	0.033	0.000
3	14.5182	6.8407	1.9838	1.1607	0.18336	92.43	91.8	−0.6	0.0827	0.087	0.004
4	20.6152	9.7134	3.0256	1.2467	0.2451	81.01	81.7	0.7	0.1591	0.169	0.010
5	25.4772	12.0044	3.9719	1.3243	0.2893	72.83	73.5	0.7	0.2497	0.271	0.022
6	30.2011	14.2302	5.0052	1.4078	0.3258	65.09	66.1	1.0	0.3771	0.409	0.032
7	31.7256	14.9484	5.3680	1.4373	0.3362	62.64	63.5	0.9	0.4341	0.469	0.035
8	33.9418	15.9927	5.9195	1.4818	0.3497	59.08	59.7	0.6	0.5083	0.557	0.049
9	34.3060	16.1643	6.0147	1.4893	0.3515	58.44	59.1	0.7	0.5292	0.576	0.047
10	37.7817	17.8020	6.9585	1.5645	0.3672	52.78	53.4	0.6	0.6897	0.777	0.087
11	41.1615	19.3945	7.9698	1.6447	0.3759	47.16	—	—	0.9150	1.031	0.116
12	44.1656	20.8053	8.9591	1.7215	0.3721	41.54	—	—	1.2187	—	—
13	46.7859	22.0446	9.9004	1.9750	0.3658	36.95	—	—	1.5471	—	—

our thermostats. The constancy of temperature control in both the thermostats (25° and 35° C) was within 0.002° C, although the absolute value of the temperature is not known to better than ±0.005° C.

EXPERIMENTAL RESULTS

The results are shown in Tables I to III. Column 6 gives the value of Λ calculated

TABLE II

DATA FOR LITHIUM NITRATE – AMMONIUM NITRATE SOLUTIONS

	1		2	3	4	5	6	7	8	9	10
Soln. No.	Weight per cent $LiNO_3$	Weight per cent NH_4NO_3	Total molarity	Density (g/cm³)	Specific conductance (mhos)	Equivalent conductance (Λ, mhos)	Calculated conductance (Λ, calc.)	Λ(calc.) – Λ(exp.)	$\frac{\eta-\eta_0}{\eta_0}$ (exp.)	$\frac{\eta-\eta_0}{\eta_0}$ (calc.)	$\frac{\eta-\eta_0}{\eta_0}$(calc.) – $\frac{\eta-\eta_0}{\eta_0}$(exp.)
					Temperature, 25° C						
14	0.3432	0.3985	0.09966	1.0009	0.01060	106.96	107.9	0.9	0.0036	0.004	0.000
15	1.8285	2.1229	0.5390	1.0163	0.04963	92.07	92.7	0.6	0.0160	0.016	0.000
16	3.1347	3.6394	0.9385	1.0303	0.07999	85.24	86.4	1.2	0.0315	0.031	0.000
17	5.9188	6.8717	1.8221	1.0613	0.1369	75.14	76.5	1.4	0.0762	0.083	0.007
18	9.4790	11.0050	3.0312	1.1024	0.1944	64.14	66.1	2.0	0.1664	0.190	0.024
19	12.1036	14.0522	3.9830	1.1344	0.2255	56.61	58.7	2.1	0.2685	0.306	0.037
20	14.8403	17.2294	5.0341	1.1694	0.2470	49.07	51.6	2.5	0.4132	0.474	0.061
21	17.4262	20.2317	6.0856	1.2039	0.2575	42.31	45.2	2.9	0.6026	0.707	0.104
22	19.7566	22.9372	7.0862	1.2365	0.2576	36.35	39.6	3.2	0.8469	0.992	0.145
23	22.0791	25.6337	8.1351	1.2702	0.2502	30.75	34.3	3.5	1.1721	1.393	0.221
24	23.7813	27.6098	8.9377	1.2956	0.2408	26.87	30.4	3.5	1.4970	1.766	0.269
25	25.7905	29.9425	9.923	1.3264	0.2236	22.53	25.8	3.3	2.0113	—	—
26	27.4651	31.8867	10.981	1.3532	0.2058	18.74	21.7	3.0	3.6197	—	—
27	29.6688	34.4452	12.124	1.4088	0.1786	14.73	—	—	4.8545	—	—
					Temperature, 35° C						
14	0.3432	0.3985	0.09933	0.9977	0.012758	128.43	130.1	1.7	0.0219	.022	0.000
15	1.8285	2.1229	0.5372	1.0129	0.059055	109.92	111.5	1.6	0.0429	0.043	0.000
16	3.1347	3.6394	0.9335	1.0266	0.09482	101.57	102.7	1.1	0.0619	0.062	0.000
17	5.9188	6.8717	1.8147	1.0569	0.16128	88.87	90.5	1.6	0.1093	0.119	0.010
18	9.4790	11.0050	3.0176	1.0975	0.22758	75.42	77.5	2.1	0.2202	0.234	0.014
19	12.1036	14.0522	3.9645	1.1292	0.26300	66.34	68.8	2.5	0.3348	0.357	0.022
20	14.8403	17.2294	5.0099	1.1638	0.28754	57.39	60.0	2.6	0.4909	0.536	0.045
21	17.4262	20.2317	6.0558	1.1980	0.29912	49.39	52.2	2.8	0.6935	0.782	0.088
22	19.7566	22.9372	7.0510	1.2304	0.29999	42.54	45.5	3.0	0.9437	1.094	0.150
23	22.0791	25.6337	8.0933	1.2637	0.29926	36.11	39.3	3.2	1.2877	1.466	0.178
24	23.7813	27.6098	8.8800	1.2873	0.28150	31.70	35.2	3.5	1.6148	—	—
25	25.7905	29.9425	9.8731	1.3197	0.26364	26.70	—	—	2.1434	—	—
26	27.4651	31.8867	10.727	1.3464	0.24449	22.79	—	—	2.7451	—	—
27	29.6688	34.4452	11.897	1.3824	0.21502	18.07	—	—	3.8916	—	—

TABLE III

DATA FOR LITHIUM NITRATE – SILVER NITRATE SOLUTIONS

	1		2	3	4	5	6	7	8	9	10
Soln. No.	Weight per cent $LiNO_3$	Weight per cent $AgNO_3$	Total molarity	Density (g/cm³)	Specific conductance (mhos)	Equivalent conductance (Λ, mhos)	Calculated conductance (Λ, calc.)	Λ(calc.) – Λ(exp.)	$\frac{\eta-\eta_0}{\eta_0}$ (exp.)	$\frac{\eta-\eta_0}{\eta_0}$ (calc.)	$\frac{\eta-\eta_0}{\eta_0}$(calc.) – $\frac{\eta-\eta_0}{\eta_0}$(exp.)
					Temperature, 25° C						
28	1.80945	4.45847	0.54923	1.0464	0.045151	82.20	82.8	0.6	0.0443	0.044	0.000
29	2.79099	6.87697	0.87025	1.0749	0.065757	75.56	76.2	0.6	0.0685	0.068	0.000
30	5.75486	14.1800	1.9540	1.1705	0.11851	60.65	61.4	0.7	0.1943	0.200	0.000
31	8.08470	19.9207	2.9466	1.2565	0.15118	51.31	52.4	1.1	0.3360	0.342	0.006
32	10.1931	25.1159	3.9768	1.3450	0.17409	43.777	44.7	0.9	0.5196	0.528	0.008
33	12.4720	30.7311	5.2672	1.4559	0.18920	35.920	37.3	1.4	0.8221	0.839	0.017
34	13.3994	33.0162	5.8441	1.5036	0.19399	33.194	34.2	1.0	0.9851	1.011	0.026
35	13.7903	33.9793	6.0976	1.5243	0.19513	32.001	32.9	.9	1.0755	1.088	0.012
					Temperature, 35° C						
28	1.80945	4.45847	0.54753	1.0428	0.053943	98.52	99.4	0.9	0.0682	0.068	0.000
29	2.79099	6.87697	0.86718	1.0711	0.078444	90.45	91.3	0.9	0.1012	0.092	−0.009
30	5.75486	14.1800	1.9460	1.1657	0.14081	72.36	73.4	1.0	0.2311	0.225	−0.006
31	8.08470	19.9207	2.9338	1.2510	0.17926	61.10	62.2	1.1	0.3822	0.370	−0.012
32	10.1931	25.1159	3.9589	1.3389	0.20579	51.98	53.1	1.1	0.5740	0.570	−0.004
33	12.4720	30.7311	5.2422	1.4490	0.22411	42.75	43.7	1.0	0.8833	0.876	−0.007
34	13.3994	33.0162	5.8166	1.4965	0.23000	39.54	40.4	0.9	1.0577	1.060	0.009
35	13.7903	33.9793	6.0687	1.5171	0.23148	38.14	39.0	0.9	1.1370	1.149	0.012

by the mixture rule from the Λ values of the individual salts in solutions of the same concentration. The mixture rule applied to conductance gives:

$$\Lambda_{mix} = x_1\Lambda_1 + x_2\Lambda_2,$$

where x_1 and x_2 are the mole fractions of salts 1 and 2 respectively and Λ_1 and Λ_2 are the equivalent conductances of the single salts at the same concentration. Since all solutions were equimolar in the two salts ($x_1 = x_2 = 0.5$), this amounts merely to taking the average of the conductances of the two single salt solutions. The values for the single salt solutions were obtained by interpolation from the previous results of this laboratory (8), and from the results for lithium nitrate at 35° C, obtained for the first time in this study and given in Table IV.

In column 7 are listed the differences between the calculated and observed equivalent conductances. Column 8 shows the increase in relative viscosity of each solution over

TABLE IV

DATA FOR LITHIUM NITRATE SOLUTIONS AT 35° C

Soln. No.	Weight per cent	Molarity	Density (g/cm³)	Relative viscosity	Specific conductance (mhos)	Equivalent conductance (mhos)
36	0.76006	0.11006	0.99843	1.0289	0.01206	109.59
37	5.73704	0.85456	1.0272	1.1212	0.07346	85.96
38	12.13645	1.8768	1.0663	1.2581	0.13172	70.32
39	17.8357	2.8538	1.1032	1.4201	0.16793	58.84
40	23.7831	3.9467	1.1442	1.6540	0.19024	48.20
41	31.8847	5.5699	1.2044	2.1411	0.19883	35.69
42	42.3407	7.9247	1.2905	3.3376	0.18141	22.89
43	50.3415	9.9537	1.3633	—	0.15549	15.62
44	56.9154	11.7966	1.4291	13.5725	0.13021	11.03

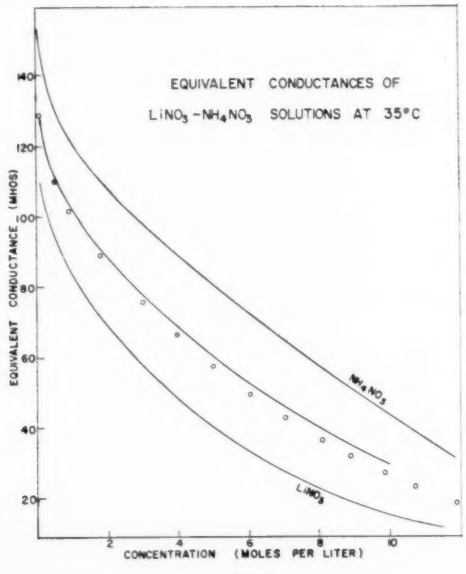

FIG. 1.

the value for water. Column 9 contains the values calculated by the mixture rule from the data for the single salts. The differences between the observed and calculated viscosity increases are listed in column 10.

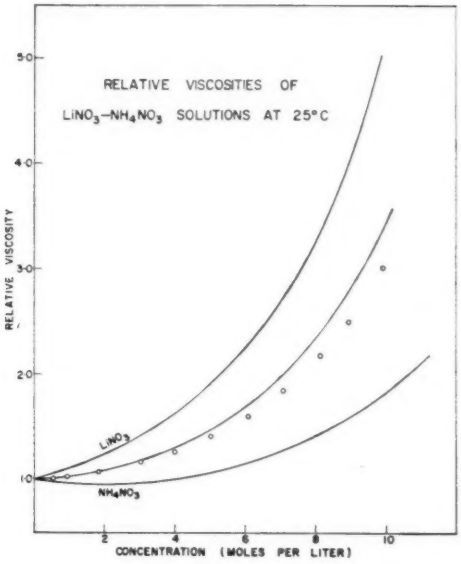

FIG. 2.

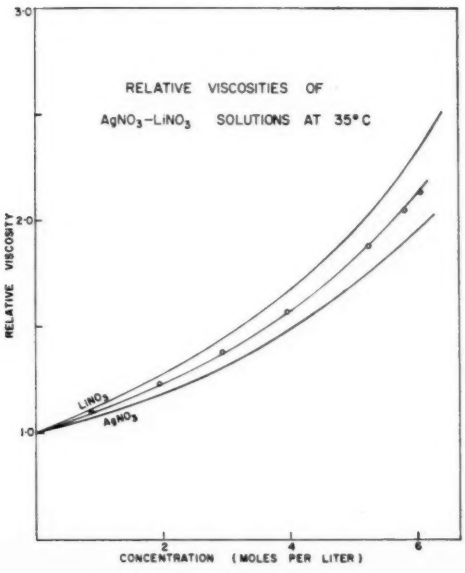

FIG. 3.

Fig. 1, a graph of equivalent conductance vs. concentration, is typical of the six sets of data. Fig. 2 illustrates graphically the relation among the viscosity of the mixed solutions, the viscosity of the single salt solutions, and the viscosity of the mixed solutions as calculated by the mixture rule, for the case of lithium nitrate – ammonium nitrate at 25° C. It can be seen from the tables of data that this type of graph is common to all the solutions, except the lithium nitrate – silver nitrate solutions at 35° C where the calculated and observed viscosities almost coincide; this graph is shown as Fig. 3. The data for lithium nitrate solutions at 35° C are given in Table IV; the graph of equivalent conductance appears in Fig. 1, and the viscosity plot in Fig. 3.

DISCUSSION OF RESULTS

The equivalent conductances of the mixed solutions were in all cases less than the values calculated by the mixture rule. If Λ_A, Λ_B, and Λ_M are the equivalent conductances of solutions of A, of B, and of an equimolar mixture of the two respectively, all at the same total ion concentration, then:

$$\Lambda_M < (\Lambda_A + \Lambda_B)/2.$$

This means that if in a solution of A one half of the A cations are replaced by B cations (the anion remaining the same), the resulting conductance will be lower than the mean conductance of the two single salt solutions. The deviations from the calculated conductances do not seem to be caused by any single ion. The deviation is large when the difference in conductances of the single salt solutions is large, and the mixture rule is more nearly applicable when the difference in conductance is small. This is in agreement with the observations of Van Rysselberghe and Nutting (6).

It is possible that differences in hydration may be concerned. For example, suppose one half of the lithium ions be replaced by ammonium ions. Since the ammonium ions are hydrated to a smaller extent than are the lithium ions, the remaining lithium ions have more water available for hydration and would therefore behave as if they were in more dilute solution. In general then, the more highly hydrated ion will be in effect in a more dilute solution. An increase in solvation and hence of the effective radius of the ion would, in the sense of Stoke's law, cause a decrease in the mobility of the ion. The increase in equivalent conductance observed on dilution of a salt solution (despite a possible increase in hydration) is due to a decrease in the interionic forces. When hydrated ions are replaced by less hydrated ions of the same charge, the number of ions presumably remains the same and the interionic forces are only slightly altered. Hence, in the case considered, the remaining lithium ions being more highly hydrated, their mobility will decrease. The contribution of the ammonium ion to conductance will be little affected, since it is only slightly hydrated. Hence it appears that the hydration effect would operate in the direction of lowering the conductance of the mixture below the value calculated by the mixture rule.

No hydration data are available for the silver ion, but from consideration of ion size and charge the primary hydration number should lie between those of sodium and potassium. Robinson and Stokes (10) from diffusion experiments assign the following values for the hydration numbers: $NH_4^+ = 0.0$; $K^+ = 0.4$; $Na^+ = 0.7$; $Li^+ = 2.3$. The nature of the experiments permits only of the determination of differences in hydration numbers but this is sufficient to show that the order of increasing hydration is $NH_4^+ < K^+ < Ag^+ < Na^+ < Li^+$. Since this is also the order of decreasing conductance, the argument developed for the lithium nitrate – ammonium nitrate solutions is consistent with our observations.

A consideration of the dielectric constant of mixed solutions leads to the same conclusion. No measurements of dielectric constant in mixed solutions have been made but certain theoretical deductions are possible. Hasted, Ritson, and Collie (11) offer the following equation to represent the change in dielectric constant of the medium with concentration of electrolyte:

$$D = D_0 + 2\bar{\delta}\sqrt{c}.$$

According to this equation, D is linear in $\sqrt{c}$. Determinations by these authors suggest that $\bar{\delta}$, the proportionality factor, is larger for smaller and more highly charged ions; this is due to the rigid orientation of the water molecules of the hydration sheath. Strict obedience to the linear equation is observed only up to a concentration of 2 molar. This is due to the inclusion of all the water molecules in the fields of the ions; the highest possible orientation of water molecules has been attained and further addition of ions can have little effect. In replacing lithium ions by ammonium ions, which are less highly hydrated, more water molecules are made available to the strong fields of the remaining lithium ions and so their power of depressing the dielectric constant is increased. Hence the dielectric constant of the mixed solution will be lower than that calculated from the mixture rule. The lower dielectric constant will increase the interionic forces and increase the tendency toward ion pair formation resulting in a lower conductance than the calculated value.

In all cases but one, the viscosities of the mixtures were lower than the values calculated by the mixture rule. The one exception, lithium nitrate – ammonium nitrate solutions at 35° C, occurs where the viscosities and conductances of the two single salt solutions are almost the same. If the viscosity were the sole factor determining conductance, this would imply that an increase in equivalent conductance would occur. Since this is not so, it is obvious that the viscosity effect is exceeded by other effects. It is difficult, however, to see why the viscosity of the solutions of two salts should be lower than the value calculated by the mixture rule. The lowering of dielectric constant, with the consequent strengthening of the interionic forces, tends to increase the viscosity. This is in agreement with the observation made by Kraus (12) in his discussion of the viscosity – dielectric constant relation. The increased hydration of the lithium ion should also increase viscosity. It therefore appears that some other factor or factors must cause this effect in mixed solutions.

REFERENCES

1. Onsager, L. and Fuoss, R. J. Phys. Chem. **36**, 2685 (1932).
2. Bray, W. C. and Hunt, F. L. J. Am. Chem. Soc. **33**, 781 (1911).
3. Longsworth, L. J. Am. Chem. Soc. **52**, 1897 (1930).
4. Bennewitz, K., Wagner, C., and Küchler, K. Physik. Z. **30**, 623 (1929).
5. Krieger, K. A. and Kilpatrick, M. J. Am. Chem. Soc. **59**, 1878 (1937).
6. Van Rysselberghe, P. and Nutting, L. J. Am. Chem. Soc. **59**, 333 (1937).
7. Van Rysselberghe, P., Grinnel, S. W., and Carson, J. M. J. Am. Chem. Soc. **59**, 336 (1937).
8. Campbell, A. N. and Kartzmark, E. M. Can. J. Chem. **28**, 43 (1950); **33**, 887 (1955). Campbell, A. N., Kartzmark, E. M., and Gray, A. P. Can. J. Chem. **31**, 617 (1953). Campbell, A. N., Kartzmark, E. M., and Debus, G. H. Can. J. Chem. **33**, 1508 (1955).
9. Swinehart, D. F. Anal. Chem. **21**, 1577 (1949).
10. Robinson, R. A. and Stokes, R. H. Electrolyte solutions. Butterworth Scientific Publications, London. 1955. p. 320.
11. Hasted, J. B., Ritson, D. M., and Collie, C. H. J. Chem. Phys. **16**, 1 (1948).
12. Kraus, C. A. Properties of electrically conducting systems. Am. Chem. Soc. Monograph Ser. The Chemical Catalog Co. Inc., New York. 1922. p. 111.

SOME THERMODYNAMIC CONSIDERATIONS OF THE EFFECTS OF STRESS ON METAL ELECTRODE POTENTIALS[1]

E. A. Flood

ABSTRACT

It is shown that the change in thermodynamic potential of a solid when elastically strained by the application of the principal stresses p_x, p_y, and p_z is given by the equation

$$\mu-\mu_0 = \tfrac{1}{3}\int_{0,T}^{p_x+p_y+p_z} v\,d(p_x+p_y+p_z)+\phi(q-q_0),$$

where v is the volume per unit mass and $\phi(q-q_0)$ is the shear strain work done on unit mass of the solid, at T and $(p_x+p_y+p_z)$ constant, as the relative values of p_x, p_y, and p_z vary, i.e., as the values of the principal stresses vary from their mean.

INTRODUCTION

Many modern authors of scientific papers assume that the work done upon a system constitutes a measure of the change of Gibbs free energy of the system concerned, quite regardless of how this work is done and regardless of its relation to the pertinent equilibrium conditions. Of course, it is well known that when a solid or liquid is in equilibrium with its vapor that work may be done on or by the system at constant temperature without change in the Gibbs free energy of the system, i.e., without change in the thermodynamic potential of the substance concerned.

The variation in thermodynamic potential of a substance corresponding to given variations in the various variables of the system will depend upon how these variables are involved in particular equilibrium conditions. Accordingly, in order to calculate the changes of potential which accompany given changes in the variables of a system it is essential that the mathematical operations correspond with the idealized experimental conditions.

THERMODYNAMIC POTENTIALS

The condition that a system be in reversible equilibrium with externally applied forces is that the heat absorbed during any change shall be equal to the increase in energy of the system plus the maximum work that the system can do against the externally applied forces. Thus to be in reversible equilibrium with its surroundings the work done *on* a system during a specified change will be the same as that done *by* the system during the exact reverse of the specified change. This is the oldest of the thermodynamic conditions for equilibrium and is, of course, the Carnot–Kelvin condition that a system have no tendency to change its state spontaneously. It will be noted that while both the energy and entropy changes of a system depend only on the initial and final states, the reversible work done and the net heat absorbed ($\int T\,dS$) depend upon how the change is carried out, i.e., upon the path of integration.

The Carnot–Kelvin condition for equilibrium was expressed by Gibbs in the more concise form $(\delta S)_E \leqslant 0$ or $(\delta E)_S \geqslant 0$, leading to similar expressions using the various other thermodynamic functions, the enthalpy, Helmholtz free energy, Gibbs free energy, etc.

[1]*Manuscript received June 13, 1958.*
Contribution from the Division of Pure Chemistry, National Research Council, Ottawa, Canada.
Issued as N.R.C. No. 4878.

The general condition that the various parts of an isolated system be in reversible equilibrium with one another with respect to heat transfer, as between its parts, is that the temperature of its parts shall be the same. If matter may interdiffuse between these parts independently of heat it is also necessary that the thermodynamic potentials of the various kinds of matter in these different parts of the system shall be the same.

Processes in which a given mass of material in "state 1" disappears, while at the same time an equal mass appears in "state 2", the natures and states of the masses, all their respective intensive variables, etc., remaining constant during the transformation, are essentially displacement processes. The condition that such processes be reversible is that the total thermodynamic potentials or displacement potentials of the masses in the two states shall be equal. Where the only externally applied forces involved are the temperature and hydrostatic pressures and we write $F = E - TS + pv$, the condition that the process be reversible is that $\Delta F = 0$ or that $\mu_1 = \mu_2$,* where the thermodynamic potential $\mu = (\partial F/\partial \mathrm{m})_{T,p}$. That this is equivalent to the Carnot–Kelvin equilibrium condition may readily be demonstrated as follows. Let the mass δm_1 disappear by reversible introduction into a reference system while at the same time the mass δm_2 appears as in a typical Washburn thermodynamic engine. If the nature and state of mass m_1 remain unchanged, the entropy and volume per unit mass remain unchanged. The condition that the mass m_1 be in reversible equilibrium with the externally applied forces requires that the decrease in energy δE_1 shall be equal to the heat evolved less the work done on the system by the external forces. If the only external force is the hydrostatic pressure p_1 the work done on the system is $p_1 \delta v$. Thus as the mass δm_1 disappears we have $-\delta E_1 = -T\,\delta S_1 + p_1 \delta v_1$, and similarly as δm_2 appears we have $\delta E_2 = T\,\delta S_2 - p_2 \delta v_2$ and the net effect of the operation is that the energy of the mass may have changed while a quantity of heat has been absorbed or rejected and work done by or on the system. If this work is the maximum work that can be done, the process as a whole is reversible and we can write $\delta F = T\,\delta S - W_{\text{rev}}$. Evidently if $F_1 = E_1 - TS_1 + p_1 v_1$ and $F_2 = E_2 - TS_2 + p_2 v_2$ per unit masses then for the process as a whole $\Delta F = F_2 - F_1 = E_2 - E_1 - T(S_2 - S_1) + p_2 v_2 - p_1 v_1 = 0$, when $p_2 = p_1$ or when

$$\int_{p_0}^{p_2} v_2\, dp = \int_{p_0}^{p_1} v_1\, dp.$$

Thus the condition that $\Delta F = 0$ for such displacement processes at constant T and p is equivalent to the Carnot–Kelvin equilibrium condition. Thus for such processes the condition for equilibrium is that $F_1 = F_2$ or that $\mu_1 = \mu_2$ and the condition that equilibrium be preserved as F_1 and F_2 are changed is that $dF_1 = dF_2$. Hence when the temperature is constant the equilibrium condition equation is $v_1\, dp_1 = v_2\, dp_2$. Evidently in the process above

$$E_2 - E_1 = \delta E = T \int_{S(p_1)}^{S(p_2)} dS - \int_{v_1,\,T}^{v_2} p\, dv = T(S_2 - S_1) - (p_2 v_2 - p_1 v_1),$$

and $p_2 = p_1$ or if phase changes are involved

$$\int_{p_0}^{p_1} v_1\, dp = \int_{p_0}^{p_2} v_2\, dp.$$

Let us consider a case where the equilibrium between δm_1 and the reference system involves only the external pressure p_1 and T as before, but where E_1' and S_1' may differ

**The subscripts refer to the "phases" or to the separate bodies of matter, not to the components as is the common convention in this respect.*

from E_1 and S_1, owing to the action of some other forces (such as the presence of a gravitational field), which are not directly involved in the displacement work terms. Thus let E_1' and S_1' be given by

$$E_1'-E_1 = T\int_{x_0.T.p_1}^{x} dS-\int_{x_0.T.p_1}^{x} p\,dv-\int_{x_0.T.p_1}^{x} f(x)\,dx$$
$$= T(S_1'-S_1)-p_1(v_1'-v_1)-\phi(x_1p_1)+\phi(x_0,p_1)$$

where

$$-\int_{x_0.T.p_1}^{x} p\,dv-\int_{x_0.T.p_1}^{x} f(x)\,dx$$

is the work done by the system on changing its position from x_0 to x in a scalar potential field.*

As before, the condition for reversibility is that

$$E_2-E_1' = T(S_2-S_1')-(p_2v_2-p_1v_1')+\phi(x)-\phi(x_0)$$

and we can write,

$$F_1' = E_1'-TS_1'+p_1v_1' = E_1-TS_1+p_1v_1-\phi(x)+\phi(x_0),$$
$$F_2 = E_2-TS_2+p_2v_2,$$

or,

$$F_1'' = E_1'-TS_1'+p_1v_1'+\phi(x),$$
$$F_2'' = E_2-TS_2+p_2v_2+\phi(x_0),$$

and the condition for reversible equilibrium in such processes is again that $\Delta F = 0$.† This leads to the well-known equation for equilibrium in an isothermal potential field $v\,dp = -d\phi(x)$.

*
$$\int_{x_0.T.p}^{x} f(x)\,dx = \int_0^m \frac{\partial}{\partial m}\int_{x_0.T.p}^{x} f'(x)d\,x\cdot d\,m$$

where $f'(x)$ is the force function per unit mass thus providing for variation in f with m, T, and p being constant.

†*We can derive F_1' from F_2' by integrating in two steps first from p_2 to p_1 at T and x_0, and second, from x_0 to x at p_1 and T so that*

$$F_1' = F_2'+\int_{p_2.x_0.T}^{p_1.x.T} d\,F$$

and during the first step

$$\int_{p_2.x_0.T}^{p_1} d\,F = \int_{p_2.x_0.T}^{p_1} d\,E-T\int_{p_2.x_0.T}^{p_1} d\,S+\int_{p_2.x_0.T}^{p_1} p\,dv+\int_{p_2.x_0.T}^{p_1} v\,dp$$
$$= \int_{p_2.x_0.T}^{p_1} v\,dp = \int_{p_2.x_0.T}^{p_1} \frac{\partial F}{\partial p}\,dp$$

while in the second step

$$\int_{x_0.p_1.T}^{x} d\,F = \int_{x_0.p_1.T}^{x} d\,E-T\int_{x_0.p_1.T}^{x} d\,S+\int_{x_0.p_1.T}^{x} p\,dv$$
$$= -\int_{x_0.p_1.T}^{x} f(x)\,dx = \int_{x_0.p_1.T}^{x} \frac{\partial F}{\partial x}\,dx.$$

Evidently the condition that $\Delta F = 0$ or that $F_1' = F_2'$ is that

$$\int_{p_2.x_0.T}^{p_1} v\,dp-\int_{x_0.p_1.T}^{x} f(x)\,dx = 0 = \int_{p_2.x_0.T}^{p_1} v\,dp-\int_{x_0.p_2.T}^{x} f(x)\,dx.$$

If we suppose that the equilibrium between the mass m_1 and the reference system necessarily involves an electric charge so that as δm_1 is forced into the reference system, reversibly, a definite electric charge is carried with it thus leaving the remaining mass with, say, a net negative charge, as in an electrolytic equilibrium where the mass is in equilibrium with positively charged ions in solution; in this case, we must write $F = E - TS + pv + \epsilon c$ where ϵ is the e.m.f. and c the charge. This leads directly to the relation

$$d\epsilon = -v\,dp/c$$

$$\epsilon - \epsilon_0 = -\frac{1}{n\mathfrak{F}}\int_{p_0}^{p} v\,dp$$

where n is the number of charges carried by the ion, $\mathfrak{F}$ is Faraday's constant, v the volume per mole, etc. Thus the potential difference between two incompressible metal electrodes which differ only in hydrostatic state of stress is $\epsilon - \epsilon_0 = -[v/n(\mathfrak{F})](p - p_0)$. Thus the electrode becomes more negative (more electropositive or less noble) as the hydrostatic pressure p increases. Of course, the electrode becomes positive (more noble) when the hydrostatic pressure p is negative.*

When the stresses acting on the electrode are not hydrostatic stresses, the situation is somewhat more complex. When the contractions $\partial x/x$, $\partial y/y$, etc., are linear functions of the normal stresses p_x, p_y, etc., and the material is isotropic, the volume change is given by the change of the sum of the normal stresses. Accordingly a definite work term is involved for given values of $(p_x + p_y + p_z)$. However, in the general case it is only when the shape remains constant that a reversible equilibrium and a definite work term can be associated with the positive or negative changes in volume which accompany the addition or removal of elements of mass. In this case, if xyz be an element of volume v, then $\delta v = yz\,dx + zx\,dy + xy\,dz$, and we can write,

$$\delta E = T\delta S - p_x yz\,dx - p_y zx\,dy - p_z xy\,dz + \mu\delta m.$$

We can integrate this equation holding T and p_x, p_y, p_z, the principal stresses, constant and obtain a definite work term only if dx, dy, and dz are related to one another in a constant manner. In this case we can write $y = a_y x$, $z = a_z x$, where a_y and a_z are constants and obtain

$$\begin{aligned}\delta E &= T\delta S - (p_x + p_y + p_z)a_y a_z x^2\,dx + \mu\delta m,\\ &= T\delta S - \tfrac{1}{3}(p_x + p_y + p_z)\delta v + \mu\delta m,\\ &= T\delta S - \bar{p}\delta v + \mu\delta m.\end{aligned}$$

This leads to

$$\epsilon - \epsilon_0 = -\frac{1}{n\mathfrak{F}}\int_{\bar{p}_0}^{\bar{p}} v\,dp$$

where $\bar{p} = \tfrac{1}{3}(p_x + p_y + p_z)$.

If, however, p_x, p_y, and p_z, the principal or normal stresses, are of relatively large magnitudes and differ from one another appreciably, shear strain energies are necessarily involved. The work term associated with the shear strain energy is not involved in the displacement work and accordingly we must add the corresponding work term to the displacement or Gibbs potential, as done above in the case of a gravitational potential

*Since an electric charge on a thin wire gives rise to an appreciable mechanical stress, a term taking this into account explicitly may be necessary. The term is equivalent to $\partial\mu_1/\partial q.\delta q$ where δq is the increased charge associated with the greater ϵ.

$\phi(x)$. This work term is always positive when taken from the unsheared state, i.e., work done on the body at constant temperature as an angular deformation occurs at constant $(p_x+p_y+p_z)$, while the relative values of p_x, p_y, and p_z change. In this case we should write $F = E_{q_0} - TS + \bar{p}v + \epsilon c + \phi(q)$, where $\phi(q)$ is the shear strain energy per unit mass

$$= \int_{q_0.T.v}^{q} \phi \, dq$$

($\phi(q)$ for elastic deformations of isotropic bodies obeying Hooke's Law is $1/12M\,[(p_x-p_y)^2 + (p_y-p_z)^2+(p_z-p_x)^2]$ where M is the modulus of rigidity).

Accordingly the electrode potential $\epsilon-\epsilon_0$ as a function of stress becomes,

$$\epsilon-\epsilon_0 = -\frac{1}{n\mathfrak{F}} \int_{\bar{p}_0}^{\bar{p}} v \, d\bar{p} - \int_{q_0.T.\bar{p}}^{q} \phi \, dq. \qquad [1]$$

Evidently purely compressional or dilational strain energies are not explicitly involved in the final formulae, since they are already contained in the E, TS, and pv terms. For elastic solids obeying Hooke's Law we can write approximately,

$$\begin{aligned} \epsilon-\epsilon_0 &= -(v/n\mathfrak{F})(\bar{p}-\bar{p}_0) - (v/12M)[(p_x-p_y)^2+(p_y-p_z)^2+(p_z-p_x)^2] \\ \delta\epsilon &= -(v/3n\mathfrak{F})(p_x+p_y+p_z) - (v/12M)[(p_x-p_y)^2+(p_y-p_z)^2+(p_z-p_x)^2], \end{aligned}$$

where $\delta\epsilon$ is the voltage difference between an electrode under no stress and one with normal stresses p_x, p_y, and p_z expressed in suitable units. Thus the shear strain energy always makes the electrode more electropositive (i.e. less noble), while the displacement work terms make the electrode more electropositive when $p_x+p_y+p_z$ is positive and makes the electrode less electropositive (i.e. more noble) when the sum of the pressures or normal stresses is negative. For small positive or negative values of p_x, p_y, and p_z, the shear strain potential will be negligible, while at very large values of the stresses the shear strain potential may be dominant. If the electrode is strained beyond its elastic limit and the stress released, a term of the type $\phi(q)$ will remain so that the strained metal will in general be more electropositive (i.e. less noble) than in the unstrained state; however, in this case the magnitude of $\phi(q)$ cannot be calculated in any very simple manner. In general, in the absence of competing chemical reactions of the electrode, electrolyte, etc., lack of reversibility will tend to reduce the magnitude of the difference $\epsilon-\epsilon_0$, i.e. to reduce the magnitude of the electrical work the cell can do.

If the stress p_x arises as a result of the application of a constant force while p_y and p_z correspond to the constant hydrostatic pressure of the electrolyte, the stress p_x will vary as material dissolves or deposits on the electrode. There can be no true equilibrium in this case. However, in the case of an electrode of reasonably large diameter the variation of p_x due to dissolution or deposition will be very small, especially when the electrolyte concentrations are small. If the electrode is reasonably uniform so that all parts of it, including the surface layer, are in thermodynamic equilibrium with one another, equation 1 should hold reasonably well for small changes in stress. If the surface of the electrode which controls the ionic equilibrium consists of largely detached particles of metal so that little of the applied stress is sustained by these surface particles, the observed $\epsilon-\epsilon_0$ will be much less than that calculated. It is also possible that the outer layer, due, say, to work hardening, may be of much greater rigidity than that of the interior material and consequently that the stress sustained by the surface material is appreciably greater than that estimated from the applied force. In this case the observed $\epsilon-\epsilon_0$ may be greater than that calculated from equation 1.

The general trend of the relevant data reported in the literature, that we have seen, appears to be consistent with the views expressed above (cf. Fryxell, R. E. and Nachtrieb, N. H. J. Electrochem. Soc. **99**, 495 (1952)).

A somewhat similar problem has been discussed by Gibbs. In the paragraph following Equation (397) of his "Equilibrium of heterogeneous substances" he appears to have made a slip (!!) when he states, "the fluids in equilibrium with the solid are all supersaturated with respect to the substance of the solid, except when the solid is in a state of hydrostatic stress". This statement is only generally correct when the mean of the principal stresses of the solid is equal to or greater than the hydrostatic stress of the fluid.

APPENDIX

The basic relations may be generalized as follows:

$$dE = T\,dS - \sum P_i\,dV_i + \sum f_j\,dx_j$$

where the terms $\sum P_i dV_i$ are all work terms which are necessarily associated with the reversible addition or removal of material, its nature and state remaining constant during the process, the terms $\sum f_j\,dx_j$ are work terms which are not associated directly with the addition or removal of the material, its nature and state remaining constant.

Thus we can write,

$$\begin{aligned} dE &= T\,dS - \sum P_i\,dV_i + \left[\sum \frac{\partial}{\partial m}\int_{x_{j0}}^{x_j} f_j\,dx_j + \mu_0\right] dm \\ &= T\,dS - \sum P_i\,dV_i + \mu\,dm. \end{aligned}$$

The nature of the work terms $\sum P_i\,dV_i$ are assumed to be such that the integration of the equation holding T, the P_i's, and μ constant has a definite meaning and corresponds to an ideal physical process. Thus we can write,

$$E = TS - \sum P_i\,V_i + \mu m$$

and

$$F = E - TS + \sum P_i\,V_i = \mu m.$$

Evidently,

$$\left(\frac{\partial F}{\partial m}\right)_{T,P_i,x_j} = \left(\frac{\partial E}{\partial m}\right)_{S,V_i,x_j} = \mu$$

$$\left(\frac{\partial F}{\partial x_1}\right)_{T,P_i,m,x_2\ldots} = \left(\frac{\partial E}{\partial x_1}\right)_{S,V_i,m,x_2\ldots} = f_1$$

The condition that the μ's be the same for two separate bodies of matter is equivalent to the condition that in any transfer of matter between the two bodies, $\delta E = 0$ when S and V_i's are constant, and that $\delta E = T\delta S - \text{work}_{(\max)}$ or that $\delta F = 0$, when T and P_i's are constant.

Similar relations hold for other thermodynamic functions, thus all of the equilibrium conditions are contained in the Carnot–Kelvin condition for reversibility.

MICROCALORIMETRY OF THE ADSORPTION OF WATER VAPOR ON SODIUM CHLORIDE[1]

HENRY M. PAPÉE[2] AND KEITH J. LAIDLER

ABSTRACT

Using a microcalorimeter of the Calvet type, measurements have been made of the heats of adsorption of water vapor on microcrystals of sodium chloride, the rate of heat production being followed as a function of time. With crystals of surface areas between 1 and 15 square meters per gram it was found that three distinct processes occurred, in the following order: (1) simple adsorption of water on the surface, (2) decrease in the surface area, and (3) penetration of water into the lattice. During the second stage no adsorption could be detected. On crystals with larger surface areas there was considerable overlapping of the three phenomena, but the general mechanisms appear to be the same.

INTRODUCTION

Detailed studies of the surface enthalpies of sodium chloride crystals have been made by Benson and his co-workers (1, 2, 3), who measured the heat evolved on the solution in water of sodium chloride crystals of high surface area. The mechanism of the adsorption of water vapor on sodium chloride is a matter of considerable importance in connection with the precipitation of rain (4, 5, 6, 7), and in order to gain further knowledge of this phenomenon a microcalorimetric investigation has been made of the heat liberated when water vapor is allowed to come into contact with sodium chloride crystals of various surface areas.

EXPERIMENTAL

Materials

The sodium chloride employed was C.P., and crystals having large specific surface areas were prepared using a special apparatus and technique developed by Young and Morrison (8; cf. also ref. 2, where the same method was employed). The essential feature of the procedure is that vapor is swept from the surface of molten sodium chloride in a turbulent stream of nitrogen and is carried into an electrostatic precipitator, where the small particles are collected. Care was taken to avoid conditions that would lead to the formation of metallic sodium and of sodium nitrate (3), and tests of purity revealed the absence of contamination. The samples of salt were kept at all times in a desiccator, and all manipulations with the material were carried out at 25.0° C in an atmosphere of dry nitrogen of less than one per cent relative humidity.

In some experiments the work was done directly with samples prepared in the electrostatic precipitator. In other cases samples were prepared by controlled sintering, under vacuum at 240° C, of samples prepared in this way. Samples of low areas (from 1 to 2 $m^2 g^{-1}$) were obtained by grinding optical crystals and sieving them to −200 mesh.

Surface areas were measured by the Brunauer–Emmett–Teller method, involving the adsorption of nitrogen at relative pressures below 0.15. Tests showed that the surface areas of the samples remained constant over considerable periods of time.

All samples were heated for 12 hours at 150° C under vacuum.

Microcalorimetry

The heat measurements were carried out in a microcalorimeter of the Tian–Calvet type (9), and the general procedures were as described in previous papers (10, 11)

[1]*Manuscript received May 26, 1958.*
Contribution from the Department of Chemistry, University of Ottawa, Ottawa, Canada.
[2]*Present address: Division of Applied Chemistry, National Research Council of Canada, Ottawa, Canada.*

dealing with work with this instrument. A special device which allowed the adsorption to take place under high vacuum was designed and constructed; it is shown schematically in Fig. 1, and further details are given on p. 264 of ref. 12. Essentially it consists of two connecting cells, each one of which is fitted into a silver thimble in the microcalorimeter block. One cell contains the salt and the other, the water and a heat exchanger. When the connections between the two cells are opened the vapor diffuses into the salt, and measurements are made of both the heat evolved in the salt cell and of the heat absorbed in the water cell. The manipulations with the cells could be made from outside the calorimeter by the turning of insulated rods.

Prior to being filled with salt the interior container was outgassed under high vacuum for 5 hours at 250° C, and the whole vacuum circuit was evacuated for 5 hours, after which it was filled with dry nitrogen. The subsequent operations were carried out in a dry box in which the relative humidity was below one per cent. The sodium chloride was introduced into the cell and its weight determined by difference.

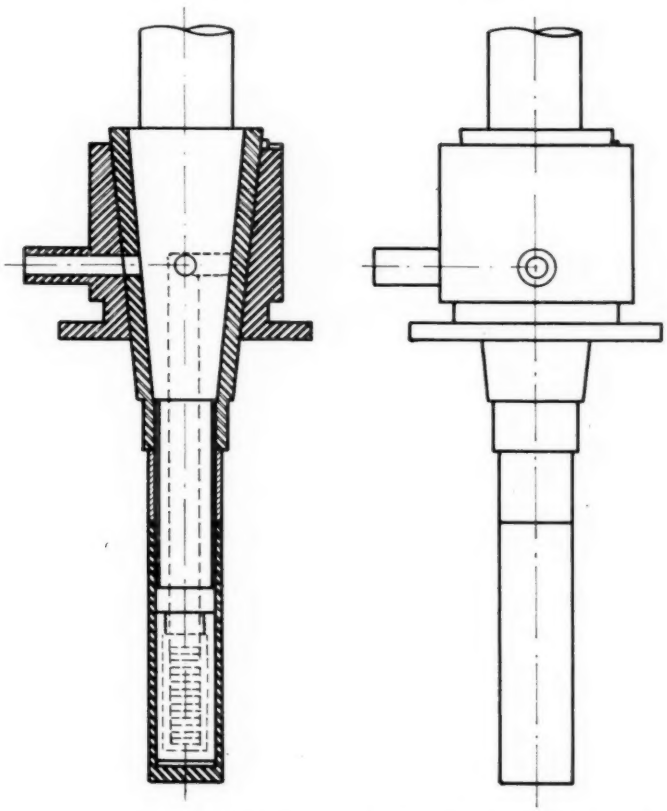

FIG. 1. Schematic representation of a high-vacuum cell for the adsorption studies. At the left is shown a section, at the right an outside view twisted through 90°. Two cells of this type are connected together by thick polythene tubing and inserted into the microcalorimeter block. The turning of valves required to connect and disconnect the two cells is performed by turning an insulated rod which comes out through the top of the apparatus.

After the introduction of the vacuum circuit into the microcalorimeter the water-containing cell was evacuated, left for 10 minutes, and the operation repeated three times. This cell was then sealed off, and the salt-containing cell was pumped down for 4 hours, using a diffusion pump. After the pump was disconnected the salt cell was sealed off and the water cell put into communication with the interconnecting bridge. The whole assembly was then left overnight to attain thermal equilibrium.

On the following day zero readings were taken over a period of several hours, and the cells then put into communication with one another. Separate recordings were made of the heat evolved in the salt cell and of the heat absorbed in the water cell. The values were corrected using results from blank experiments in which the salt container was empty but in which all other operations were identical.

All heat measurements were carried out at $25.00 \pm 0.01°$ C, and the runs were continued for a considerable number of hours in each case. The calorimeter records the rate of heat evolution (Q/t) as a function of time,* and heats are determined by mechanical integration using a planimeter. The values quoted in the present paper are 'thermochemical' calories, equal to 4.1840 joules. The instrument was calibrated electrically.

General Procedure

Two series of experiments were carried out, as follows:

Series 1.—In this group of measurements calorimetric measurements were made using different weights of a given sample of sodium chloride, the surface area being 19.68 $m^2 g^{-1}$.

Series 2.—In this series the work was done with salt samples weighing from 0.4 to 2.0 g but with specific surface areas ranging from 1 to 20 $m^2 g^{-1}$.

Work was done with various degrees of connection between the two cells, and it was found that the most useful results, in which the separate stages were distinctly revealed, were obtained when the rate of diffusion was moderate.

RESULTS

When the rate of diffusion of water vapor into the salt cell is caused to be small, points of discontinuity are observed in the record of Q/t against t for the salt cell, as shown schematically in Fig. 2. By comparing the records for the salt cell and the water cell, and using the known heat of vaporization of water, it is possible to estimate the amount of water that interacts with the salt during each of the separate processes.

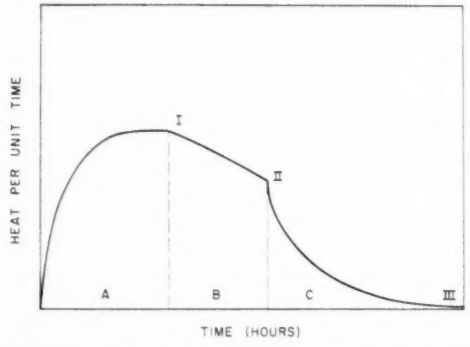

FIG. 2. Schematic plot of rate of heat production against time, showing the two inflection points observed on the microcalorimetric records.

**This is very close to the truth because of the slowness of the process.*

Fig. 2 shows that Q/t at first increases progressively with time until finally a steady value is obtained. This first process is ended by a point of discontinuity after which Q/t decreases gradually until a second point is reached. This second point could be detected only when larger crystals, with surface areas below 15 $m^2\ g^{-1}$, were used. Such points of discontinuity were well defined when the surface area was between 1 and 15 $m^2\ g^{-1}$, but difficult to detect in samples of areas of about 20 $m^2\ g^{-1}$; this was the case in experiments of series 1.

The process can therefore be regarded as occurring in three stages, corresponding to the areas A, B, and C in Fig. 2. Heats corresponding to the three stages were determined by measuring the appropriate areas.

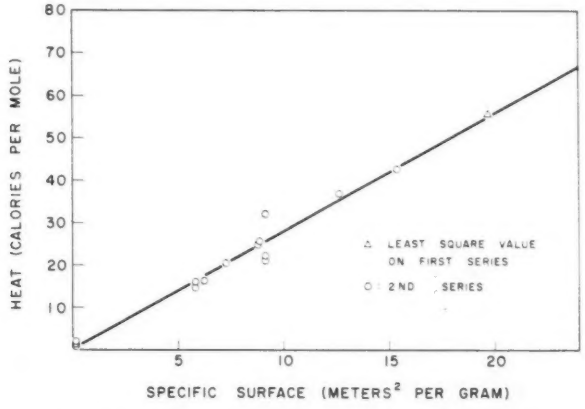

FIG. 3. Plot of heat evolved up to the first inflection point (area A in Fig. 2) against the specific surface area.

TABLE I

HEATS CORRESPONDING TO THE VARIOUS STAGES

Figure	Stage	Series of experiments	Cell	Slope
3	A	1 and 2	Salt	2.77 ± 0.06 (cal $mole^{-1}$)/($m^2\ g^{-1}$) = 0.047 ± 0.001 cal m^{-2}
4	A	1 and 2	Water	-0.75 ± 0.02 (cal $mole^{-1}$)/($m^2\ g^{-1}$) = -0.0128 ± 0.0003 cal m^{-2}
5	A + B	2	Salt	$5.91+0.08$ (cal $mole^{-1}$)/($m^2\ g^{-1}$) = 0.101 ± 0.001 cal m^{-2}
6	A + B	2	Water	-0.76 ± 0.02 (cal $mole^{-1}$)/($m^2\ g^{-1}$) = -0.0130 ± 0.0003 cal m^{-2}
7	C	1	Salt	3.93 ± 0.03 (cal $mole^{-1}$)/($m^2\ g^{-1}$) = 0.0673 ± 0.0005 cal m^{-2}
8	C	1	Water	-1.34 ± 0.17 (cal $mole^{-1}$)/($m^2\ g^{-1}$) = -0.023 ± 0.003 cal m^{-2}
9	C	2	Salt	0.30 ± 0.02 cal g^{-1}
10	C	2	Water	-0.388 ± 0.04 cal g^{-1}

Mole refers to sodium chloride.

TABLE II

SUMMARY OF RESULTS

Stage	Heat: Salt cell	Heat: Water cell	Units	Phenomenon
A	0.047 ± 0.001	-0.0128 ± 0.0003	cal m^{-2}	Adsorption on surface
B	0.054 ± 0.001	0.000 ± 0.0001	cal m^{-2}	Increase in surface area
C	17.5 ± 1	24.5 ± 3	cal $mole^{-1}$	Penetration of water into lattice; condensation of water on salt

Mole refers to sodium chloride.

The results are summarized in Figs. 3–10, and in Tables I and II. The figures show plots of heats against either the surface area or the weight of sample, and it is to be seen that reasonably linear behavior is found in both cases. Figs. 3, 5, 7, and 9 refer to the cell in which the salt is contained, and therefore are concerned with heat evolution; Figs. 4, 6, 8, and 10 show results for the cell from which the water was evaporating, and heat is therefore absorbed. The lines in Figs. 3–10 all appear to pass through the origin, and least-square calculations were made in such a way that the line was forced to go through the origin. The resulting slopes, and the standard deviations, are given in Table I. In the case of stage C in the second series of experiments it was found that there was no relationship between the heat and the surface area, but only between the heat and the weight of the sample.

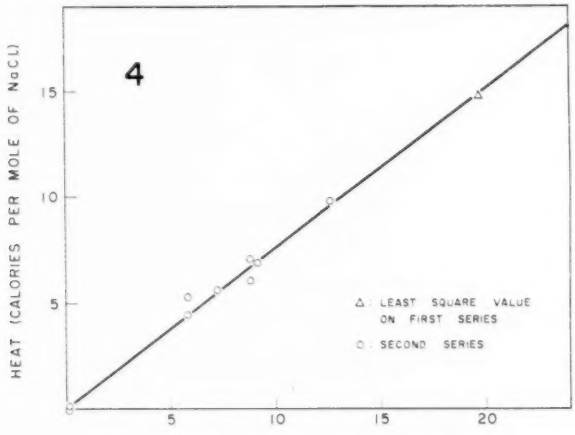

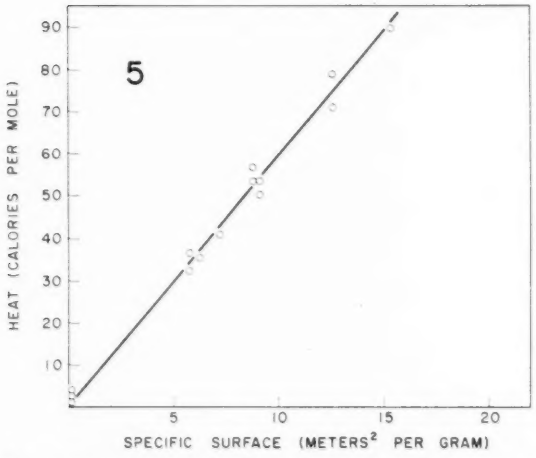

FIG. 4. Plot of heat absorbed up to the first inflection point against the specific surface area, for the cell from which the water was evaporating.

FIG. 5. Plot of heat evolved up to the second inflection point (areas A and B in Fig. 2) against the specific surface area.

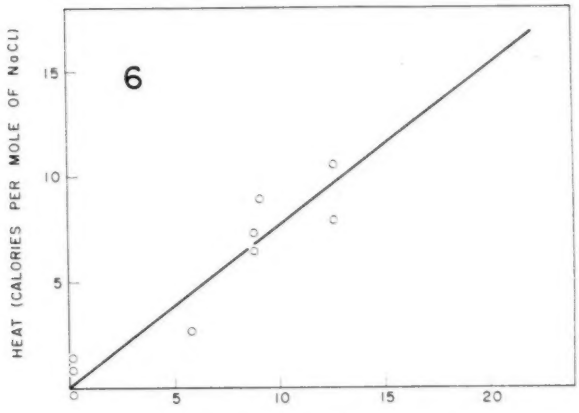

FIG. 6. Plot of heat absorbed up to the second inflection point, for the cell from which the water was evaporating.

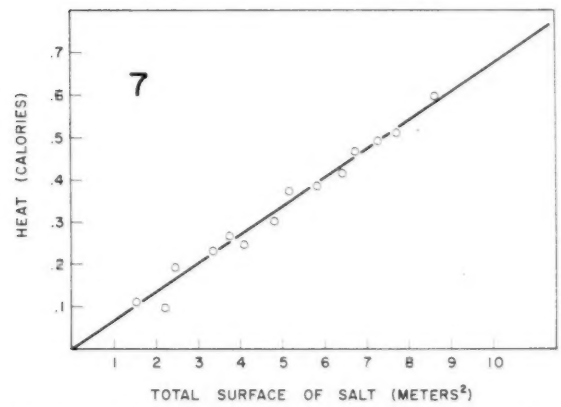

FIG. 7. Plot of heat evolved after the second inflection point (area C in Fig. 2) against the total surface area.

Table II summarizes the main results of the investigation, and shows, for each of the three stages A, B, and C, the heats evolved in the salt cell and absorbed in the water cell.

DISCUSSION

The most striking result of the present investigation is that during stage B there is, within the experimental error, no heat absorbed in the water cell. This means that there is no evaporation of water during the process and therefore no uptake of water by the salt. Stage B thus represents simply a change in the nature of the surface of the salt. The picture that therefore emerges is that the three stages are as follows:

Stage A.—Adsorption of water on the surface of the salt.

Stage B.—Change in the surface area of the salt. Presumably the salt crystals to some extent coalesce, with a decrease in surface area, and during this process there is no uptake of water.

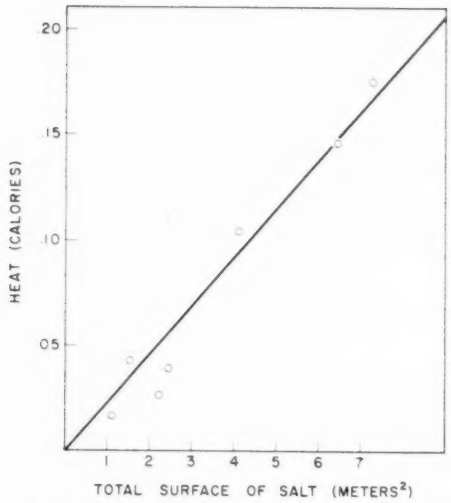

FIG. 8. Plot of heat absorbed after the second inflection point against the total surface area, for the cell from which the water was evaporating.

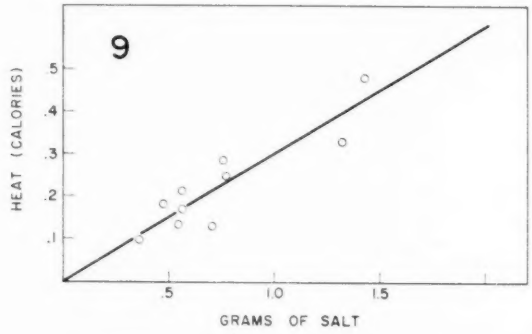

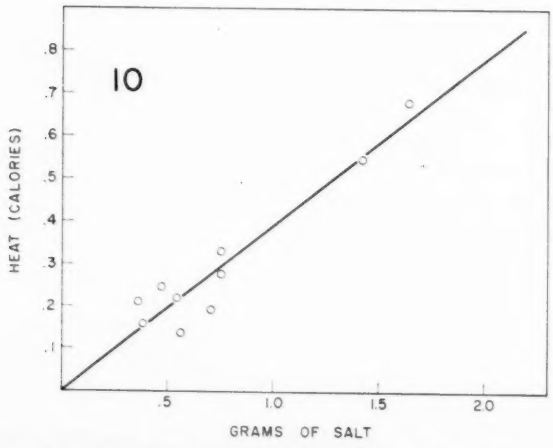

FIG. 9. Plot of heat evolved after the second inflection point against weight of salt.

FIG. 10. Plot of heat absorbed after the second inflection point against weight of salt, for the cell from which the water was evaporating.

Stage C.—Penetration of water into the crystal lattice, and condensation of additional water on the surface.

It is unlikely, however, that the stages are to be distinguished sharply. Thus the heat evolved in the salt cell during stage A is equal to about 36 kcal per mole of water, and this is too large to correspond to a simple physical adsorption; presumably some change in the surface is occurring at the same time.

It is significant that during stages A and B the heat evolution is proportional to the surface area; the heats per unit area were found to be uninfluenced by whether the material was prepared by electrostatic precipitation, by sintering, or by grinding. However, the magnitude of the heat evolved in stage C is proportional to the total weight of the sample and not to the surface area. These facts are consistent with the mechanisms proposed above for the three stages. During stage C the crystals are considered to have undergone a pronounced change in surface area, and the heat is therefore independent of the initial areas.

The amount of water evaporated in stage A, estimated from the heat absorption and the latent heat of evaporation, is found to be about one twelfth of that required to form a monolayer.* The significance of this may well be that this is the amount required to induce the crystals to undergo a structural change in which a decrease of surface occurs.

It is of interest to compare the results obtained in the present work with the value of Benson *et al.* (3) for the total surface energy of sodium chloride. Their value is

$$0.0659 \text{ cal m}^{-2}.$$

This value is seen from Table II to be greater than the value for stage A (0.047 cal m^{-2}) but less than the sum of the values for stages A and B (0.101 cal m^{-2}). This result further suggests that stages A and B are not sharply separated from one another, although it would appear that all of the surface has been broken down by the end of stage B.

ACKNOWLEDGMENTS

The authors are indebted to Mr. T. W. Zawidzki for preparing the sodium chloride of high surface area, and for help in many other ways. They are also indebted to Drs. G. C. Benson and J. A. Morrison of the National Research Council for the use of their electrostatic precipitator and for much help and valuable advice. Thanks are also due to Professor M. Proulx for the preparation of Fig. 1.

The work was performed under a contract between the U.S. Air Force Cambridge Research Center and the University of Ottawa.

REFERENCES

1. Benson, G. C. and Benson, G. W. Can. J. Chem. **33**, 232 (1955).
2. Van Zeggeren, F., Schreiber, H. P., and Benson, G. C. Can. J. Chem. **34**, 1501 (1956).
3. Benson, G. C., Schreiber, H. P., and Van Zeggeren, F. Can. J. Chem. **34**, 1553 (1956).
4. Woodcock, A. H. Artificial stimulation of rain. Pergamon Press, Ltd., New York. 1957. p. 202.
5. Byers, H. R., Sievers, J. R., and Tufts, B. J. Artificial stimulation of rain. Pergamon Press, Ltd., New York. 1957. p. 47.
6. Nakaya, U. Artificial stimulation of rain. Pergamon Press, Ltd., New York. 1957. p. 36.
7. Papée, H. M. J. Meteorol. (To be published).
8. Young, D. M. and Morrison, J. A. J. Sci. Instr. **31**, 90 (1954).
9. Calvet, E. and Prat, H. Microcalorimetrie. Masson et Cie., Paris. 1956.
10. Papée, H. M., Canady, W. J., and Laidler, K. J. Can. J. Chem. **34**, 1677 (1956).
11. Canady, W. J., Papée, H. M., and Laidler, K. J. Trans. Faraday Soc. **54**, 502 (1958).
12. Rossini, R. D. Experimental thermochemistry. Interscience Publishers, Inc., New York. 1956.

**This estimate is based on a value of 10.6 Å² for the area occupied by each water molecule; a monolayer would therefore consist of 9.43×10^{18} molecules or 2.82×10^{-4} g of water per square meter. The heat absorbed in the water cell during stage A was 1.28×10^{-2} cal per square meter of salt. This corresponds to the evaporation of 2.33×10^{-5} g of water.*

L'ARYLATION DES QUINONES PAR LES SELS DE DIAZONIUM

IV. SUR LA RÉACTION DE CES SELS AVEC LA 2,5-DIHYDROXY-*p*-BENZOQUINONE ET LA SYNTHÈSE DE LA 3-HYDROXY-2,5-BISPHENYL-*p*-BENZOQUINONE[1]

P. Brassard[2] et P. L'Écuyer

RÉSUMÉ

L'accumulation des fonctions phénoliques sur l'anneau de la *p*-benzoquinone rend la molécule particulièrement apte à la copulation avec les sels de diazonium au détriment de l'arylation. La réaction de la 2,5-dihydroxy-*p*-benzoquinone avec ces sels donne, en solution aqueuse et en présence d'un excès de 25% de la quantité stoechiométrique d'hydroxyde de potassium, la 2,5-dihydroxy-3-phénylazo-*p*-benzoquinone. Lorsqu'on effectue la réaction en présence d'au moins deux fois la quantité calculée de la base, on isole la 2,5-dihydroxy-3-phényl-6-phénylazo-*p*-benzoquinone. La 2,5-dihydroxy-3,6-bis-(*o*-tolyl)-*p*-benzoquinone est la seule 2,5-dihydroxy-3,6-bisaryl-*p*-benzoquinone que nous avons réussi à synthetiser par cette réaction. Au cours de nos travaux nous avons synthétisé la 3-hydroxy-2,5-bisphényl-*p*-benzoquinone selon un autre procédé décrit dans la partie expérimentale.

INTRODUCTION

La synthèse de la 2,5-dihydroxy-3,6-bisphényl-*p*-benzoquinone ou acide polyporique (1) et de ses dérivés naturels, l'atromentine (2) et la leucomélone (3) a été, jusqu'à présent, l'objet d'un certain nombre de travaux. Fichter (4) a d'abord réalisé la préparation de l'acide polyporique et Kögl (5) celle du diméthyléther de l'atromentine avec des rendements respectifs de 0.14 et 1.28%. Adams (6), Asano et Kameda (7), Kvalnes (8), Ghigi (9) et Fieser et Oxford (10) publièrent d'autres synthèses de l'acide polyporique, et Akagi (3) réalisa celle de la leucomélone.

Il est relativement difficile d'obtenir la 2,5-dichloro- et les 2,5-bisaryl-*p*-benzoquinones (11), les intermédiaires indispensables à la préparation des 2,5-dihydroxy-3,6-bisaryl-*p*-benzoquinones. Pour cette raison, il nous a semblé opportun de tenter d'obtenir directement ces dernières à partir de la 2,5-dihydroxy-*p*-benzoquinone en utilisant une technique analogue à celle qu'a suivie Neunhoffer (12) pour l'arylation de la 2-hydroxy-1,4-naphtoquinone avec les sels de benzène-diazonium.

La 2,5-dihydroxy-*p*-benzoquinone se prépare avec grande facilité par la méthode de Jones et Shonle (13), mais l'accumulation des fonctions phénoliques sur l'anneau de la quinone rend la molécule particulièrement apte à la copulation avec les sels de diazonium au détriment de l'arylation.

Lorsqu'on fait réagir une solution aqueuse du chlorure de diazonium avec de la 2,5-dihydroxy-*p*-benzoquinone dissoute dans de la potasse contenant 25% d'hydroxyde de potassium en excès de la quantité stoechiométrique et qu'ensuite on acidifie légèrement le mélange (pH = 5) par l'addition d'acide acétique, une certaine quantité de substances indésirables précipitent. Si on filtre alors et acidifie fortement le filtrat (pH = 2) avec de l'acide chlorhydrique on obtient la 2,5-dihydroxy-3-arylazo-*p*-benzoquinone. Il est nécessaire d'employer un excès de 25% de la quantité calculée d'hydroxyde de potassium, car autrement le rendement diminue considérablement.

Influence de la température de réaction et de la concentration d'hydroxyde de potassium

Lorsqu'on effectue la réaction du sel de diazonium avec la 2,5-dihydroxy-*p*-benzoquinone en présence de deux fois la quantité théorique d'hydroxyde de potassium, on isole de la même façon que précédemment, une autre classe de composés, soit les

[1]*Manuscrit reçu le 9 juin, 1958.*
Contribution du Département de Chimie, Université Laval, Québec, P.Q.
[2]*Adresse actuelle: Chemisches Institut der Universität, Zürich, Suisse.*

2,5-dihydroxy-3-aryl-6-arylazo-*p*-benzoquinones. En élevant la température de réaction de 50 à 85°, et en augmentant en même temps la concentration de la base jusqu'à un excès de 200%, on obtient encore les mêmes substances. Le seul effet de ces variations croissantes de la température et de la concentration de la base est de faire baisser proportionnellement les rendements (Tableau I).

TABLEAU I

INFLUENCE DE LA TEMPÉRATURE DE RÉACTION ET DE LA CONCENTRATION D'HYDROXYDE DE POTASSIUM

Réaction du chlorure de benzène-diazonium (0.1 mole) avec la 2,5-dihydroxy-*p*-benzoquinone (0.05 mole) en solution aqueuse (600 ml)

Température	% d'excès de KOH	Rendement, en %
45–50°	100	28
45–50°	150	18
45–50°	200	11
80–85°	100	20

Influence du substituant dans le sel de diazonium

Dans la synthèse des dihydroxyarylazoquinones comme dans la préparation des 2-hydroxy-3-aryl-1,4-naphtoquinones en milieu alcalin, la réactivité des sels de diazonium semble être l'inverse de celle qui se manifeste lors de la réaction normale avec la *p*-quinone en l'absence de base. Dans ce dernier cas la stabilité du sel de diazonium favorise l'arylation de la quinone non-hydroxylée. Par contre, lors de la réaction avec la 2-hydroxy-1,4-naphtoquinone d'après la méthode de Neunhoffer, l'*o*-toluidine diazotée donne un rendement de 65%, tandis que le chlorure de *p*-chlorobenzène-diazonium n'en fournit plus qu'un de 40%.

Nous avons observé la même relation dans la réaction des sels de diazonium avec la 2,5-dihydroxy-*p*-benzoquinone en milieu alcalin. Les meilleurs résultats ont été obtenus avec la *m*-toluidine diazotée tandis que le rendement est nul avec la chlorure de *p*-chlorobenzène-diazonium.

Dans un cas seulement, il nous a été possible de synthétiser une 2,5-dihydroxy-3,6-bisaryl-*p*-benzoquinone par cette réaction. C'est en utilisant un sel de diazonium particulièrement instable, le chlorure d'*o*-methylbenzène-diazonium, et en employant des quantités équimoléculaires de la quinone et du réactif diazoique. Nous avons alors obtenu la 2,5-dihydroxy-3,6-bis-(*o*-tolyl)-*p*-benzoquinone avec un rendement de 32%.

Enfin nous avons synthétisé la 3-hydroxy-2,5-bisphényl-*p*-benzoquinone, à partir de la 2,5-bisphényl-*p*-benzoquinone, en suivant la façon de procéder décrite dans la partie expérimentale.

PARTIE EXPÉRIMENTALE*

2,5-Dihydroxy-3-phénylazo-p-benzoquinone

On diazote de la façon habituelle de l'aniline (9.3 g, 0.10 mole) dissoute dans une solution diluée d'acide chlorhydrique (25 ml d'acide concentré dans 100 ml d'eau). On ajoute lentement (l'opération doit durer 5 minutes), la solution du sel de diazonium à une solution de 2,5-dihydroxy-*p*-benzoquinone (7.0 g) et d'hydroxyde de potassium (20.0 g) dans l'eau (500 ml) tout en maintenant la température entre 45 et 50° et en agitant vigoureusement. On continue d'agiter pendant 20 minutes à la même température. On

*Les points de fusion ont été pris à l'aide de l'appareil de Johns.

dilue alors à environ 1 litre, et on acidifie à pH = 5 avec de l'acide acétique. On filtre, on rend le filtrat fortement acide par l'addition d'acide chlorhydrique et on essore le précipité. Après deux cristallisations dans le dioxane, la 2,5-dihydroxy-3-phénylazo-*p*-benzoquinone (6.2 g, 51% de la théorie), aiguilles rouges, contient du dioxane de cristallisation. Elle perd ce dioxane par séchage sous vide à 60° en se transformant en une poudre rouge vif qui se décompose entre 220 et 225°. Calculé pour $C_{12}H_8O_4N_2$: C, 59.02%; H, 3.30%; N, 11.46%. Trouvé: C, 59.0%; H, 3.3%; N, 11.2%.

2,5-Dihydroxy-3-(o-tolylazo)-p-benzoquinone

On opère exactement comme précédemment. Après deux cristallisations dans le dioxane on obtient 8.4 g (65% de la théorie) de 2,5-dihydroxy-3-(*o*-tolylazo)-*p*-benzoquinone pure sous la forme d'aiguilles brun-rouge. Après avoir éliminé le dioxane de cristallisation par chauffage sous-vide à 60° pendant 3 heures, la substance devenue pulvérulente est de couleur rouge foncé et se décompose entre 225 et 228°. Calculé pour $C_{13}H_{10}O_4N_2$: C, 60.46%; H, 3.90%; N, 10.81%. Trouvé: C, 60.7%; H, 3.8%; N, 10.7%.

2,5-Dihydroxy-3-phényl-6-phénylazo-p-benzoquinone

On procède comme pour la préparation de la 2,5-dihydroxy-3-phénylazo-*p*-benzoquinone sauf qu'on utilise 40.0 g d'hydroxyde de potassium au lieu de 20.0 g. On essore 6.9 g de produit brut. Par cristallisation dans le dioxane on obtient 4.5 g (28%) de 2,5-dihydroxy-3-phényl-6-phénylazo-*p*-benzoquinone pure sous la forme de fines aiguilles orangées. Elle se sublime au-dessus de 200°. P.f. 256–257°. Calculé pour $C_{18}H_{12}O_4N_2$: C, 67.49%; H, 3.78%; N, 8.85%. Trouvé: C, 67.7%; H, 4.0%; N, 8.9%.

2,5-Dihydroxy-3-(m-tolyl)-6-(m-tolylazo)-p-benzoquinone

On suit le même mode opératoire que pour la préparation précédente. On obtient ainsi 11.5 g de produit brut, qui après cristallisation dans le dioxane, donne 8.4 g (48% de la théorie) de 2,5-dihydroxy-3-(*m*-tolyl)-6-(*m*-tolylazo)-*p*-benzoquinone pure sous la forme d'aiguilles rouge-brun. Elle contient du dioxane de cristallisation. Elle le perd par chauffage sous vide à 60° et se transforme en une poudre brune qui se sublime au-dessus de 200°. P.f. 224–225°. Calculé pour $C_{20}H_{16}O_4N_2$: C, 68.95%; H, 4.63%; N, 8.04%. Trouvé: C, 69.2%; H, 4.6%; N, 8.0%.

2,5-Dihydroxy-2,6-bis-(o-tolyl)-p-benzoquinone

En procédant comme pour la synthèse de la 2,5-dihydroxy-3-phénylazo-*p*-benzoquinone, mais en employant 30.0 g d'hydroxyde de potassium au lieu de 20.0 g, on obtient une substance que l'on cristallise une première fois dans un mélange de dioxane et d'éthanol (1:1) et une deuxième fois dans un peu de dioxane. La 2,5-dihydroxy-3,6-bis-(*o*-tolyl)-*p*-benzoquinone pure se présente sous la forme d'aiguilles jaunes. On se débarrasse des molécules de solvant de cristallisation par chauffage sous vide à 60°. Transformée en une poudre brun-pâle, la 2,5-dihydroxy-3,6-bis-(*o*-tolyl)-*p*-benzoquinone se sublime au-dessus de 200°. P.f. 243–244°. Calculé pour $C_{20}H_{16}O_4$: C, 74.98%; H, 5.03%. Trouvé: C, 75.1%; H, 5.0%.

3-Hydroxy-2,5-bisphényl-p-benzoquinone

On laisse reposer, pendant 24 heures, un mélange d'anhydride acétique (100 ml), de 2,5-bisphényl-*p*-benzoquinone (10.0 g) et d'acide perchlorique à 40% (10 gouttes). On verse alors le mélange dans 1000 ml d'eau froide, on essore le précipité, on le dissout dans le méthanol (100 ml), on ajoute de l'acide chlorhydrique concentré (5 ml) et on bout à reflux pendant 1 heure. On refroidit la solution, on la rend alcaline par l'addition d'une solution diluée d'hydroxyde de sodium et on dilue avec de l'eau à environ 500 ml.

Le 1,3,4-trihydroxy-2,5-bisphényl-benzène s'oxyde alors spontanément à l'air. Après quelques minutes on filtre et avec de l'acide chlorhydrique dilué on acidifie à pH = 3. La 3-dihydroxy-2,5-bisphényl-*p*-benzoquinone cristallise dans le dioxane en longues aiguilles rouges qui contiennent des molécules de solvant. Elle effleurit à l'air pour donner une poudre rouge qui se sublime au-dessus de 200° sans fondre. Le rendement pour les trois étapes est excellent. Calculé pour $C_{18}H_{12}O_3$: C, 78.25%; H, 4.38%. Trouvé: C, 78.3%; H, 4.1%.

REMERCIEMENTS

Nous remercions le Conseil National de Recherches du Canada et la Shell Oil Company pour des bourses d'études accordées à l'un de nous (P.B.).

BIBLIOGRAPHIE

1. KÖGL, F. Ann. **447**, 78 (1926).
2. KÖGL, F. et BECKER, H. Ann. **465**, 211 (1928).
3. AKAGI, M. J. Pharm. Soc. Japan, **62**, 129, 202 (1942); Chem. Abstr. **45**, 2898 (1951).
4. FICHTER, F. Ann. **361**, 363 (1908).
5. KÖGL, F. Ann. **465**, 243 (1928).
6. SCHILDNECK, P. R. et ADAMS, R. J. Am. Chem. Soc. **53**, 2373 (1931).
7. ASANO, M. et KAMEDA, Y. J. Pharm. Soc. Japan, **59**, 768 (1939); Chem. Abstr. **34**, 2345 (1940).
8. KVALNES, D. E. J. Am. Chem. Soc. **56**, 2478 (1934).
9. GHIGI, E. Boll. sci. fac. chim. ind. univ. Bologna, **5**, 38 (1944–47).
10. FIESER, L. F. et OXFORD, A. E. J. Am. Chem. Soc. **64**, 2060 (1942).
11. NEUNHOFFER, O. et WEISE, J. Ber. **22**, 2127 (1889).
12. JONES, R. G. et SHONLE, H. A. J. Am. Chem. Soc. **67**, 1034 (1945).
13. BRASSARD, P. et L'ÉCUYER, P. Can. J. Chem. **36**, 709 (1958).

LIGHT ABSORPTION STUDIES

PART XI. ELECTRONIC ABSORPTION SPECTRA OF NITROBENZENES[1]

W. F. Forbes

ABSTRACT

The spectra of nitrobenzenes are discussed in terms of previously proposed hypotheses relating electronic interactions and ultraviolet absorption spectra.

INTRODUCTION

In previous parts of this series it was proposed that *B*- and *C*-bands of a large number of benzene derivatives are determined mainly by mesomeric and steric interactions and only to a lesser extent by other factors. These hypotheses, which, if true, have important implications, are consistent with a large body of data. For example, whenever primary mesomeric interactions or steric effects are assumed to operate, the spectral changes are normally much larger than the spectral changes which are ascribed to other interactions, such as field effects, inductive effects, and various types of solvent–solute interactions. The present purpose is to extend these hypotheses to nitrobenzenes. The substituent in nitrobenzene possesses a negative mesomeric effect. However, this negative mesomeric effect is greater in nitro-compounds than in the previously studied acetophenones and benzoic acids, and other interactions may also play a different part.

The spectra of nitrobenzenes have recently been described by a number of workers (for example, 1, 2, 3, 4, 5), and the spectra have been noted to cause anomalous effects (6, 7; cf. also the greater ethylenic stretching frequency at 1600 cm^{-1} in nitrobenzenes (8*a*), and the absence of the usual correlations for C–H bending vibrations in the region 1000–650 cm^{-1} (8*c*)).

ULTRAVIOLET ABSORPTION SPECTRA

Nitrobenzene

The ultraviolet absorption spectra of nitrobenzene in different solvents are listed in Table I.

A broad symmetrical absorption band, structureless even in the gas phase (3), occurs near 260 mμ, which is classified as the *B*-band, by analogy with the *B*-band near 240 mμ in acetophenones. The bands are of comparable intensity and undergo parallel changes on alteration of the dielectric constant or polarity of the solvent. The nitrobenzene band at 260 mμ will also be shown to be highly susceptible to steric effects, causing hypsochromic shifts and reduced absorption intensities, which represents a characteristic property of the *B*-band in acetophenones and benzoic acids (11).

Next, no appreciable concentration dependence could be discerned for various nitrobenzene solutions. This indicates that nitrobenzene is apparently not appreciably associated in solution within the investigated concentration range (see Table I). The observed bathochromic wavelength displacement with increased dielectric constant of the solvent is parallel, but more pronounced for nitrobenzene than for acetophenone. This suggests increased solvent stabilization of the excited state relative to the ground state and may be related to the greater contribution of dipolar excited states in nitrobenzene (cf. also ref. 3). Change of pH of the solution does not cause any additional wavelength shift,

[1]*Manuscript received in original form January 21, 1958, and, as revised, June 19, 1958.*
Contribution from the Memorial University of Newfoundland, St. John's, Newfoundland.

TABLE I

ABSORPTION SPECTRA OF NITROBENZENE

(Values in italics represent inflections in this and subsequent tables)

Solvent	*B*-Band		*C*-Band		Source
	λ_{max} (mμ)	ϵ_{max}	λ_{max} (mμ)	ϵ_{max}	
Gas phase	239.9	7600			Ref. 3
Naphtha	251	9200			Ref. 9
Cyclohexane (conc. = 2.2–88 mg/liter)	252	9000	*ca. 285*	*1500*	*
Iso-octane	252	8620	—	—	Ref. 1
Ethanol (conc. = 70 mg/liter)	257	8100	—	—	*
Ethanol (conc. = 1.75 mg/liter)	258	7700	—	—	*
95% Aqueous ethanol	260	8000			See Ref. 10
Dioxane (conc. = 90.5 mg/liter)	257–258	8400	—	—	*
Dioxane (conc. = 1.81 mg/liter)	259	7400	—	—	*
50% Aqueous dioxane	263–265	7800	—	—	*
Water (conc. = 2.4–95 mg/liter)	265–266	7900	—	—	*
N NaOH	266	6900	*ca. 304*	*2000*	*
0.1 *N* HCl	266	7800	—	—	*
Conc. H_2SO_4	287.5	8600	*ca. 302*	*7200*	*

*This series of papers.

which emphasizes the importance of the dielectric constant, compared with the presence or absence of hydrogen ions in determining the location of the *B*-band. On the other hand, media of high acidity, such as sulphuric acid (see Table I and ref. 3), have a marked effect on the spectrum.

Further, the *B*-band of nitrobenzene lies at considerably longer wavelength than that of acetophenone. Since the *B*-band of monosubstituted benzenes is predominantly determined by mesomeric interaction (cf., for example, ref. 12), it follows that in the absence of other considerations the nitro-group would be expected to exert a greater negative mesomeric interaction than the acetyl-group and in this way nitrobenzene absorbs at longer wavelength. It may be noted that the large mesomeric effect of the nitro-group can be used to explain the large frequency shift of the C–H bending vibration in nitrobenzene (13), and also the extremely high intensity of the $R-NO_2$ stretching vibration (8*f*) and the enhanced intensities of the aromatic bands at 1600–1500 cm^{-1} for nitrobenzenes (8*b*), since absorption intensities in the infrared region are probably largely proportional to resonance interaction (14, 15).

The *C*-band in nitrobenzene is identified only with difficulty. This is explained by the hypothesis (11) that a large mesomeric effect causes a low intensity *C*-band. There is little doubt that this band corresponds to the band in benzene at *ca.* 260 mμ (9, 11).

Para-Substituted Nitrobenzenes

The ultraviolet absorption spectra of some para-substituted nitrobenzenes are listed in Table II.

Para-disubstituted compounds provide a good method of studying mesomeric interactions because inductive-type interactions and steric effects may be assumed to be small (12) for a number of compounds of this type, and if the para-substituent is electron donating, a large mesomeric interaction would be expected. The data for this type of

TABLE II

ABSORPTION MAXIMA OF PARA-SUBSTITUTED NITROBENZENES

Substituent	Solvent	*B*-Band λ_{max} (mμ)	*B*-Band ϵ_{max}	*C*-Band λ_{max} (mμ)	*C*-Band ϵ_{max}	Source
p-Amino-	2 *N* HCl	258	8,700	—	—	Ref. 6
p-Nitro-	Methanol	258	14,700			Ref. 10
p-Acetyl-	Cyclohexane	258	14,000	*292* *308*	*2000* *1000*	*
	Ethanol	261	14,000	*ca. 298* *ca. 312*	*2200* *1200*	*
p-Carboxy-	Cyclohexane	255	13,000	*ca. 294*	*2000*	*
	Ethanol	258	12,000	*ca. 294*	*2500*	*
	Water	271	10,000			*
	0.1 *N* HCl	263.5	12,500			*
	N NaOH	272	10,600			*
p-Formyl-	Hexane	259	13,800	*ca. 284* *ca. 295* *ca. 305*	*3400* *2100* *1200*	*
	Const. boiling ethanol	265	11,400	—	—	Ref. 16
	Water	266	14,500	*ca. 301* *ca. 314*	*3000* *1800*	*
p-Fluoro-	Iso-octane	256	7,600			Ref. 17
	95% Aqueous ethanol	*ca.* 266	7,900	—	—	Ref. 4
p-Chloro-	95% Aqueous ethanol	*ca.* 272	10,000	—	—	Ref. 4
	pH 6	280	10,300	—	—	Ref. 6
p-Bromo-	95% Aqueous ethanol	*ca.* 276	11,100	—	—	Ref. 4
p-Iodo-	95% Aqueous ethanol	*ca.* 294	11,700	—	—	Ref. 4
p-Methyl-	Iso-octane	264	10,250	—	—	Ref. 1
	pH 6	285	9,250	—	—	Ref. 6
p-*i*-Propyl-	Iso-octane	265	10,430	—	—	Ref. 1
p-*t*-Butyl-	Iso-octane	265	10,720	—	—	Ref. 1
p-Hydroxy-	Cyclohexane	295	11,000	—	—	*
	Ethanol	314	13,000	—	—	Ref. 18
	Water	314	9,500			*
	pH 3	317.5	10,000	—	—	Ref. 6
	N NaOH	402.5	19,200	—	—	Ref. 6
p-Methoxy-	Ethanol	305	13,000	—	—	Ref. 18
	Water	313	10,500	—	—	*
p-Amino-	Naphtha	320	14,600			Ref. 9
	Ethanol	371	15,500	—	—	Ref. 19
	Water	373–377	13,000	—	—	*
	0.1 *N* HCl	372	5,600	—	—	*
	N NaOH	373–379	13,000	—	—	*
p-Dimethyl-amino-	Ethanol	387	18,300			See Ref. 10

*This series of papers.

compound, as discussed in the following paragraph, are in fact consistent with the hypothesis that a mesomeric type of interaction predominantly determines the spectra and that inductive and other types of interactions are again only of secondary importance (cf. Introduction). To investigate this mesomeric interaction, the data in Table II are first divided into two groups. The first group comprises the earlier values in Table II which do not show any appreciable mesomeric interaction. This is either because acid conditions prevent mesomeric interaction, as for *p*-nitroaniline in acid solution, or alternatively because primary mesomeric interaction may be negligible, as for *p*-dinitrobenzene, where by analogy with the electron-withdrawing properties of the nitro-group in the ground state, neither of the two nitro-substituents would be expected to act effectively as an electron donor in the electronic excited state.

For the latter type of example, moreover, both para-substituents will also tend to deactivate the benzene ring, that is, cause a withdrawal of π-electrons from the benzene

ring. This latter deactivation is also suggested by other data. For example, the carbonyl stretching frequencies in dilute chloroform solution for *p*-nitrobenzaldehyde (λ_{max} 1721 cm^{-1} (8*d*)) and *p*-nitroacetophenone (λ_{max} 1700 cm^{-1} (12)) are considerably displaced from those of benzaldehyde (λ_{max} 1709 cm^{-1}) and acetophenone (λ_{max} 1691 cm^{-1}) (12). This indicates that at least some of the conjugation, which causes the initial shift to lower frequency in aromatic carbonyl compounds, because of the aromatic nucleus, is no longer available. Although this argument again is evidently applicable only to the ground state, it is not unreasonable to assume that a similar deactivation occurs in the electronic excited state. Consequently, the carbonyl stretching frequencies data indirectly support the hypothesis. The supposed absence of mesomeric interaction may also be related to Hammett's observation (20) that for nitrobenzenes two different substitution constants must be used (cf. also ref. 21). Further, ultraviolet data indicate a reduced force constant in the N-nuclear bond for compounds like *p*-dinitrobenzene, since an increased extinction coefficient, as is observed in the early examples of Table II relative to nitrobenzene, may be ascribed to a reduced force constant. A number of similar examples have previously been discussed (22) and the relation between a reduced force constant and an increased extinction coefficient *in the absence of primary mesomeric interaction* has previously been suggested as a "secondary" effect in electronic spectra (22) and this hypothesis accounts well for the observed spectral changes. For example, the para-formyl group is assumed to decrease the double-bond character of the N-nuclear bond and in this way decreases the force constant of this bond, and hence increases the molecular

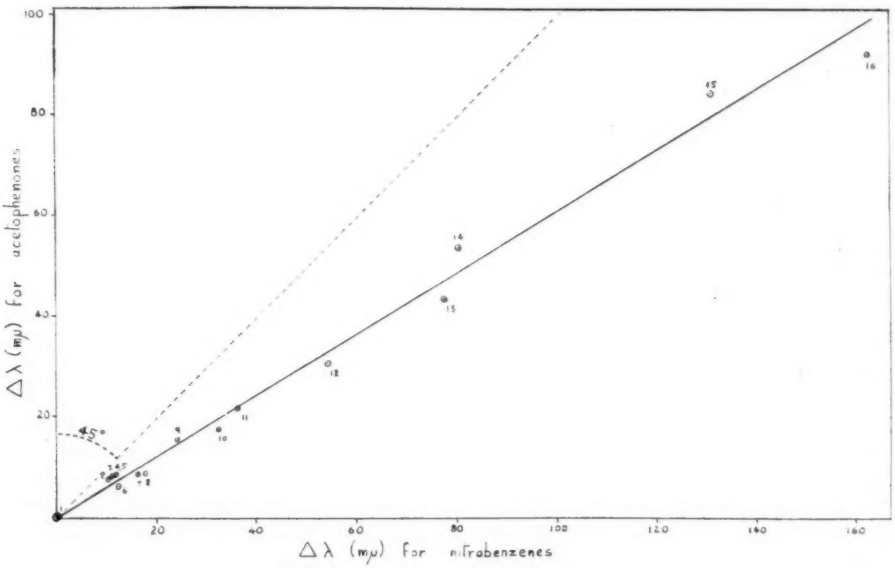

FIG. 1. Wavelength shifts ($\Delta\lambda$) of the *B*-band obtained on introducing a para-substituent in nitrobenzene and acetophenone. 1—H (gas phase); 2—Me (gas phase); 3—Et (gas phase); 4—*i*-Pr (gas phase); 5—*t*-Bu (gas phase); 6—H (hexane); 7—F (iso-octane, hexane); 8—H (ethanol); 9—Me (iso-octane, hexane); 10—Cl (95% ethanol, ethanol); 11—Br (95% ethanol, ethanol); 12—I (95% ethanol, ethanol); 13—OH (aqueous acid); 14—NH_2 (hexane, naphtha); 15—NH (ethanol); 16—OH (aqueous base). Values obtained from Table II, ref. 3, and previous papers in this series.

extinction coefficient. This decreased force constant may incidentally explain the relatively more pronounced *C*-band in compounds like *p*-nitroacetophenone (see Table II and ref. 11) compared with the *C*-band in nitrobenzene.

For the second group of data in Table II the primary mesomeric interaction which predominantly affects the electronic excited state is supposed to be the main factor determining the maximal wavelength of the *B*-band. In support of this hypothesis the following may be cited. First, an increased dielectric constant in the para-substituted nitrobenzenes, where primary mesomeric interaction is supposed to occur, causes bathochromic displacements parallel, but usually more pronounced, to those observed for nitrobenzene itself (see Tables I and II). This suggests that both changes are related to one and the same, mesomeric, interaction. Next, Fig. 1 shows that the wavelength displacements, and consequently the energy changes, for acetophenones and nitrobenzenes tend to be directly proportional to each other whenever mesomeric interaction is assumed to determine the *B*-band. This again is consistent with the hypothesis that both wavelength displacements are proportional to one electronic interaction, which is predominantly mesomeric in character.

The slope of the straight line obtained in Fig. 1 also indicates that mesomeric interaction is greater in nitro-compounds. This is ascribed to increased resonance contributions of dipolar excited states in nitrobenzene because of the greater negative mesomeric effect of the nitro-group. Two additional points may be noted. First, although the concept of resonance structures is implied in this discussion, molecular orbital theory provides, at least qualitatively, a similar picture (cf. ref. 9). Secondly, intensity values (ϵ) of para-substituted compounds compared to intensity values of unsubstituted compounds (ϵ_0) are less suitable than wavelength changes in the study of mesomeric interactions. This follows not only because overlapping of bands may interfere with the quantitative estimation of absorption intensities, but also because intensity values are more sensitive to other, secondary, interactions, such as slight changes in the force constant of the N-nuclear bond caused by solvent–solute interactions.

Meta-Substituted Nitrobenzenes

The spectra of meta-substituted nitrobenzenes are listed in Table III.

In meta-substituted nitrobenzenes primary mesomeric interaction between the meta-substituents is theoretically impossible and hence the observed *B*-bands would be expected to correspond to the *B*-bands of the two monosubstituted parent compounds. This explanation is taken to account for the frequent occurrence of two distinct *B*-bands in a meta-disubstituted benzene derivative. This is illustrated by some of the data in Table III, and the band assignment is also supported by a number of unpublished data. One of the *B*-bands, the nitrobenzene *B*-band, is usually identified without difficulty for the compounds listed in Table III. The second *B*-band is ascribed to benzenoid absorption involving the non-nitro substituent. It may be noted in passing that Doub and Vandenbelt sometimes designate this second *B*-band as a "secondary primary band" (7). For example, the maximal absorption at 251.5 mμ for *m*-nitrophenol is assumed to be a secondary primary band, whereas we would ascribe this absorption to phenolic *B*-band absorption.

However, the observed *B*-bands will not necessarily correspond closely to the *B*-bands of the mono-substituted parent compounds, since a secondary interaction also occurs between the two substituents in meta-substituted compounds. This interaction has previously been discussed in general terms (25), and we will therefore at present consider

TABLE III

ABSORPTION MAXIMA OF META-SUBSTITUTED NITROBENZENES

Substituent	Solvent	*B*-Band λ_{max} (mμ)	*B*-Band ϵ_{max}	*C*-Band λ_{max} (mμ)	*C*-Band ϵ_{max}	Source
m-Nitro-	Cyclohexane	228	20,500	*ca. 275* 283 294	*1150* 1000 770	*
	96% Aqueous ethanol	235	17,400			See Ref. 10
	Water	241.5	16,300	305	1100	Ref. 7
m-Acetyl-	Cyclohexane	224 *254*	23,000 *7000*	*288* 298	*1100* 750	*
	Ethanol	226 *ca. 260*	22,500 *6500*	*ca. 300*	*800*	*
m-Formyl-	Cyclohexane	225 *ca. 242* *ca. 252*	26,000 *11,000* *6800*	287 298	1000 700	*
	Ethanol	*ca. 256*	*7,700*	—	—	
m-Carboxy-	Cyclohexane containing 2% ether	250–251	7400	*ca. 285* *ca. 296*	*1150* *650*	*
	Ethanol	215 255	22,500 7000	—	—	*
	Water	212.5 265	20,000 7000			*
	0.1 *N* HCl	261	7100			*
	N NaOH	266	7350			*
m-Fluoro-	Iso-octane	246	7400	284	1700	Ref. 17
	95% Aqueous ethanol	*ca.* 255	7700	*ca. 300*	*1900*	Ref. 4
m-Chloro-	95% Aqueous ethanol	*ca.* 258	7200	*ca. 300*	*1500*	Ref. 4
	Water	224 264	6800 7100	313	1300	Ref. 7
m-Bromo-	95% Aqueous ethanol	*ca.* 259	6200	*ca. 303*	*1200*	Ref. 4
m-Iodo-	Light petroleum	*ca. 260*	*6200*	*ca.* 308	1000	Ref. 23
	95% Aqueous ethanol	*ca.* 262	6400	*ca.* 315	1000	Ref. 4
m-Methyl-	Iso-octane	256.5	8160	*ca. 292*	*1500*	Ref. 1
m-*t*-Butyl-	Iso-octane	258	8220	*ca. 292*	*1500*	Ref. 1
m-Hydroxy-	Cyclohexane containing *ca.* 1% ether	225–226 262	11,000 5750	319	2200	*
	Ethanol	270.5	6900	332.2	2700	Ref. 18
	Water	228 272	7600 6000	323 328	1900 1950	*
	pH 3	228.5 273.5	7900 6000	333	1960	Ref. 7
	0.1 *N* NaOH	251.5 291	11,000 4500	392	1500	Ref. 7
m-Methoxy-	Cyclohexane	223 260	13,000 6100	313	2400	*
	Ethanol	268	6400	325.2	2400	Ref. 18
	Water	228 273.5	8900 6000	330	2050	Ref. 7
m-Amino-	Ethanol	233	18,000	375	1600	Ref. 24
	Water	224 278–279	13,500 4500	350–358	1400	*
	N NaOH	224 278–279	14,000 4650	354	1400	*
	0.1 *N* HCl	256	7500			*
m-Dimethyl-amino-	Ethanol	246	23,000	400.3	1350	Ref. 24

*This series of papers.

only the effect of a meta-nitro substituent on the *B*-band of a monosubstituted benzene derivative. The relevant data (see Tables III, I, and previous parts of this series) are collected in Table IV.

TABLE IV

THE NON-NITROBENZENE *B*-BAND OF META-SUBSTITUTED NITROBENZENES, AND THE *B*-BAND OF REFERENCE COMPOUNDS

Solvent	*m*-Substituted nitrobenzene	λ_{max} (mμ)	ϵ_{max}	Reference compound	λ_{max} (mμ)	ϵ_{max}	Δλ (in mμ)
Cyclohexane	*m*-Dinitrobenzene	228	20,500	Nitrobenzene	252	9000	−24
95% Aqueous ethanol	*m*-Dinitrobenzene	235	17,400	Nitrobenzene	260	8000	−25
Water	*m*-Dinitrobenzene	241.5	16,300	Nitrobenzene	265–266	7900	−24
Cyclohexane	*m*-Nitroaceto-phenone	224	23,000	Acetophenone	237.5	12,500	−13.5
Ethanol	*m*-Nitroaceto-phenone	226	22,500	Acetophenone	240	12,500	−14
Cyclohexane	*m*-Nitrobenzalde-hyde	225	26,000	Benzaldehyde	241	14,000	−16
0.1 *N* NaOH	*m*-Nitroaniline	224	14,000	Aniline	230	8400	−6
Aqueous acid	*m*-Nitrophenol	228.5	7900	Phenol	210	6000	+18.5
Water	*m*-Nitrophenol	228	7600	Phenol	210	6000	+18
Aqueous NaOH	*m*-Nitrophenol	251.5	14,500	Phenol	234	10,500	+17.5
Water	*m*-Nitroanisole	228	8900	Anisole	217	4300	+11

Table IV shows that a meta-nitro substituent indeed affects the absorption band, usually giving rise to an appreciable displacement. This displacement is positive or negative, presumably depending on the dipolar forms contributing to the electronic excited state. In this way, a nitro-group apparently exerts a negative wavelength displacement on chromophores like acetophenone or nitrobenzene, but a positive wavelength displacement on chromophores like anisole or phenol. The different effect of the nitro-group in meta-disubstituted benzene derivatives may be rationalized by assuming that either structure I or II may preferentially contribute to the electronic excited state. Assuming structures of this type, one may visualize the way in which the formation of a positive or negative charge near the *m*-nitro-group may have opposite effects, as illustrated for *m*-nitrophenol and *m*-dinitrobenzene. The relatively large extinction coefficients, which are noted in the *B*-band of the meta-substituted nitrobenzenes listed in Table IV, are again tentatively ascribed to a reduced force constant caused by the electron-withdrawing effect of the nitro-substituent (cf. ref. 22).

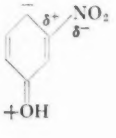

I

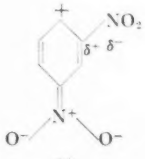

II

The nitrobenzene *B*-band is evident in most of the compounds listed in Table III, and is subject to the usual secondary interactions. One of these, the buttressing effect, would be expected to occur in meta-substituted nitrobenzenes (cf. ref. 26), and this effect would be expected to be greatest for *m*-dinitrobenzene. In this way, the buttressing effect may contribute to the variation in the observed wavelength displacement (see Table IV). The *C*-band in meta-substituted nitrobenzenes usually becomes more pronounced, an observation which has previously received an explanation (11).

Ortho-Substituted Nitrobenzenes

The ultraviolet absorption spectra of ortho-substituted nitrobenzenes are listed in Table V.

TABLE V

ABSORPTION MAXIMA OF ORTHO-SUBSTITUTED NITROBENZENES

Substituent	Solvent	*B*-Band λ_{max} (mμ)	*B*-Band ϵ_{max}	*C*-Band λ_{max} (mμ)	*C*-Band ϵ_{max}	Source
o-Acetyl-	Cyclohexane	254	6000	—	—	*
	Ethanol	257	6000	—	—	*
o-Formyl-	Cyclohexane	222	15300	*ca.* 285	1700	*
		247	7000			
	Ethanol	220	8500	270	3600	Ref. 16
		252	4700			
o-Carboxy-	Cyclohexane containing *ca.* 2% ether	—	—	*ca. 278*	*1350*	*
	Ethanol	*ca. 250*	*3500*	—	—	*
	Water	*ca.* 266	5300			*
	0.1 *N* HCl	*ca.* 262.5	5500			*
	N NaOH	267	5500			*
o-Fluoro-	Iso-octane	242	7250	278	1850	Ref. 17
	95% Aqueous ethanol	*ca.* 250	6900	*ca. 285*	*2200*	Ref. 4
o-Chloro-	95% Aqueous ethanol	*ca.* 252	3500	*ca.* 290	1200	Ref. 4
	Water	228	4400	310	1400	Ref. 7
		260	4000			
o-Bromo-	95% Aqueous ethanol	*ca.* 255	3000	*ca.* 292	1300	Ref. 4
o-Iodo-	95% Aqueous ethanol	*ca. 260*	*3500*	*ca.* 310	1500	Ref. 4
o-Methyl-	Iso-octane	250	5950	*ca. 290*	*1500*	Ref. 1
o-*i*-Propyl-	Iso-octane	247	3760	*ca. 290*	*1300*	Ref. 1
o-*t*-Butyl-	Iso-octane	—	—	*ca. 275*	*700*	Ref. 1
o-Methyl-	Water	266	5300	325	1300	Ref. 7
o-Hydroxy-	Cyclohexane	269–270	7500	342	3800	*
	Ethanol	273	6600	343.5	3600	Ref. 18
	Water	*ca. 230*	*3700*	346	3000	*
		276	6350			
	pH 3	*230*	*3900*	351	3200	Ref. 7
		278.5	6600			
	0.1 *N* NaOH	*250*	*5000*	416	4800	Ref. 7
		282	4300			
o-Methoxy-	Cyclohexane	249	3400	304	2500	*
	Ethanol	258.5	3450	317.2	2850	Ref. 18
	Water	264	4300	333	2900	*
o-Amino-	Cyclohexane	227	18000	370	5000	*
		268	5000			
	Ethanol	275.2	5100	403.6	5400	Ref. 24
	Water	233	17000	400–405	4500	*
		280	5500			
	0.1 *N* NaOH	245	7000	412	4500	Ref. 7
		282.5	5400			
o-Dimethyl-amino-	Ethanol	245.5	21500	416	2950	Ref. 24

*This series of papers.

The ortho-effect of alkyl groups in nitrobenzenes has previously been ascribed to steric inhibition of resonance (1) and it was noted that the decreased intensity of absorption is qualitatively in agreement with the increased size of the substituent, i.e. *t*-butyl > *i*-propyl > methyl. For alkylnitrobenzenes in iso-octane solution a hypsochromic shift is also observed compared with the wavelength of maximal absorption in the meta-isomers. This is explained by assuming that in certain ortho-isomers not only does the alkyl group fail to contribute to mesomeric interaction between the two substituents,

but the vicinal alkyl-group also causes the nitro-group to twist about the C–NO_2 axis. Consequently, absorption in the ortho-isomer occurs at shorter wavelength, and with decreased absorption intensity (cf. ref. 25, 27).

By considering the two types of *B*-bands in ortho-isomers (cf. preceding section), we can further relate changes in the *B*-bands with the ease of dislodging a particular group from the plane of the benzene ring. For example, in *o*-nitrophenol (basic solution) the band corresponding to nitrobenzene occurs at λ_{max} 282 mμ, ϵ = 4300, similar in intensity to the band in *m*-nitrophenol, which occurs at λ_{max} 291 mμ, ϵ = 4500. The other *B*-band, which occurs in the meta-isomer at λ_{max} 251.5 mμ, ϵ = 11,000, and which is ascribed to the phenolate ion, occurs in the ortho-isomer only as an inflection at 250 mμ, ϵ = 5000. This suggests that the $-O^-$ substituent is more readily dislodged from the plane of the benzene ring than the nitro-group.

The ease of dislodging a particular group from the plane of the benzene ring may also depend on the solvent. This is illustrated in Fig. 2 for the spectrum of *o*-nitrobenzoic acid.

Fig. 2 shows that the nitrobenzene *B*-band in aqueous medium is more pronounced

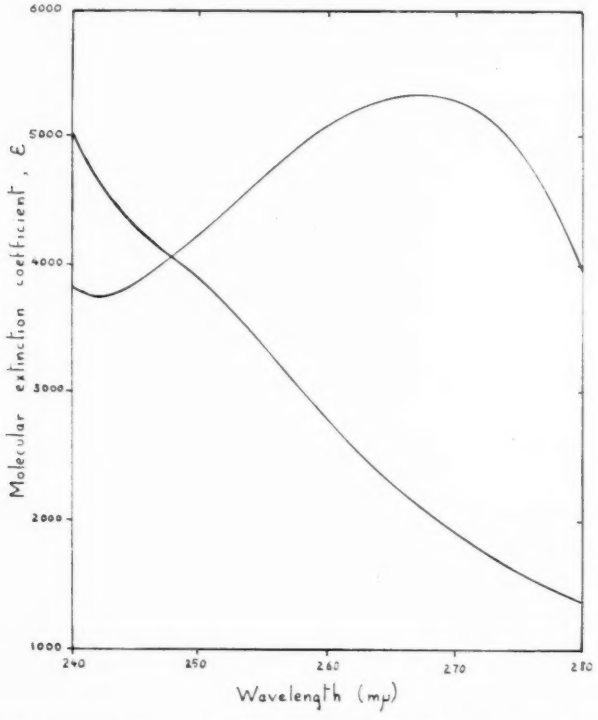

FIG. 2. The *B*-band (nitrobenzene band) of *o*-nitrobenzoic acid in 1—water; 2—cyclohexane containing 2% ether. Strictly speaking, for comparison purposes, the spectrum should have been determined in acidified aqueous solution, since in water the molecule will actually absorb as the anion and not as the undissociated acid. (We are grateful to a referee for drawing our attention to this.) However, in fact, the spectrum in acidified water also shows a similar maximum (see Table V) undergoing only the usual displacement associated with the change from neutral to acidic medium (cf. ref. 25).

and, as such, more readily recognized. This has some application from an analytical point of view (see next section). It can be explained by assuming that in aqueous solution the nitrobenzene band is strengthened at the expense of benzoic acid coplanarity. This explanation may be related to the appreciable wavelength displacement observed for nitrobenzene absorption on passing from hexane to ethanol and water, since this also suggests solvent–solute interaction between the nitro-group and the solvent. In terms of the previously proposed classification of steric effects (cf. ref. 12 and references cited there), this observation implies that *in aqueous solutions ortho-substituted nitrobenzenes will more frequently give rise to type I steric effects* (that is, an intensity decrease without appreciable wavelength displacement will be observed), *whereas in hexane media other steric effects will often be observed.*

As expected, steric interactions in ortho-substituted nitrobenzenes are also evident from a number of other physical data (cf. also ref. 5). For example, while the characteristic Raman frequency of the nitro-group is around 1367 cm^{-1}, in nitrobenzene the interaction of the nitro-group with the aromatic nucleus causes a frequency drop to 1341 cm^{-1}. In *o*-nitrotoluene some of this interaction is destroyed, and absorption again occurs at higher frequency (1345 cm^{-1}). In nitromesitylene the interaction is almost completely destroyed and the frequency occurs at 1363 cm^{-1}, close to the frequency of the unconjugated nitro-group (28; cf. also refs. 29, 30). This latter absorption may be compared with the ultraviolet absorption of nitromesitylene (1), which also indicates the virtual absence of conjugation.

Apart from steric interactions, the operation of other forces, especially intermolecular hydrogen bonding, would be expected to be evident in ortho-substituted nitrobenzenes. Examples of intermolecular hydrogen bonding may be provided by the nitrobenzene *B*-bands of nitrophenol and nitroanisole. In ethanol, the meta-isomers absorb maximally within 3 mμ (see Table III), whereas the corresponding ortho-isomers show a bathochromic shift of 14.5 mμ for the phenol (see Table V). It may be noted that this wavelength displacement is qualitatively similar to the displacement observed in the corresponding acetophenones (11) and that intramolecular hydrogen bonding in nitrobenzenes is also suggested from infrared data (cf. refs. 8*d*, 31).

The *C*-band of ortho-substituted nitrobenzenes again is normally more pronounced than that of the corresponding para-isomers, but tends to disappear in compounds where steric inhibition of resonance is large (11).

APPLICATIONS

Since the negative mesomeric effect is large for a nitro-group, the mesomeric interaction in nitrobenzene will be large, and will not be too easily inhibited by steric interactions. Consequently the prerequisite for a type I steric effect is available; namely, the electronic excited state, where mesomeric interaction is presumed to be greater than in the ground state, remains frequently at a similar energy level for the prevalent conformations in both the sterically hindered compounds and reference compounds, and hence no appreciable wavelength displacements are observed. Steric effects of type I are in fact often observed, and are found to be more probable in aqueous solution, where solvent–solute interactions are assumed to further facilitate the mesomeric interaction.

Thus, the characteristic nitrobenzene band near 260 mμ will often be evident in aqueous solution, even in a reasonably complex molecule. Conversely, the occurrence of a band near 260 mμ under those conditions, for a compound containing a nitro-group, indicates the presence of the nitrobenzene chromophore. It should be noted, however, that for

ortho- or meta-substituted nitrobenzene chromophores more than one band may occur in this region, and that for certain para-substituents the band may be considerably displaced towards longer wavelength (cf. Table II).

If a definite absorption band occurs near 260 mμ, the absorption intensity of the band can also be used to estimate steric effects. This type of spectral analysis has recently been employed in the discussion of the structures of 2-carboxy-4,5-dimethoxy-2′-nitrobiphenyl and 2-carboxy-4,5-dimethoxy-2′-nitro-3′-methylbiphenyl (26) and of (+)6,6′-dinitro-2,2′-di-(2,4-dimethylbenzoyl)biphenyl (32). Qualitative spectral investigation of the nitro-group is also possible in the infrared region (8*e*, 33), since the nitro-group causes characteristic bands near 1550 cm^{-1} and in the region 1360–1300 cm^{-1}. Lastly, the *B*-band in the ultraviolet region appears to be well suited to the quantitative determination of compounds containing a nitrobenzene chromophore. This is so, because the extinction coefficients obey Beer's law fairly accurately and in additon the absorption is not particularly sensitive to slight changes in pH. In this way, the method may offer advantages, for example, in the study of reaction mechanisms involving a nitro-substituent.

EXPERIMENTAL

The ultraviolet absorption spectra were determined in quartz cells using a Unicam SP500 spectrophotometer. For each compound at least two independent sets of observations were made. Some of the spectra, for example the acetophenone spectra used in constructing Fig. 1, have already been described in previous parts of this series. Little disagreement was found between our values and those reported elsewhere in the literature. The estimated precision of our values for extinction coefficients is $\pm 5\%$ or better. On theoretical grounds the use of oscillator strengths, *f*, would be preferred, but for practical reasons we have not used this quantity so far (cf. also Wepster (5), who has found a reasonably linear relationship between ϵ_{max} and *f*). The estimated precision of our values for the maximal wavelengths is ± 0.5 mμ.

The nitrobenzenes were purified from the commercially available compounds. Solvents also were purified by standard methods.

ACKNOWLEDGMENTS

The author gratefully acknowledges the assistance of Mr. J. C. Dearden, Miss Rosemarie Gosine, and Mr. J. F. Templeton in the experimental work, and in the preparation of the diagrams (Mr. J. C. Dearden).

Lastly, it is a pleasure to thank the National Research Council of Canada for grants supporting this work.

REFERENCES

1. Brown, W. G. and Reagan, H. J. Am. Chem. Soc. **69**, 1032 (1947).
2. Hammond, G. S. and Modic, F. C. J. Am. Chem. Soc. **75**, 1385 (1953).
3. Schubert, W. M., Robins, J., and Haun, J. L. J. Am. Chem. Soc. **79**, 910 (1957).
4. Ungnade, H. E. J. Am. Chem. Soc. **76**, 1601 (1954).
5. Wepster, B. M. Rec. trav. chim. **76**, 335 (1957).
6. Doub, L. and Vandenbelt, J. M. J. Am. Chem. Soc. **69**, 2714 (1947).
7. Doub, L. and Vandenbelt, J. M. J. Am. Chem. Soc. **71**, 2414 (1949).
8. Bellamy, L. J. The infrared spectra of complex molecules. Methuen & Co. Ltd., London. 1954. (*a*) p. 60; (*b*) p. 62; (*c*) p. 68; (*d*) p. 134; (*e*) p. 250; (*f*) p. 252.
9. Nagakura, S. J. Chem. Phys. **23**, 1441 (1955).
10. Kamlet, M. J. and Glover, D. J. J. Am. Chem. Soc. **77**, 5696 (1955).
11. Forbes, W. F., Mueller, W. A., Ralph, A. S., and Templeton, J. F. Can. J. Chem. **35**, 1049 (1957).
12. Forbes, W. F. and Mueller, W. A. Can. J. Chem. **35**, 488 (1957).

13. KROSS, R. D., FASSEL, V. A., and MARGOSHES, M. J. Am. Chem. Soc. **78**, 1332 (1956).
14. BARROW, G. M. J. Chem. Phys. **21**, 2008 (1953).
15. JONES, R. N., FORBES, W. F., and MUELLER, W. A. Can. J. Chem. **35**, 504 (1957).
16. WALKER, E. A. and YOUNG, J. R. J. Chem. Soc. 2041 (1957).
17. GRUBER, W. Can. J. Chem. **31**, 1020 (1953).
18. BURAWOY, A. and CHAMBERLAIN, J. T. J. Chem. Soc. 2310 (1952).
19. TIMMONS, C. J. J. Chem. Soc. 2613 (1957).
20. HAMMETT, L. P. Physical organic chemistry. McGraw-Hill Book Co., Inc., New York. 1940. p. 188.
21. FREEDMAN, L. D. and DOAK, G. O. J. Org. Chem. **21**, 811 (1956).
22. FORBES, W. F. and TEMPLETON, J. F. Can. J. Chem. **36**, 180 (1958).
23. FERGUSON, J. and IREDALE, T. J. Chem. Soc. 2959 (1953).
24. MORTON, R. A. and MCGOOKIN, A. J. Chem. Soc. 901 (1934).
25. FORBES, W. F. and RALPH, A. S. Can. J. Chem. **36**, 869 (1958).
26. FORBES, W. F. and MUELLER, W. A. J. Am. Chem. Soc. **79**, 6495 (1957).
27. FORBES, W. F. and MUELLER, W. A. Can. J. Chem. **34**, 1340 (1956).
28. SAUNDERS, R. H., MURRAY, M. J., and CLEVELAND, F. F. J. Am. Chem. Soc. **63**, 3121 (1941).
29. FRANCK, B., HÖRMANN, H., and SCHEIBE, S. Ber. **90**, 330 (1957).
30. LITTLEJOHN, A. C. and SMITH, J. W. J. Chem. Soc. 2476 (1957).
31. FRANCEL, R. J. J. Am. Chem. Soc. **74**, 1265 (1952).
32. FORBES, W. F., WALLENBERGER, F. T., O'CONNOR, W. F., and MORICONI, E. J. J. Org. Chem. **23**, 224 (1958).
33. HASZELDINE, R. N. J. Chem. Soc. 2525 (1953).

LIGHT ABSORPTION STUDIES

PART XII. ULTRAVIOLET ABSORPTION SPECTRA OF BENZALDEHYDES[1]

J. C. Dearden and W. F. Forbes

ABSTRACT

The electronic spectra of benzaldehydes in the region 220–360 mμ are recorded and discussed in terms of previously stated hypotheses. The formyl group is shown to endow benzene derivatives with spectral properties similar to those of the acetyl group in acetophenones, except that steric interactions are slightly modified.

INTRODUCTION

The ultraviolet absorption spectra of benzaldehydes are of interest because they provide additional examples in the study of the various interactions which determine electronic spectra. The spectra would be anticipated to be related to the previously studied spectra of acetophenones (1, 2, 3), benzoic acids (4), and nitrobenzenes (5), since in all these compounds a negative mesomeric effect operates.

The spectra of some of the benzaldehydes have previously been recorded (6, 7, 8, 9, 10), but, whenever it proved convenient, spectra were redetermined in order to obtain data under near-identical conditions. The terminology employed in this paper is identical with that employed in previous parts of this series.

THE SPECTRUM OF BENZALDEHYDE

The absorption maxima of benzaldehyde in different solvents are listed in Table I.

TABLE I

ABSORPTION MAXIMA OF BENZALDEHYDE IN DIFFERENT SOLVENTS*

		B-Band		*C*-Band	
Solvent	Concentration (mg/liter)	λ_{max} (mμ)	ϵ_{max}	λ_{max} (mμ)	ϵ_{max}
Cyclohexane	1.01	241	14,000†		
		247	*11,500*	277–278	1200
	40.5	241	14,500	*287*	*1000*
		247	*12,500*		
Ether	3.6	241	14,000	*ca. 270*	*1000*
		ca. 247	*12,000*	277–278	1200
				285	1000
Dioxane	41.2	243	*ca.* 12,500	278–279	1200
50% Aqueous dioxane	1.01	247	10,500†	279–280	1350
	40.4	247	12,500		
Water	0.98	248	12,000†	278–279	1400
	39.1	248	12,500		
N NaOH	1.02	248	10,000	*ca. 279*	*1200*
	40.8				
0.1 *N* HCl	1.03	249	13,500	280	1500
	41.2				
Conc. H_2SO_4	2.5	293	21,000	*ca. 330*	*2000*

*Values in italics represent inflections in this and subsequent tables.
†Intermediate values for extinction coefficients were obtained at intermediate concentrations.

[1]*Manuscript received May 5, 1958.*
Contribution from the Memorial University of Newfoundland, St. John's, Newfoundland.

Benzaldehyde in cyclohexane solution appears to show a slight concentration dependence, which may be caused by intermolecular hydrogen bonding (11). Unfortunately, the changes in the extinction coefficients are not sufficiently large to permit any conclusions at this stage. None of the *C*-bands listed in Table I shows concentration dependence within the accuracy of the experiments. Extinction coefficients are also altered on changing the solute concentration for dioxane solutions (see Table I), and some aspects of these spectral changes will be examined in a separate study. It is noticeable, however, that some interaction occurs between solvent and solute in solvents other than cyclohexane, as witnessed by the spectral changes occurring in various solvents. In particular, the characteristic doublet, observed in cyclohexane and to a small extent in ether solution, disappears in all other solvents.

This doublet is more pronounced for both *B*- and *C*-bands on reducing the temperature (12). In acetophenone, in the gas phase and in heptane, the spectrum is also reported to be slightly unsymmetrical at the *B*-band maximum and shows a small shoulder at about 7 mμ to the red of the peak. Again in all other solvents, this maximum was found to be symmetrical and the shoulder was absent. For nitrobenzenes, the *B*-band is structureless, even in the gas phase, and quite symmetrical about the maximum (13). An explanation involving hydrogen bonding cannot perhaps be ruled out completely, at least at this stage (cf. 14), but seems improbable. Any complete explanation for this fine structure effect must take into account the above and also the following observations:

(i) The fine structure occurs for all benzaldehyde *B*-bands described in this paper, with the exception of the band at 225 mμ for *m*-nitrobenzaldehyde, which exhibits no fine structure (see following sections). For this compound, the benzaldehyde band is considerably displaced.

(ii) The fine structure disappears for certain *C*-bands (see following sections).

(iii) In the *B*-band of *o*-hydroxybenzaldehyde the fine structure is slightly different inasmuch as the longer wavelength peak is more pronounced (see Table V). This is the only *B*-band for which this different band shape was noted.

The occurrence of the doublet for solutions of benzaldehyde in hexane is also of some practical importance, since it frequently allows the identification of the benzaldehyde

TABLE II

VARIATION OF ABSORPTION MAXIMA WITH DIELECTRIC CONSTANT OR ACIDITY

Solvent	Benzaldehyde		Acetophenone		Nitrobenzene	
	λ_{max} (mμ)	ϵ_{max}	λ_{max} (mμ)	ϵ_{max}	λ_{max} (mμ)	ϵ_{max}
			B-Bands			
Dioxane	243	*ca.* 12,500	239	12,000	257–259	8000
50% Aqueous dioxane	247	10,500–12,500	243	12,000	264	8000
Water	248	12,000–12,500	244	12,000	265–266	8000
N NaOH	248	10,000	244	11,500	266	7000
0.1 *N* HCl	249	13,500	244	12,000	266	8000
Conc. H_2SO_4	293	21,000	293	20,000	287.5	8500
			C-Bands			
Dioxane	278–279	1200	277	1000	—	—
50% Aqueous dioxane	279–280	1350	278	1150	—	—
Water	278–279	1400	276–278	1250	—	—
N NaOH	*ca. 279*	*1200*	277	1250	*ca. 304*	*2000*
0.1 *N* HCl	280	1500	277	1250	—	—
Conc. H_2SO_4	*ca. 330*	*2000*	*ca. 325*	*2500*	*ca. 302*	*7200*

band, not only in simple benzaldehydes (see following sections) but also in more complicated molecules (cf. 15).

Finally in this section it may be noted that the maximal absorption of the *B*-band for benzaldehyde normally occurs at longer wavelength than for acetophenone. This prompts the speculation that benzaldehyde exists, at least at room temperature, with a larger proportion of planar or near-planar conformations. This hypothesis also correlates with the known lesser susceptibility of benzaldehydes to steric interactions (cf. 1, 16). On the other hand, the carbonyl stretching frequency of benzaldehyde lies at 1709 cm^{-1} (mean integrated absorption intensity, A = 2.56 $mole^{-1}$. liter. $cm^{-2} \times 10^{-4}$), whereas the corresponding frequency for acetophenone under identical conditions occurs at 1691 cm^{-1} (A = 2.20), that is, at shorter frequency or longer wavelength (2). This wavelength shift therefore is in the reverse order from that observed in the ultraviolet spectra. An explanation of these observations may be provided if it is remembered that steric effects in the *B*-band are predominantly caused by interactions between vicinal atoms in the electronic excited state (cf. 2, 16, 17), and consequently the observed opposite wavelength displacements may represent a previously discussed type of steric effect in which ground and excited states are displaced in opposite directions compared with a non-hindered reference compound (cf. Fig. 2 in Part VII (2) of this series). Although the positions of the maximal wavelengths are displaced in opposite directions for the vibrational and electronic spectra, the integrated absorption intensities (A) of the vibrational spectra relate to the wavelength changes in the electronic spectra. This is as anticipated, since the integrated absorption intensities have been related to the resonance energies of conjugation (18), which also predominantly determine the *B*-band in electronic absorption spectra. This hypothesis, incidentally, is consistent with the observation that in sulphuric acid the two compounds absorb at identical maximal wavelength in the ultraviolet region and with similar absorption intensity. That is, it is assumed that the increased solvent–solute interaction in this solvent overcomes the steric interactions between the methyl-group and the ortho-hydrogen atoms in acetophenone.

THE SPECTRA OF PARA-SUBSTITUTED BENZALDEHYDES

The spectra of para-substituted benzaldehydes are listed in Table III and wavelength displacements compared with benzaldehyde are also related to similar wavelength displacements obtained in the acetophenone and nitrobenzene series (see Table III and Fig. 1).

Most of the values in Table III are for hexane solution, but some of the values are for ethanolic solution. In compiling the wavelength shifts for Fig. 1, the mean maximal wavelength was used. This introduces an uncertainty, since the maximum of the hypothetical "unresolved" band may not exactly coincide with this mean. However, this uncertainty does not appear to introduce any appreciable deviation from the observed relations, since Fig. 1 shows that the wavelength displacements are approximately proportional to each other, indicating that the electronic interactions are comparable for the compounds under investigation. An exception is provided by the hydroxy-compounds in alkaline ethanol, which appear to show a relatively smaller wavelength displacement for the benzaldehyde. This effect may tentatively be ascribed to the relative absence of steric interactions in benzaldehydes (see previous section), since, in this way, the alkaline medium will tend to overcome steric interactions in acetophenones and nitrobenzenes.

Table III shows that the *B*-bands of all para-substituted benzaldehydes obtained by us possess fine structure in hexane solution, except the *B*-band of *p*-nitrobenzaldehyde.

TABLE III

ABSORPTION MAXIMA OF PARA-SUBSTITUTED BENZALDEHYDES AND THE EFFECT OF PARA-SUBSTITUENTS ON THE *B*-BAND FOR BENZALDEHYDES, ACETOPHENONES, AND NITROBENZENES IN *n*-HEXANE OR CYCLOHEXANE SOLUTION

(Wavelength displacements for ethanol are given in parentheses in this and subsequent tables)

	B-Band			*C*-Band		Wavelength shifts with reference to parent compound in:			
Benzaldehyde	λ_{max} (mμ)	ϵ_{max}	Mean λ_{max}	λ_{max} (mμ)	ϵ_{max}	Benzaldehydes	Acetophenones	Nitrobenzenes	Ref.
(Benzaldehyde)	241	14,000	244	277–278	1200	—	—	—	*
	247	*12,000*		287	1000				
p-Methyl-	251	15,000	254	279	1200	10	10.5	12	*, †
	257	12,500		*284*	*1000*				
p-Fluoro-	244	13,000	244	Not given		3	1.5	4	*, ‡
	Not given								
p-Chloro-	253	19,000	256	276	1500	12	10.5	14	*, ‡
	259	*15,500*		286	1000				
p-Bromo-	257.5	18,500	257.5	Not given		16.5	14.5	18.5	*, ‡
	Not given								
p-Iodo-	268	19,500	274	*ca. 290*	*4000*	30	24.5	35	*, ‡
	275	16,000				(26)	(22)	(34.5)	
	280	14,500							
p-Methoxy-	265	18,500	275	—	—	31	27	39	*, §
	ca. 272	*16,000*				(32)	(29)	(47)	*, ‖
	278	12,500							
	286	5,500							
p-Hydroxy-	265–266	19,000	277	—	—	33	28	35	*, §
	ca. 274	*15,500*				(37)	(35)	(56)	*, ‖
	281	12,000							
	288	6,000							
[In alkaline ethanol	336	30,000	336	—	—	88	84	134	¶]
p-Amino-	291	16,300	293.5	—	—	49.5	46	69	*, **
	296	16,100							
p-Carboxy-	249	17,500	253	279	1650	9	—	3	*
	257	15,500		288	1950				
				298	1600				
p-Nitro-	[259	13,800]	—	*ca. 284*	*3400*	—	—	—	*
				ca. 295	*2100*				
				ca. 305	*1200*				
[In aqueous solution	266	14,500]		*ca. 301*	*3000*				
				ca. 314	*1800*				

*This series of papers. †Ref. 6. ‡Ref. 8. §Ref. 19. ‖Ref. 7. ¶Ref. 20. **Solvent: cyclohexane containing 2% ether.

Partly because of this, the *B*-band of *p*-nitrobenzaldehyde is assigned to nitrobenzene absorption. On the other hand, the spectrum of *p*-carboxybenzaldehyde shows the typical benzaldehyde doublet. The former assignment, indicated in Table III by square brackets, also receives support, since this band not only shows the absence of the characteristic benzaldehyde doublet, but also shows the characteristic properties of nitrobenzene absorption. For example, the *B*-band of *p*-nitrobenzaldehyde in aqueous solution undergoes an appreciable bathochromic wavelength displacement to 266 mμ, that is, to the wavelength associated with nitrobenzene absorption in aqueous solution (5) (see Table III). These assignments therefore suggest the absence of any appreciable interaction between two electron-withdrawing substituents in para-disubstituted benzene derivatives. Further, the assignments for para-substituted benzaldehydes may be rationalized in terms of competing mesomeric interactions, the suggested order of mesomeric interaction being $-NO_2 > -CHO > -COOH$; and this order is supported by the relative locations of the maximal absorption for nitrobenzene, benzaldehyde, and benzoic acid

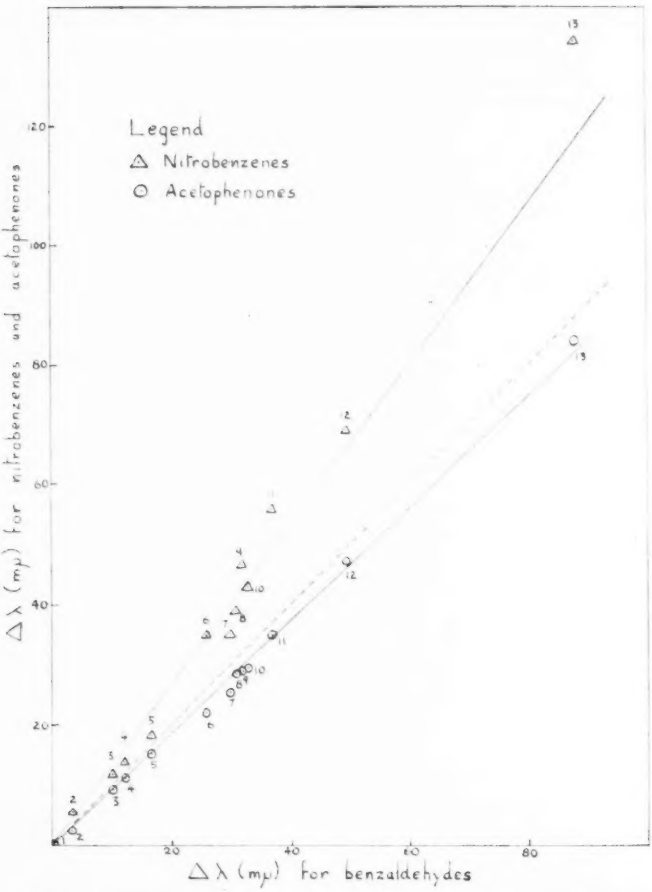

FIG. 1. Wavelength displacements ($\Delta\lambda$) in the *B*-band obtained on introducing para-substituents in benzaldehyde, acetophenone, and nitrobenzene. Values in hexane unless otherwise stated. 1—H; 2—F; 3—Me; 4—Cl; 5—Br; 6—I (in ethanol); 7—I; 8—MeO; 9—MeO (in ethanol); 10—OH; 11—OH (in ethanol); 12—NH_2; 13—OH (in alkaline ethanol) (values from Table III).

(3). This order is again suggested by the *B*-bands of ortho-substituted benzaldehydes (see Table V), since for example the fine structure of the *B*-band of *o*-carboxybenzaldehyde points to this band being due to benzaldehyde absorption. This in turn suggests that the carboxyl-group is preferentially dislocated.

Whenever the para-substituent can act as electron donor, appreciable interactions occur in para-substituted benzaldehydes and the resulting displacements to longer wavelength are shown in Fig. 1 to be directly proportional to corresponding displacements in the acetophenone and nitrobenzene series. This suggests that the displacements are proportional to one "basic" electronic interaction, which acts along the extremities of a conjugated system and which is characteristic for each substituent. This interaction

has already been associated with the mesomeric effect of a substituent, although in its assignment of the order for halogens the interaction affords a different order from that usually accepted for the mesomeric interactions of the halogens (17).

The slope of the line in Fig. 1 relating wavelength displacements in para-substituted acetophenones and benzaldehydes is less than tan 45°, whereas the slope of the line relating wavelength displacements for nitrobenzenes and benzaldehydes is greater than tan 45° (see Fig. 1). This confirms the expected order of mesomeric effect, that is $-NO_2 > -CHO$, and also suggests a mesomeric electron-withdrawing ability $-CHO > -COCH_3$. This latter observation should be related with the fact that benzaldehyde absorbs maximally at longer wavelength than acetophenone.

The *C*-band for each of the compounds listed in Table III could normally be identified only with difficulty. It disappeared in compounds where there is appreciable interaction between the two para-substituents. These tendencies have previously been noted and discussed (3).

THE SPECTRA OF META-SUBSTITUTED BENZALDEHYDES

The spectra of *m*-substituted benzaldehydes and the displacements due to the meta-substituent in benzaldehydes, acetophenones, and nitrobenzenes are listed in Table IV.

Table IV shows that the effect of substituents on the location of the benzaldehyde *B*-band is usually small and similar for benzaldehydes, acetophenones, and nitrobenzenes.

Table IV also shows that meta-substituted benzaldehydes may give rise to two distinct *B*-bands. One of these *B*-bands is the expected benzaldehyde band, somewhat modified

TABLE IV

ABSORPTION MAXIMA OF META-SUBSTITUTED BENZALDEHYDES AND THE EFFECT OF META-SUBSTITUENTS ON THE *B*-BAND FOR BENZALDEHYDES, ACETOPHENONES, AND NITROBENZENES IN *n*-HEXANE OR CYCLOHEXANE SOLUTION

	B-Band			*C*-Band		Wavelength shifts with reference to parent compound in:			
Benzaldehyde	λ_{max} (mμ)	ϵ_{max}	Mean λ_{max}	λ_{max} (mμ)	ϵ_{max}	Benzaldehydes	Acetophenones	Nitrobenzenes	Ref.
(Benzaldehyde)	241	14,000	244	277–278	1200	—	—	—	*
	247	*12,000*		287	1000				
m-Methyl-	245	13,500	248	280	1000	4	5	4.5	*, †
	251	12,000		290	800		(4.5)		
m-Fluoro-	238	12,800	242	282–283	2100	−2	−3.5	−6	*
	246	11,600		290	1750				
				ca. 293	*1700*		(−4)	(−5)	
m-Chloro-	241–242	11,500	245	288	1400	1	0.5		*
	248	10,000		298	1200		(0)	(−2)	
m-Bromo-							4		*
							(0)	(−1)	
m-Iodo-	*244*	*8000*	249	295–296	1300	5	9.5		*
	249	7600		303	1235		(10)	(2)	
	251	*7400*							
	253	*6850*							
m-Hydroxy-	244	10000	247	302–303	2900	3	7.5		*, ‡, §
	250	9500		*ca. 307*	*2800*	(9)		(12.5)	
m-Methoxy-	247	6800	249	304	3000	5	7.5		*, ‡, §
	ca. 251	*6500*		*ca. 313*	*2700*	(8)		(10)	
m-Amino-	*ca. 245*	*9000*	250.5			6.5	7.5		*
	ca. 256	*7500*					(15)		
m-Nitro-	225	26000	225	287	1000	−19			*, ‖
	[*ca. 245*	*8000*]		298	700		(−25)		
	([*ca. 256*	*7700*])							

*This series of papers. †Ref. 6. ‡Ref. 8. §Ref. 7. ‖Ref. 21.

because of the secondary short-range interaction of the non-formyl substituent (5, 22). The second *B*-band corresponds to the absorption of the other substituent, with the formyl group acting as the secondary substituent. These latter bands are again indicated by square brackets. Thus, for example, in the spectrum of *m*-nitrobenzaldehyde in cyclohexane two bands occur, one at λ_{max} 225 mμ ascribed to benzaldehyde absorption and a much weaker absorption at *ca.* 245 mμ ascribed to nitrobenzene absorption. This assignment may be questioned on the grounds that the benzaldehyde band is appreciably displaced and also because the band does not show the doublet characteristic of benzaldehyde absorption in inert media. On the other hand, a nitro-group normally gives rise to appreciable changes in the spectra of meta-disubstituted benzene derivatives (5). Also, our assignment receives support from the spectrum of *m*-nitrobenzaldehyde in ethanol (see Table IV). There, the presence of ethanol would be expected to displace the nitrobenzene absorption to longer wavelength and this is in fact observed.

Steric effects in meta-substituted benzaldehydes would not be expected to be significant, since the formyl group is relatively small. However, the fairly low extinction coefficient for the *B*-band of *m*-iodobenzaldehyde may be caused, at least partly, by a buttressing interaction. Similarly, the unusual wavelength displacement, as shown in Table IV, for *m*-iodonitrobenzene compared to those for *m*-iodoacetophenone and *m*-iodobenzaldehyde also points to the operation of a buttressing effect in this type of compound (cf. 23).

The *C*-bands, as anticipated, are well defined for meta-substituted benzaldehydes (cf. 3).

THE SPECTRA OF ORTHO-SUBSTITUTED BENZALDEHYDES

The spectra of ortho-substituted benzaldehydes are listed in Table V, together with the spectra of ortho-substituted acetophenones.

All the *B*-bands, with the exception of that of *o*-nitrobenzaldehyde, occur as doublets. The *B*-band of *o*-nitrobenzaldehyde at 247 mμ is again assigned to nitrobenzene absorption, as indicated by square brackets in Table V. This is confirmed by the absorption of this compound in ethanol, which, as anticipated, occurs in the more polar solvent at longer wavelength at 252 mμ (ϵ = 4700) (21). The greatly reduced absorption intensity of the band, particularly in ethanolic solution, compared with the corresponding band in the meta-isomer, is ascribed to the increased steric interaction between the two vicinal substituents in *o*-nitrobenzaldehyde.

Information concerning the nature of the ortho-effect can also be obtained by comparing the spectra of *o*-substituted benzaldehydes with the spectra of *o*-substituted acetophenones (see Table V). At least three interpretations may be advanced for the observed ortho-effects and the data assist in deciding between these. The first interpretation is to ascribe the ortho-effect to intramolecular hydrogen bonding; a second interpretation (cf. 22) is to ascribe the ortho-effect to steric interaction between vicinal atoms or groups *with the molecule occupying only one ground state* (6); a third interpretation is to assume that the ortho-effect may also sometimes be caused by the molecule existing in more than one conformation, for example an *s-cis* and *s-trans* conformation, which however do not all contribute to the observed absorption (16).

Examination of Table V shows that an explanation based on intramolecular hydrogen bonding is consistent with the observed similarity of the *B*-bands for the *o*-hydroxy and *o*-methoxy derivatives of benzaldehyde and acetophenone. On the other hand, hydrogen bonding would not account for the generally decreased absorption intensities in the

acetophenone series, nor in particular would it account, for example, for the spectrum of *o*-chloroacetophenone, where the molecular extinction coefficient is reduced to a much greater extent than in the corresponding benzaldehyde. Therefore, steric interactions evidently also determine the ortho-effects and intramolecular hydrogen bonding is not the sole explanation for the observed ortho-effects. Experiments to differentiate between the two types of steric effects will be reported separately.

The *C*-bands show the usual changes (3), although it may be noted that in *o*-tolualdehyde and in salicylaldehyde the *C*-band does not occur as a doublet (see Table V).

TABLE V

ABSORPTION MAXIMA OF ORTHO-SUBSTITUTED BENZALDEHYDES AND ACETOPHENONES IN *n*-HEXANE OR CYCLOHEXANE SOLUTION

	Benzaldehyde				Acetophenone		
	B-Band		*C*-Band		*B*-Band		
Substituent	λ_{max} (mμ)	ϵ_{max}	λ_{max} (mμ)	ϵ_{max}	λ_{max} (mμ)	ϵ_{max}	Ref.
(Benzaldehyde)	241	14,000	277–278	1200	238–239	12,500	*
	247	*12,000*	287	1000			
o-Methyl-	243	12,500	291	1700	237	11,500‡	†
	251	13,000			245.5	9060	
			284	2400			
o-Fluoro-	240	13,300	291	2000	233	9500	*
	ca. 247	*9,700*	294	2000			
o-Chloro-	246	11,000	292	1750	235	5700	*
	252	8,500	300	1400			
			302	1400			
o-Bromo-	245.5	12,500	292	2100	234–236	4900	*
o-Iodo-	*252*	*10,000*	301	1750	—	—	*
o-Hydroxy-	250	11,000	324–325	3600	251	9700	*, §
	257	11,700					
o-Methoxy-	246	10,500	306	4600	246	8000	*, §
	ca. 253	*8500*	*ca. 314*	*4200*			
o-Amino-	255	5600	352	4600	252	5500	*
	ca. 262	*3500*					
o-Carboxy-	224	8000	269	800			*
	ca. 231	*7000*	276	850			
			ca. 286	*400*			
o-Nitro-	222	15,300					
	[247	7000]	*ca. 285*	*1700*	[254	6000]	*, ‖
	([252	4700]	270	3600	[256	4800])	

*This series of papers. †Ref. 6. ‡Values in isopentane, E. S. Waight, unpublished information. §Acetophenone values in ether (14). ‖ Values in constant-boiling ethanol (21).

EXPERIMENTAL

The benzaldehydes were obtained commercially or prepared by standard methods as described in the literature. The physical constants, after purification, of the compounds not previously reported in this series are listed in Table VI.

The ultraviolet absorption spectra were determined in specially calibrated quartz cells of various path lengths using a Unicam SP 500 spectrophotometer. Dioxane–water mixtures were prepared as previously described (11). For each compound at least two independent sets of observations were made. Where previous data are available, our data compare well with the published values. For the *m*- and *p*-aminobenzaldehydes the purified solutions in ether were directly diluted with cyclohexane to about 2% ether. This procedure avoided polymerization, which otherwise occurred. The spectrum was determined on each solution, and the concentration was subsequently obtained by evaporating to dryness and weighing the residue.

TABLE VI

PHYSICAL CONSTANTS OF BENZALDEHYDES

Benzaldehyde	Melting point, or boiling point and refractive index	Literature value of physical constants
(Benzaldehyde)	b.p. 41°, 1 mm, $n_D^{22.5}$ 1.5444	b.p. 62°, 10 mm, $n_D^{17.6}$ 1.5463 (24, 25)
o-Fluoro-	b.p. 51°, 11 mm, n_D^{22} 1.5212	b.p. 175° (24)
m-Fluoro-	$n_D^{21.3}$ 1.5173	b.p. 173° (24)
o-Chloro-	b.p. 213°, n_D^{22} 1.5656	b.p. 213–214°, $n_D^{21.7}$ 1.5656 (24, 25)
m-Chloro-	b.p. 55°, 1 mm, $n_D^{25.8}$ 1.5613	b.p. 213–214°, $n_D^{20.2}$ 1.5650 (25)
p-Chloro-	m.p. 47.5°	m.p. 47.5° (25)
m-Iodo-	m.p. 57°	m.p. 57° (24)
p-Iodo-	m.p. 76°	m.p. 77–78° (24)
o-Hydroxy-	b.p. 45°, 3 mm, $n_D^{22.5}$ 1.5722	b.p. 196.5°, $n_D^{19.7}$ 1.5736 (25)
m-Hydroxy-	m.p. 104°	m.p. 108° (106°) (24, 25)
p-Hydroxy-	m.p. 117°	m.p. 115–116° (24)
o-Methoxy-	b.p. 71°, 2 mm, n_D^{21} 1.5604	m.p. 36°, n_D^{20} 1.5600 (24)
m-Methoxy-	b.p. 62°, 1 mm, n_D^{25} 1.5511	b.p. 230°, n_D^{20} 1.5530 (24)
p-Methoxy-	b.p. 83°, 2 mm, n_D^{22} 1.5717	b.p. 248°, $n_D^{13.7}$ 1.5764 (24, 25)
o-Nitro-	m.p. 42°	m.p. 43–44° (24)
m-Nitro-	m.p. 57°	m.p. 58° (24)
p-Nitro-	m.p. 106°	m.p. 106° (24)
o-Carboxy-	m.p. 97.2°	m.p. 97° (25)
p-Carboxy-	m.p. *ca.* 250°	m.p. 248–250° (256°) (25)

ACKNOWLEDGMENT

The authors gratefully acknowledge the receipt of a research grant from the National Research Council of Canada.

REFERENCES

1. FORBES, W. F. and MUELLER, W. A. Can. J. Chem. **33**, 1145 (1955).
2. FORBES, W. F. and MUELLER, W. A. Can. J. Chem. **35**, 488 (1957).
3. FORBES, W. F., MUELLER, W. A., RALPH, A. S., and TEMPLETON, J. F. Can. J. Chem. **35**, 1049 (1957).
4. FORBES, W. F. and SHERATTE, M. B. Can. J. Chem. **33**, 1825 (1955).
5. FORBES, W. F. Can. J. Chem. **36**, 1350 (1958).
6. BRAUDE, E. A. and SONDHEIMER, F. J. Chem. Soc. 3754 (1955).
7. BURAWOY, A. and CHAMBERLAIN, J. T. J. Chem. Soc. 2310 (1952).
8. BURAWOY, A. and THOMPSON, A. R. J. Chem. Soc. 4314 (1956).
9. GRAMMATICAKIS, P. Compt. rend. **231**, 278 (1950).
10. GRAMMATICAKIS, P. Bull. soc. chim. France, 821 (1953).
11. FORBES, W. F. and TEMPLETON, J. F. Can. J. Chem. **36**, 180 (1958).
12. JONES, R. N., FORBES, W. F., and MUELLER, W. A. Unpublished information.
13. SCHUBERT, W. M., ROBINS, J., and HAUN, J. L. J. Am. Chem. Soc. **79**, 910 (1957).
14. MORRIS, H. H. and YOUNG, R. H. J. Am. Chem. Soc. **79**, 3408 (1957).
15. FORBES, W. F., MORICONI, E. J., WALLENBERGER, F. T., and O'CONNOR, W. F. J. Org. Chem. **23**, 224 (1958).
16. FORBES, W. F. and MUELLER, W. A. Can. J. Chem. **34**, 1347 (1956).
17. FORBES, W. F. and RALPH, A. S. Can. J. Chem. **34**, 1447 (1956).
18. BARROW, G. M. J. Chem. Phys. **21**, 2008 (1953).
19. DANNENBERG, H. Z. Naturforsch. **4b**, 327 (1949).
20. LEMON, H. W. J. Am. Chem. Soc. **69**, 2998 (1947).
21. WALKER, E. A. and YOUNG, J. R. J. Chem. Soc. 2041 (1957).
22. FORBES, W. F. and RALPH, A. S. Can. J. Chem. **36**, 869 (1958).
23. FORBES, W. F. and MUELLER, W. A. J. Am. Chem. Soc. **79**, 6495 (1957).
24. HEILBRON, Sir I. and BUNBURY, H. M. Dictionary of organic compounds. Eyre and Spottiswoode Ltd., London. 1946.
25. HODGMAN, C. D. *et al.* Handbook of chemistry and physics. 37th ed. Chemical Rubber Publishing Co., Cleveland, Ohio.

LIGHT ABSORPTION STUDIES

PART XIII. THE ELECTRONIC ABSORPTION SPECTRA OF RING-SUBSTITUTED ANILINES[1]

W. F. Forbes and I. R. Leckie

ABSTRACT

A spectral analysis of benzene derivatives in terms of steric and electronic interactions is extended to ring-substituted anilines.

INTRODUCTION

In previous parts of this series spectral analyses were carried out for substituted acetophenones, benzaldehydes, and nitrobenzenes, that is, for compounds in which one substituent possesses a *negative* mesomeric effect. The purpose of the present communication is to consider in greater detail the effect of the amino group on the electronic spectra, that is, the effect of a group which possesses a *positive* mesomeric effect.

Systematic investigations of the electronic spectra of anilines have also recently been carried out by Wepster (1) and by Klevens and Platt (2). The emphasis of our work will be to relate the available data to the hypotheses developed for other benzene derivatives in this series and, whenever convenient, we have also redetermined the reported data, in order that data would be obtained under near-identical conditions.

THE ANILINE SPECTRUM

The absorption maxima of aniline for different solvents in the region 220–300 mμ are listed in Table I.

TABLE I

Main absorption maxima of aniline in different solvents

Solvent	*B*-Band		*C*-Band		Source
	λ_{max} (mμ)	ϵ_{max}	λ_{max} (mμ)	ϵ_{max}	
Vapor phase	229		*ca.* 280		*, †
Cyclohexane	233–234	9000	286	1900	*
Ethanol	234–235	8000	284–285	1700	*
Water	230	8000	278	1400	*
0.1 *N* HCl	202	7500	247 252 258	150 170 150	*
N NaOH	230	8400	279	1400	*
Ether	238	10,000	288	1900	*
Cyclohexane containing 3% ether	234	9000	285	1800	*

*This series of papers.
†ϵ_{max} values not determined.

The two bands listed in Table I are described as *B*- and *C*-bands, implying that these bands correspond to the similar bands in acetophenone, benzaldehyde, and nitrobenzene (cf. 3, 4, 5). Consequently the corresponding electronically excited states may be visualized as involving dipolar resonance forms of type I.

I

[1]*Manuscript received June 16, 1958.*
Contribution from the Memorial University of Newfoundland, St. John's, Newfoundland.

The *B*-band of aniline appears to be symmetrical and shows no fine structure if the spectra are determined in solution. Some fine structure occurs in cyclohexane for the *C*-band, but this is not evident in other solvents, for example in ether or water. In the vapor phase, fine structure is shown by both *B*- and *C*-bands. Further, in cyclohexane both *B*- and *C*-bands do not show any appreciable concentration dependence within the investigated concentration range (2×10^{-3} to 3.36×10^{-4} moles/liter for the *B*-band, and 1×10^{-2} to 3.36×10^{-4} moles/liter for the *C*-band). This may be related to information deduced from infrared data, which suggests that aniline in carbon tetrachloride solution occurs as the monomer up to a concentration of 10^{-2} moles/liter (6).

The data in Table I also show that although no appreciable spectral change occurs between the spectra in ethanol and cyclohexane, a more pronounced spectral change occurs between the spectra in cyclohexane and aqueous solution. Analogous wavelength displacements are observed for the spectrum of N,N-dimethylaniline in hexane, ethanol, and water (7), and this therefore suggests that the observed spectral changes are not caused by hydrogen bonding involving the nitrogen-linked hydrogen atoms. In addition, it has previously been shown that if an aqueous solution of aniline is examined within a temperature range sufficient to affect any hydrogen bonding present, no spectral changes are observed (8). Searching for a possible explanation of the spectral changes, one may note that the reduced extinction coefficient between ethanol and water for N,N-dimethylaniline, which is not observed for aniline, may be tentatively ascribed to steric interaction. Ungnade has previously pointed out (see footnote 17 of ref. 7) that it is necessary to assume a hydrate, involving the unshared electron pair, in aromatic amines in order to account for the basic properties of these substances, and that the formation of such hydrates is subject to steric effects. Consequently, the most probable explanation of the wavelength displacement is provided by assuming that in aqueous solution the molecular species $C_6H_5NH_3OH$ contributes appreciably to the observed absorption. However, this species must surely involve some form of hydrogen bonding, although it may not be the same type of hydrogen bond as will be described below. The aniline or N,N-dimethylaniline molecule presumably in some way accepts the proton of the water molecule by means of the non-bonding electrons of the nitrogen atom. It has been suggested that by partially isolating the $2p_z$ electrons of the nitrogen atom in this way, the hydrogen bond reduces the interaction between the $2p_z$ electrons and the benzene ring and thus the absorption band is displaced to shorter wavelength (9).

In aqueous solution, the equilibrium

$$C_6H_5.NH_3OH \longleftrightarrow C_6H_5.NH_3^+ + OH^-$$

may also be sufficiently displaced to the right to contribute to the observed wavelength displacements. However, within the investigated concentration range, this effect does not appear to be important. That is, the *B*-band in aqueous solution was found to be unchanged within the concentration range 2×10^{-3} to 3.25×10^{-4} moles/liter and the *C*-band was found to be unchanged within the concentration range 10^{-2} to 3.25×10^{-4} moles/liter. In acidic media, there occurs a hypsochromic wavelength displacement which may be related to the non-availability of the unshared *p*-electrons in the electronic excitation. That is, the non-bonded electrons are now predominantly involved in the nitrogen–hydrogen bond, and are consequently unable to participate in the transitions leading to the *B*-band. This wavelength displacement is incidentally quite characteristic for aniline and ring-substituted anilines (see Tables I, II, III, and IV), and may therefore be used in the identification of an amino substituent. No appreciable wavelength displacement occurs in weakly basic media (see Table I).

The observed wavelength displacement in ether solution for the *C*-band has been attributed to hydrogen bonding between the amino group and the oxygen atom of the solvent (cf. refs. 10 and 11). This wavelength displacement between heptane and ether is observed for aniline, but a similar displacement is now not observed for N,N-dimethylaniline (10) where this type of hydrogen bonding is ruled out. Further, the dipole moment increases markedly for aniline in ether, compared with the dipole moment in heptane, whereas a similar increase in dipole moment is not observed for N,N-dimethylaniline (10). On the other hand, we have found that the addition of 3% by weight of ether to a solution of aniline in cyclohexane does *not* change the absorption spectrum to a spectrum similar to that of aniline in ether (see Table I and cf. also ref. 10 for the spectrum of aniline in heptane containing various amounts of dioxane). This latter observation therefore does not support the concept of a stoichiometric, permanent, hydrogen bond. Lastly, it may be noted that the wavelength displacements observed between cyclohexane and vapor phase spectra suggest that some interaction also occurs between aniline and cyclohexane molecules.

THE SPECTRA OF PARASUBSTITUTED ANILINES

The spectra of parasubstituted anilines are listed in Table II.

TABLE II

ABSORPTION MAXIMA OF PARASUBSTITUTED ANILINES

(Values in italics represent inflections in this and subsequent tables)

Substituent	Solvent	*B*-Band		*C*-Band		Source
		λ_{max} (mμ)	ϵ_{max}	λ_{max} (mμ)	ϵ_{max}	
p-Hydroxy-	Cyclohexane containing 2% ether	235	7000	304	2500	*
	Water	229	6000	294	2000	*
p-Amino-	Cyclohexane	246	8500	315	2000	*
p-Methyl-	Iso-octane	237	9610	293	1910	Ref. 1
	Ethanol	236	10000			Ref. 12
p-Fluoro-	Hexane	230.5	7000			Ref. 13
	Ethanol	233.4	7000			Ref. 13
	Ethanol–HCl (99:1)	207.8	3400			Ref. 13
p-Chloro-	Hexane	241.4	12500			Ref. 13
	Ethanol	244.5	12500			Ref. 13
	Ethanol–HCl (99:1)	216.7	8000			Ref. 13
p-Bromo-	Cyclohexane	241	14000	297 *ca. 306*	1750 *1150*	*
	Ethanol	245	13300	296–297	1600	*
	Ethanol–HCl (99:1)	219	8400			Ref. 13
	0.1 *N* NaOH	239.5	12800	290	1340	Ref. 14
p-Iodo-	Hexane	246.3	17500			Ref. 13
	Ethanol	250.2	18500			Ref. 13
	Ethanol–HCl (99:1)	232.4	12500			Ref. 13
p-Acetyl-	Cyclohexane	285	19000	—	—	*
	Ethanol	316	20000	—	—	*
	Water	308–309	16500	—	—	*
	0.1 *N* HCl	*ca.* 260	6000	—	—	*
	N NaOH	308–309	11000	—	—	*
p-Formyl-	Cyclohexane containing 2% ether	291 296	16300 16100			*
p-Nitro-	Naphtha	320	14600	—	—	Ref. 15
	Ethanol	371	15500	—	—	Ref. 5
	Water	373–377	13000	—	—	*
	0.1 *N* HCl	372	5600	—	—	*
	N NaOH	373–379	13000	—	—	*
p-Carboxy-	Ether	277	20600			Ref. 16
	Ethanol	288	19000	—	—	*
	2 *N* HCl	226.5	12300	270	970	Ref. 14
	0.1 *N* NaOH	265	14900	—	—	Ref. 14

*This series of papers.

The early examples in Table II provide illustrations where both substituents are electron donating and the molecule absorbs essentially as aniline. It may be noted that for these examples the maximal extinction coefficient (ϵ_{max}) is frequently *reduced* relative to aniline, whereas in disubstituted benzene derivatives, when the substituents are electron withdrawing, the values of ϵ_{max} are usually *increased* relative to the monosubstituted parent compound (cf. 17, 18, 19).

Table II also shows that parasubstitution usually displaces the *B*-band of aniline towards longer wavelength. This is well illustrated by the spectra of the parahalogen-substituted anilines, and the magnitude of the displacements, compared with the wavelength displacements observed for meta- and ortho-isomers (see Tables III and IV), supports the postulate of dipolar forms, which may be associated with electron mobility acting along systems of conjugated bonds. However, resonance forms are evidently not entirely satisfactory in representing the relevant dipolar excited states (cf. ref. 13), although structures of type II may be used to provide a picture of the orbital delocalizations occurring in the electronic excited state.

Further, the bands are described as displaced aniline *B*-bands, but it should be noted that significant changes occur on parasubstitution. For example, whereas changing the solvent from cyclohexane to ethanol for aniline does not cause any appreciable wavelength displacement, precisely such a displacement is observed in parahalogen-substituted anilines; this displacement usually becomes increasingly pronounced with increased mesomeric interaction. Next, although normally the aniline band disappears in dilute acid media, for compounds such as *p*-nitroaniline where the mesomeric interaction is large, the band does not completely disappear, although the intensity is very greatly reduced (see Table II). Again, while for both *p*-aminoacetophenone and aniline the characteristic *hypsochromic* wavelength displacement is observed on changing the solvent from ethanol to water, in *p*-nitroaniline a *bathochromic* displacement is observed on changing the solvent from ethanol to water.

II

III

The absorptions at much longer wavelength for compounds like *p*-nitroaniline or *p*-aminoacetophenone may be associated with favorable resonance forms of type III contributing appreciably to the electronic excited state. The more appreciable contribution of resonance forms of type III, even in the ground state, presumably also accounts for the large dipole moments of these compounds (20) and the various effects noted by Wepster, who ascribed these effects, at least partly, to a decrease in the average angle of twist in the nitro group on substitution of an amino group in the para position (1, 21).

THE SPECTRA OF METASUBSTITUTED ANILINES

The spectra of metasubstituted anilines are listed in Table III.

For many of the spectra listed in Table III, the aniline B-band is readily discernible, as for example in *m*-methyl- or *m*-halogen-substituted anilines. It may be noted that the sensitiveness of the B-band to solvent changes is again different for metasubstituted anilines, such as *m*-aminoacetophenone, than for aniline.

As previously mentioned (18, 19), two B-bands can frequently be discerned in the spectra of metadisubstituted benzene derivatives, and these B-bands have been associated with transitions involving the two monosubstituted parent compounds. In this way, the

TABLE III

ABSORPTION MAXIMA OF METASUBSTITUTED ANILINES

Substituent	Solvent	Aniline *B*-band λ_{max} (mμ)	Aniline *B*-band ϵ_{max}	2nd *B*-band λ_{max} (mμ)	2nd *B*-band ϵ_{max}	*C*-Band λ_{max} (mμ)	*C*-Band ϵ_{max}	Source
m-Hydroxy-	Cyclohexane containing 2% ether	234	6800			283.5	2300	*
	Water	229	6400			278	1900	*
	0.1 *N* HCl	*ca. 211*	*6300*	217	6500	269	2000	*, †
						ca. 273	*1700*	
m-Amino-	Cyclohexane	*ca. 240*	*7000*	—	—	293	2600	*
	pH 9	*240*	*7300*	—	—	289	2100	Ref. 22
m-Methyl-	Cyclohexane	237	8300			289	1900	*
m-Chloro-	Cyclohexane	238	8500			289	2100	*
m-Bromo-	Cyclohexane	237–238	7800			290	2400	*
m-Iodo-	Cyclohexane	*239*	*8700*	*ca. 232*	*10400*	292	2700	*, †
						299	*2200*	
m-Acetyl-	Cyclohexane	226	26500	*246*	*9000*	320	2500	*
	Ethanol	231	23000	*ca. 255*	*7000*	338	1900	*
	Water	226	21000	*ca.* 255	7000	324	1900	*
	0.1 *N* HCl			238	12000	277	1000	*
	N NaOH	226.5	20000	*ca.* 255	7000			*
m-Formyl-	Cyclohexane containing 0.2% ether	227	17500	*ca. 243*	*9000*	327.5	2000	*
				ca. 256	*7500*			
m-Nitro-	Ethanol	233	18000			375	1600	Ref. 23
	Water	224	13500	278–279	4500	354	1400	*
	0.1 *N* HCl			256	7500			*
	N NaOH	224	14000	278–279	4650	354	1400	*
m-Carboxy-	Ethanol			*ca. 241*	*7000*	319	2100	*
	Ether			244	7800	320	2800	Ref. 16
	pH 3.73	218.5	14000	250	2400	310	650	Ref. 22
	pH 11			*241*	*7400*	300	1800	Ref. 22

*This series of papers.

†B-band assignment doubtful.

maximum at 226 mμ for *m*-aminoacetophenone in cyclohexane solution, the maximum for the same compound at 231 mμ in ethanol, the maximum at 233 mμ for *m*-nitroaniline in ethanol, and the maximum for the same compound at 224 mμ in *N* NaOH are all ascribed to aniline absorption. On the other hand, the inflections at 243 and 256 mμ for *m*-aminobenzaldehyde in cyclohexane are ascribed to the benzaldehyde chromophore, the inflection at 246 mμ for *m*-aminoacetophenone in cyclohexane is ascribed to the acetophenone chromophore, and the inflection at 241 mμ for *m*-aminobenzoic acid in ethanol is ascribed to the benzoic acid chromophore. Some typical features of the *B*-band assist in the assignments. For example, the characteristic doublet of the benzaldehyde *B*-band (cf. 19) appears in the spectrum of *m*-aminobenzaldehyde for the inflection near 250 mμ.

The meta-amino substituent, as expected, gives rise to a secondary interaction, which frequently causes an appreciable bathochromic wavelength displacement for the compounds listed in Table III (cf. 24). For example, in ethanol, the *B*-band of acetophenone at 240 mμ occurs as an inflection near 255 mμ in *m*-aminoacetophenone, and the *B*-band of benzoic acid at 227 mμ occurs as an inflection near 241 mμ in *m*-aminobenzoic acid. Similar displacements for other compounds, caused by the secondary effect of the meta-amino group, may be deduced from Table III. It is found that the wavelength displacement is reasonably constant, at least for similar compounds. Thus, whenever the non-amino substituent is electron withdrawing, the corresponding *B*-band appears to show an appreciable bathochromic wavelength displacement. An exception is provided in acid media, where the unshared electron pair of the amino substituent is presumably unable to contribute efficiently to the interaction with the benzene ring. Likewise, the

non-amino substituent affects the aniline *B*-band in a manner which seems susceptible to generalization. For example, if the non-amino substituent is electron withdrawing, the effect on the aniline absorption appears to be quite generally a displacement to shorter wavelength accompanied by increased absorption intensity (see Table III).

This relatively greater intensity of the band associated with aniline absorption suggests that the amino group gives rise to greater mesomeric interaction in the electronic excited state. Structures, which may be crudely represented by resonance forms of of type IV, would again contribute to the electronic excited state, and these resonance

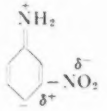

IV

forms, by analogy with the previously discussed resonance structures of that type (18), would be expected to be favored by an electron-withdrawing substituent in the meta position. On the other hand, if the meta substituent is electron donating, the band intensity of the aniline *B*-band is usually decreased (see Tables III and I). This decrease is qualitatively similar to the intensity decrease observed for the corresponding para isomers (see Table II). Both the changes may again be rationalized by resonance structures of type IV.

Since the amino group is relatively small, no appreciable buttressing interaction would be expected for metasubstituted anilines. In fact, buttressing effects are not readily discernible except possibly for the spectrum of *m*-iodoaniline (cf. 25). A buttressing interaction may also contribute to the spectral changes in the series aniline, *o*-toluidine, and 2,3-dimethylaniline. These compounds are reported to absorb in iso-octane solution at about 250 mμ with ϵ values of 9130, 8800, and 7550 respectively (1). Further, 2,3,5,6-tetramethylaniline, compared with 2,6-dimethylaniline, shows a reduced absorption intensity (1).

The *C*-band, as anticipated, is frequently more pronounced in metasubstituted anilines, compared with the *C*-band in aniline or parasubstituted anilines (26). Difficulties have arisen because of different assignments; for example, Morton and McGookin (23) note that wavelength displacements are observed in opposite senses for *m*- and *p*-nitro-N,N-dimethylaniline on changing the solvent from ethanol to water. An explanation for this apparent anomaly is provided if it is accepted that the relevant bands of the para isomer are *B*-bands, whereas the "similar" bands of the meta isomer are *C*-bands. In this way, we believe that the band of *p*-nitrodimethylaniline, which occurs in ethanol at 368.5 mμ, and the band of the same compound, which occurs in water at 422 mμ, are *B*-bands (cf. 18). On the other hand, we assume that the band of *m*-nitrodimethylaniline, which in ethanol occurs at 400.3 mμ, and which in aqueous solution is hypsochromically displaced to 385 mμ, is a *C*-band. A similar hypsochromic displacement on changing the solvent from ethanol to water is incidentally also observed for the *C*-band of *m*-nitroaniline (see Table III).

THE SPECTRA OF ORTHOSUBSTITUTED ANILINES

The spectra of orthosubstituted anilines are listed in Table IV.

The *B*-bands listed in Table IV can again be classified into the two types of *B*-bands

TABLE IV

ABSORPTION MAXIMA OF ORTHOSUBSTITUTED ANILINES

Substituent	Solvent	Aniline *B*-band		2nd *B*-band		*C*-Band		Source
		λ_{max} (mμ)	ϵ_{max}	λ_{max} (mμ)	ϵ_{max}	λ_{max} (mμ)	ϵ_{max}	
o-Hydroxy-	Cyclohexane containing 2% ether	235	7000			288	3300	*
	Water	229	6200			281	2700	*
	0.1 *N* HCl			209–210	6500	268	2100	*, †
						ca. 273	*1800*	
o-Amino-	Cyclohexane	235.5	6600	—	—	289	3500	*
	pH 9	233	6900	—	—	289	2900	Ref. 22
o-Methyl-	Cyclohexane	234	8850			283	2350	*
o-Ethyl-	Iso-octane	234	8030			286	2330	Ref. 1
o-Isopropyl-	Iso-octane	234	7780			286	2280	Ref. 1
o-Chloro-	Cyclohexane	235	8700			288	2900	*
o-Bromo-	Cyclohexane	235	8500			289	3000	*
o-Iodo-	Cyclohexane	237	8400			292	3200	*
o-Acetyl-	Cyclohexane	224	23500	252	5500	347	4350	*
	Ethanol	226	21000	254	5600	359	4350	*
	Water			254–255	5900	350	3500	*
	Dioxane			253–255	5000	354–357	4500	*
	25% Aqueous dioxane			255	5800	356–358	3800	*
o-Formyl-	Cyclohexane			255	5600	352	4700	*
				ca. 262	*3400*			
o-Nitro-	Cyclohexane	227	18000	268	5000	370	5000	*
	Ethanol	231	17000	276	5000	402	5500	Ref. 5
	Water	223	17000	280	5300	400–405	4400	*
	0.1 *N* NaOH	245	7000	282.5	5400	412	4500	Ref. 22
o-Carboxy-	Ethanol			247	6700	332	4500	*
	Ether			252	7400	333	5200	Ref. 16
	pH 3.73	216.5	18500	*248*	*3900*	327	1940	Ref. 22
	pH 11			240	7100	310	2800	Ref. 22

*This series of papers.
†B-band assignment doubtful.

as described in the previous section. Table IV then shows that both *B*-bands are frequently weakened in the ortho isomer compared with the corresponding *B*-bands in the meta isomer (see Table III). Examples of this are provided by the ortho and meta isomers of iodoaniline in cyclohexane, of aminoacetophenone in cyclohexane and ethanol, of aminobenzaldehyde in cyclohexane, and of aminobenzoic acid in ethanol and ether. In the absence of intermolecular hydrogen bonding (see below), one would expect steric effects to occur and the observed intensity decreases in the examples cited are in fact ascribed to steric interactions. Steric interactions may also occur in a number of other orthosubstituted anilines, such as *o*-toluidine and *o*-chloroaniline, for which, however, the data do not permit any definite conclusions. In this connection, it may be noted that, *compared with the B-band of the para isomer*, a hypsochromic wavelength displacement and a pronounced intensity decrease is almost invariably observed in the *B*-band of the ortho isomer. Since the resonance forms contributing to the ortho and para isomers may be regarded as similar to a first approximation, one might expect the *B*-bands of the ortho and para isomers to be similar *in the absence of steric* and other short-range *interactions*. A steric contribution to this "ortho effect" is also indicated by the fact that the decrease in absorption intensity becomes more pronounced for N,N-dimethylanilines (cf., for example, the ϵ_{max} values and integrated absorption intensities of N,N-dimethylaniline and of the corresponding *o*-methyl derivative (1)).

In the previous paragraph decreases in the absorption intensities have been used as indications of steric interactions, but unusual wavelength displacements may evidently

also indicate steric interactions. However, the wavelength displacements caused by steric interactions in this series of compounds appear to be small. For example, *o*-ethyl- and *o*-isopropyl-N,N-dimethylaniline, which presumably represent appreciably hindered compounds, still absorb maximally at 249 mμ (ϵ = 4950) and 248 mμ (ϵ = 4300) respectively, that is, at a similar maximal wavelength to N,N-dimethylaniline under identical conditions (λ_{max} 251 mμ, ϵ = 15,500) (1). This lack of an appreciable wavelength displacement, which has also recently been discussed from a theoretical viewpoint (4), may be related to the large mesomeric effect of the amino group. That is, it may be supposed that the appreciable double-bond character of the N-nuclear bond tends to keep the aniline chromophore planar and the second substituent does not contribute to the observed absorption. This mechanism has recently been described as a type III steric effect (27).

Generally, the amino group does not appear to be as sensitive to steric effects as, for example, the nitro group, which also causes appreciable mesomeric interaction. For example, an ortho-methyl group produces an appreciable intensity decrease in the *B*-band of nitrobenzene and similar compounds, whereas only a small intensity decrease is observed in the *B*-band of aniline, even compared with the *B*-band of the para isomer. Two, not mutually exclusive, explanations may account for the smaller steric effects in anilines. First, the amino group may not, because of its small size, cause appreciable steric interactions. One of the factors contributing to the relatively smaller size of the amino group may be the partial positive charge associated with excited states of the aniline chromophore. A second explanation may be that π–p electronic interaction, like π–π electronic interaction, gives rise to considerable double bond character in the N-nuclear bond, but that π–p interaction is less sensitive to steric interactions, compared with π–π electronic interaction.

Apart from steric interactions, which will tend to oppose the existence of coplanar resonance forms, other short-range interactions must also be considered. Intramolecular hydrogen bonding would be expected to be one of the most important of such interactions. For some examples, there is reasonably good evidence for an intramolecular hydrogen bond. For example, comparing the ortho and meta isomers of a number of compounds in which an intramolecular hydrogen bond would be anticipated, the following bathochromic wavelength displacements are obtained from the data listed in Tables III and IV: Aminoacetophenone in cyclohexane, *B*-band, 6 mμ; *C*-band, 27 mμ. Aminobenzoic acid in ether, *B*-band, 8 mμ; *C*-band, 13 mμ. Aminobenzoic acid in ethanol, *B*-band, 6 mμ; *C*-band, 13 mμ. Aminophenol in cyclohexane containing 2% ether, *B*-band, 1 mμ; *C*-band, 4.5 mμ. In all these compounds the ortho isomer absorbs at *longer* wavelength than the meta isomer, and the wavelength displacement may therefore be attributed, at least partly, to an intramolecular hydrogen bond.

Evidence for intramolecular hydrogen bonding may also be deduced from displaced and intensified *C*-bands in some ortho isomers, but this evidence is somewhat ambiguous (cf. ref. 26). Quite generally, and not unexpectedly, for a number of compounds the

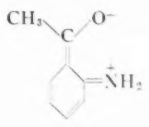

V

evidence for intramolecular hydrogen bonding from ultraviolet spectroscopy is not convincing. A number of reasons suggest themselves for this observation. For example, apart from intramolecular hydrogen bonded forms, ortho-resonance forms of type V may contribute to the ground and excited states, and this may partly account for the observed bathochromic displacements of some of the *B*-bands listed in Table IV. Next, intramolecular hydrogen bond formation may be opposed by steric interactions; the two interactions, by giving rise to opposite spectral effects, may cause different displacements depending on which interaction predominates. Further, various forms of solute–solvent interaction, including intermolecular hydrogen bonding, may interfere with intramolecular hydrogen bonding. This, in fact, is suggested by the frequent absence of the spectral effects, associated with intramolecular hydrogen bond formation, in other than inert media (cf. Tables III and IV).

The *C*-band in orthosubstituted anilines gives rise to the expected changes (see ref. 26). It is generally more pronounced in orthosubstituted anilines.

EXPERIMENTAL

The ultraviolet absorption spectra were determined by standard methods using a Unicam SP500 or a Beckman Model DU spectrophotometer. For each compound at least two independent sets of observations were made. The spectrum in the vapor phase was determined at room temperature in a 2-cm cell against air. The spectral data obtained compare well with other data whenever these were previously recorded in the literature. Where comparisons are made involving the extinction coefficients at maximal absorption (ϵ_{max}) the change in ϵ_{max} may be qualitatively related to corresponding changes in the oscillator strengths f, as far as can be discerned from the shape of the absorption bands. The precision of λ_{max} values is estimated to be ± 0.5 mμ, and the precision of ϵ_{max} values $\pm 5\%$ or better. Values were normally reproducible to $\pm 2\%$.

The physical constants, after purification, of compounds, the spectra of which have not previously been reported in this series, are listed in Table V.

TABLE V

PHYSICAL CONSTANTS OF RING-SUBSTITUTED ANILINES

Substituent	Melting point, or boiling point, and refractive index	Literature values of physical constants (28)
[Aniline	B.p. 81°, 27 mm, n_D^{23} 1.5840	B.p. 184.4°, n_D^{20} 1.5863]
m-Amino-	M.p. 62°	M.p. 62.8°
p-Amino-	M.p. 138°	M.p. 139.7°
o-Methyl-	B.p. 95.5°, 27 mm, n_D^{23} 1.5717	B.p. 200°, n_D^{20} 1.5728
m-Methyl-	B.p. 86.8°, 17 mm, n_D^{21} 1.5672	B.p. 203.3°, n_D^{22} 1.5711
o-Chloro-	B.p. 119°, 55 mm, $n_D^{24.5}$ 1.5869	B.p. 208.8°, n_D^{20} 1.5895
o-Bromo-	B.p. 152°, 117 mm, n_D^{25} 1.6165	B.p. 229°
o-Iodo-	M.p. 56°	M.p. 56.5°
o-Formyl-	M.p. 38°	M.p. 39–40°
o-Nitro-	M.p. 71.5°	M.p. 71.5°
m-Nitro-	M.p. 114°	M.p. 111.8°
p-Nitro-	M.p. 147°	M.p. 147.5°

The phenylenediamines were purified by vacuum sublimation, and the spectra of these compounds as well as the spectra of the aminophenols were determined as quickly as possible.

ACKNOWLEDGMENTS

The authors gratefully acknowledge the assistance of Mr. J. F. Templeton, in some of the preliminary work of the reported experimental data. They are also greatly indebted to the National Research Council for a research grant in support of these studies.

REFERENCES

1. WEPSTER, B. M. Rec. trav. chim. **76**, 357 (1957).
2. KLEVENS, H. B. and PLATT, J. R. J. Am. Chem. Soc. **71**, 1714 (1949).
3. MURRELL, J. N. Proc. Phys. Soc. A, **68**, 969 (1955).
4. MURRELL, J. N. J. Chem. Soc. 3779 (1956).
5. TIMMONS, C. J. J. Chem. Soc. 2613 (1957).
6. FUSON, N., JOSIEN, M. L., POWELL, R. L., and UTTERBACK, E. J. Chem. Phys. **20**, 145 (1952).
7. UNGNADE, H. E. J. Am. Chem. Soc. **75**, 432 (1953).
8. COGGESHALL, N. D. and LANG, E. M. J. Am. Chem. Soc. **70**, 3283 (1948).
9. ROBIN, M. and TRUEBLOOD, K. N. J. Am. Chem. Soc. **79**, 5138 (1957).
10. NAGAKURA, S. and BABA, H. J. Am. Chem. Soc. **74**, 5693 (1952).
11. MASAMUNE, T. J. Am. Chem. Soc. **79**, 4418 (1957).
12. BURAWOY, A. and SPINNER, E. J. Chem. Soc. 2085 (1955).
13. BURAWOY, A. and THOMPSON, A. R. J. Chem. Soc. 4314 (1956).
14. DOUB, L. and VANDENBELT, J. M. J. Am. Chem. Soc. **69**, 2714 (1947).
15. NAGAKURA, S. J. Chem. Phys. **23**, 1441 (1955).
16. DANNENBERG, H. Z. Naturforsch. **4b**, 327 (1949).
17. FORBES, W. F. and TEMPLETON, J. F. Can. J. Chem. **36**, 180 (1958).
18. FORBES, W. F. Can. J. Chem. **36**, 1350 (1958).
19. DEARDEN, J. C. and FORBES, W. F. Can. J. Chem. **36**, 1362 (1958).
20. SMITH, J. W. and WALSHAW, S. M. J. Chem. Soc. 3217 (1957).
21. WEPSTER, B. M. Rec. trav. chim. **76**, 335 (1957).
22. DOUB, L. and VANDENBELT, J. M. J. Am. Chem. Soc. **71**, 2414 (1949).
23. MORTON, R. A. and MCGOOKIN, A. J. Chem. Soc. 901 (1934).
24. FORBES, W. F. and RALPH, A. S. Can. J. Chem. **36**, 869 (1958).
25. FORBES, W. F. and MUELLER, W. A. J. Am. Chem. Soc. **79**, 6495 (1957).
26. FORBES, W. F., MUELLER, W. A., RALPH, A. S., and TEMPLETON, J. F. Can. J. Chem. **35**, 1049 (1957).
27. FORBES, W. F. The classification of steric effects in ultraviolet absorption spectra. *In* Steric effects in conjugated systems. *Edited by* G. W. Gray, Butterworth Scientific Publications, London. 1958. In press.
28. HODGMAN, C. D. *et al.* Handbook of chemistry and physics. 35th ed. Chemical Rubber Publishing Co., Cleveland, Ohio. 1953.

SUR LA SYNTHÈSE DE QUELQUES XANTHONES POLYSUBSTITUÉES[1]

R. Constantin et P. L'Écuyer

RÉSUMÉ

La synthèse de la 4,6,7-triméthoxy- et de la 1-méthyl-4,6,7-triméthoxy-9-xanthone a été réalisée en faisant agir un mélande d'anhydride acétique et d'acide sulfurique sur l'acide 6-(2′-méthoxy)- ou 6-(2′-méthoxy-5′-méthylphénoxy)-vératrique. La préparation de ces deux acides a été effectuée en condensant le 6-bromovératrate de méthyle avec le guaïacolate ou l'isocréosolate de potassium en présence de cuivre. La 1-carboxy-4,6,7-triméthoxy-9-xanthone, un produit de dégradation de la cularine, a été obtenue en oxydant la 1-méthyl-4,6,7-triméthoxy-9-xanthone par l'acide chromique en solution dans l'acide éthanoïque.

Manske (1, 2) a suggéré la formule I pour la cularine en se basant sur la structure des produits de dégradation qu'il en a obtenus et, en particulier, sur celle de la 2-styrolène-4,6,7-triméthoxy-dibenz[*b*,*f*]oxépine (II), provenant de la méthylation destructive de l'alcaloïde. L'oxydation de II lui a donné, en plus de l'acide dicarboxylique correspondant, une xanthone qui, selon toute probabilité, devait être la 1-carboxy-4,6,7-triméthoxy-9-xanthone (III, R = CO_2H). Manske n'a pas synthétisé cette xanthone, parce qu'il ne

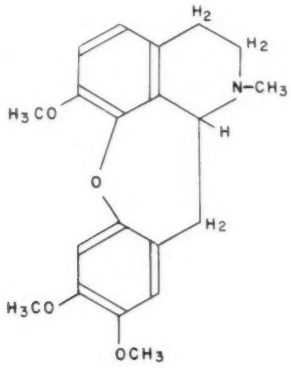

(I)

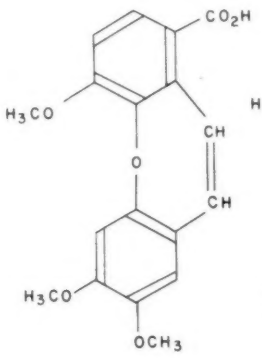

(II)

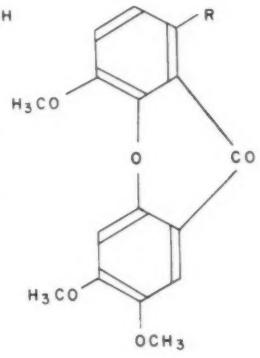

(III)

R = H, $-CH_3$ ou CO_2H

connaissait aucune méthode facile de synthèse conduisant aux xanthones polysubstituées.

Manske et Kulka (3), en appliquant la réaction de Gattermann au 2,3′,4′-triméthoxydiphényl éther et au 2,3′,4′-triméthoxy-5-méthyldiphényl éther ont déjà synthétisé les aldéhydes 6-(2′-méthoxyphénoxy)- et 6-(2′-méthoxy-5′-méthylphénoxy)-vératriques qu'ils ont transformés par oxydation en acides 6-(2′-méthoxyphénoxy)- et 6-(2′-méthoxy-5′-méthylphénoxy)-vératriques avec des rendements respectifs de 12 et 10%. En condensant le 6-bromovératrate de méthyle avec le guaïcolate ou l'isocréosolate de

[1]*Manuscrit reçu le 23 juin, 1958.*
Contribution du Département de Chimie, Faculté des Sciences, Université Laval, Québec, P.Q. Ce mémoire est tiré de la thèse de doctorat de R. Constantin.

potassium en présence de poudre de cuivre et en saponifiant les esters qui se sont formés nous avons obtenu les mêmes acides 6-(2′-méthoxyphénoxy)- et 6-(2′-méthoxy-5′-méthylphénoxy)-vératriques avec des rendements respectifs de 45 et 30%.

L'action d'un agent déshydratant sur un acide arylsalicylique constitue une méthode pratique pour la préparation d'une xanthone simple (4, 5). En faisant agir un mélange d'anhydride acétique et d'acide sulfurique sur l'acide 6-(2′-méthoxy)- ou 6-(2′-méthoxy-5′-méthylphénoxy)-vératrique nous avons pu synthétiser la 2,3,5-triméthoxy-9-xanthone (III, R = H) et la 1-méthyl-4,6,7-triméthoxy-9-xanthone (III, R = CH_3).

L'oxydation de III (R = H) par l'acide chromique dans l'acide acétique glacial nous a permis de synthétiser la 1-carboxy-4,6,7-triméthoxy-9-xanthone (III, R = CO_2H). Le point de fusion de cette xanthone mélangée à un échantillon du produit que Manske a obtenu au cours de la dégradation de la cularine n'est pas déprimé et les spectres d'absorption dans l'ultraviolet (figures 1 et 2) des deux échantillons différents de la xanthone, sont identiques. Ceci confirme donc l'exactitude de la structure que Manske a suggérée pour la xanthone qu'il a obtenue à partir de la cularine et aussi de celle qu'il a proposée pour l'alcaloïde lui-même.

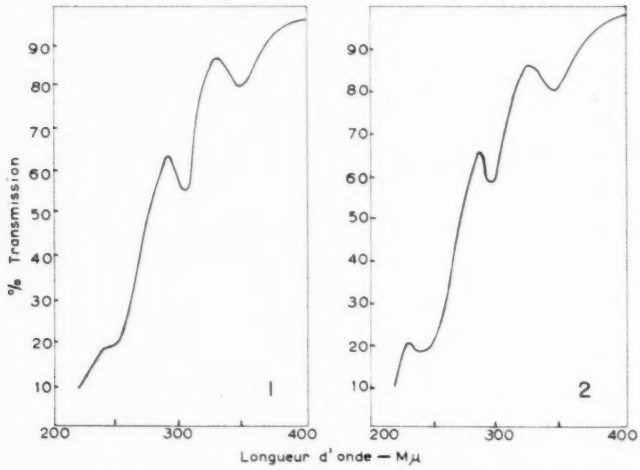

FIG. 1. Spectre d'absorption dans l'ultraviolet de la 1-carboxy-4,6,7-triméthoxy-9-xanthone synthétique.
FIG. 2. Spectre d'absorption dans l'ultraviolet de la xanthone obtenue par la dégradation de la cularine.

PARTIE EXPÉRIMENTALE*

Acides 6-(2′-méthoxyphénoxy)- et 6-(2′-méthoxy-5′-méthylphénoxy)-vératriques

On pulvérise dans un mortier un mélange de 6-bromovératrate de méthyle (0.01 mole), de guaïacolate ou d'isocréosolate de potassium (0.011 mole) et de la poudre de cuivre. On chauffe ensuite le mélange à 150° pendant 2 heures, puis à 180° pendant 15 minutes. Une fois la masse brune refroidie, on la pulvérise et on l'extrait à l'éther (3 fois avec 30 ml). Les extraits éthérés combinés sont lavés successivement à la soude 0.1 *N* et à l'eau, puis séchés et évaporés à siccité. Le résidu est saponifié en le chauffant à reflux en présence d'une solution à 3% d'hydroxyde de potassium dans le méthanol. On chasse la majeure partie du méthanol par ébullition, on dilue et on acidifie à l'acide

**Les points de fusion ont été pris à l'aide de l'appareil de Johns.*

sulfurique. Les acides 6-(2′-méthoxyphénoxy)- et 6-(2′-méthoxy-5′-méthylphénoxy)-vératriques sont essorés et cristallisés dans le benzène. Les p.f. sont respectivement 184 et 186°, et les rendements 1.37 g (45%) et 0.95 g (30% de la théorie).

4,6,7-Triméthoxy-9-xanthone (III, R = H)

A de l'acide 6-(2′-méthoxyphénoxy)-vératrique (1.6 g; 0.005 mole) dans le d'anhydride acétique (15 ml) on ajoute 2 ml d'acide sulfurique concentré. On porte la solution à 60° sur le bain-marie pendant 1 heure et on la verse ensuite sur de la glace. On essore le précipité et on le lave successivement à la soude 0.1 *N* et à l'eau. La 4,6,7-triméthoxy-9-xanthone cristallise dans le méthanol en fines aiguilles blanches de p.f. 238°. Rendement: 0.86 g (65% de la théorie). Calculé pour $C_{16}H_{14}O_5$: C, 67.11%; H, 4.92%. Trouvé: C, 66.4%; H, 5.0%.

1-Méthyl-4,6,7-triméthoxy-9-xanthone (III, R = CH_3)

On procède exactement de la même façon que pour la synthèse précédente, mais en utilisant l'acide 6-(2′-méthoxy-5′-méthylphénoxy)-vératrique comme matière première. La 1-méthyl-4,6,7-triméthoxy-9-xanthone s'obtient en fines aiguilles blanches en la cristallisant dans le méthanol ou l'éthanol. P.f. 211°. Rendement 0.26 g (40% de la théorie). Calculé pour $C_{17}H_{16}O_5$: C, 67.99%; H, 5.37%. Trouvé: C, 67.4%; H, 5.4%.

1-Carboxy-4,6,7-triméthoxy-9-xanthone (III, R = CO_2H)

On chauffe au bain-marie pendant 2 heures une solution de 1-méthyl-4,6,7-triméthoxy-9-xanthone (0.2 g) et d'oxyde chromique (0.3 g) dans l'acide acétique glacial (10 ml). On verse ensuite la solution sur de la glace et on essore le précipité qui s'est formé. La 1-carboxy-4,6,7-triméthoxy-9-xanthone cristallise dans l'acide éthanoique en fines aiguilles jaunâtres de p.f. 301°. Rendement: 0.15 g (70% de la théorie). Le p.f. mixte d'un échantillon de cette xanthone mélangée à un échantillon du produit que Manske a obtenu par la dégradation de la cularine est aussi 301°. Le spectre d'absorption dans l'ultraviolet des deux échantillons de provenance différente est aussi identique. Calculé pour $C_{17}H_{14}O_7$: C, 61.20%; H, 4.27%. Trouvé: C, 60.7%; H, 4.4%.

REMERCIEMENTS

Nous remercions le Dr. R. H. F. Manske pour nous avoir gracieusement fourni un échantillon du produit provenant de la dégradation de la cularine, puis le Conseil National de Recherches, l'office de Recherches de la Province de Québec et les Canadian Industries Limited, pour l'octroi de bourses d'études à l'un de nous (R. Constantin).

BIBLIOGRAPHIE

1. MANSKE, R. H. F. J. Am. Chem. Soc. **72**, 55 (1950).
2. MANSKE, R. H. F. et LEDINGHAM, A. E. J. Am. Chem. Soc. **72**, 4797 (1950).
3. MANSKE, R. H. F. et KULKA, M. J. Am. Chem. Soc. **75**, 1322 (1953).
4. ULLMANN, F. et ZLOKOSOFF, M. Ber. **38**, 2111 (1905).
5. ULLMANN, F. et WAGNER, C. Ann. **355**, 359 (1907).

THE KINETICS OF MOLECULAR SIEVE ACTION. SORPTION OF NITROGEN–METHANE MIXTURES BY LINDE MOLECULAR SIEVE 4A[1,2]

H. W. Habgood

ABSTRACT

This system illustrates "partial molecular sieve action". Methane has a higher affinity for the sorbent and hence is preferentially sorbed at equilibrium, while nitrogen diffuses through the crystal more rapidly and thus is preferentially taken up during the early stages of sorption. Measurements were made with the pure gases and with mixtures at 0° and −79.4° C. The sorption isotherms fit Langmuir equations and the isosteric heats of sorption are essentially independent of concentration. The sorption rates for the pure gases may be characterized by diffusion coefficients, D, calculated in the usual manner assuming the flux of diffusion to be proportional to the concentration gradient. The resultant values for D increase with increasing sorbate concentration. Diffusion of a mixture may be formally characterized by D's for each component. While that for methane is approximately the same as for methane alone, D for nitrogen in mixtures is much larger than for the pure gas and also varies with composition. This, as well as the existence of a temporary maximum in the amount of nitrogen sorbed, may be explained by considering the driving force for diffusion to be the gradient in chemical potential rather than in concentration.

INTRODUCTION

"Molecular sieve" behavior during sorption by dehydrated crystalline zeolites results from the small and uniform size of the intracrystalline pores left by removal of the water of hydration. Molecules having a significantly larger cross section are totally excluded but somewhat smaller molecules may be sorbed slowly. Here the rate-determining step appears to be diffusion through the crystal channels with a significant energy of activation being required. With a mixture of two such sorbates, *partial* molecular sieve action may occur. The component having the lesser affinity for the solid may move faster through the lattice and, consequently, the sorbed phase would show an initial enrichment in this substance, followed by an equilibrium enrichment in the other, more strongly sorbed, component. Since there is often a rough correlation between molecular size and adsorptive affinity, such cases should be fairly common.

Most of our knowledge of this interesting class of sorbents is from the extensive work of R. M. Barrer and his students over the past fifteen years (1). Studies by Barrer and Robins on the sorption of binary gas mixtures (2) indicate that argon–krypton mixtures with dehydrated mordenite and ethane–propane mixtures with dehydrated chabazite show the behavior described above. These experiments in which sorption was carried out in a series of finite steps from a gas phase of constant volume and hence of varying composition were not, however, amenable to detailed analysis.

The present study was intended to examine a single system in some detail, primarily to investigate the relationship between the diffusion properties of the gases individually and in mixtures. The sorption of nitrogen, methane, and their mixtures by Linde Molecular Sieve 4A* (a dehydrated synthetic crystalline zeolite) was studied. This system proved to be a very satisfactory choice. The effective collision diameters of nitrogen and methane,

[1]*Manuscript received March 17, 1958.*
Contribution No. 71 from the Research Council of Alberta, Edmonton.
[2]*Presented in part to the 40th Annual Conference of the Chemical Institute of Canada, Vancouver, June 1957.*
**Manufactured by the Linde Company, Division of Union Carbide Corporation, New York.*

3.71 Å and 3.82 Å (3), are almost the same but nitrogen would be expected to have a significantly smaller minor diameter of around 3.0 Å. Since methane is, in general, more strongly adsorbed than nitrogen, the expected behavior, if the adsorbent pores are a suitable size, is initial preferential sorption of nitrogen changing to the preferential sorption of methane at equilibrium. The present work demonstrates that such behavior does indeed occur, although, as with many other diffusion phenomena, the simple Fick's Law approach is inadequate for a complete description.

EXPERIMENTAL

Apparatus and Method

Measurements were made of the progress of sorption with time and of the equilibrium sorption for the pure gases and for mixtures. For some of the work with the pure gases a conventional constant volume system was used in which the sorption was followed by change in pressure. For all of the measurements on gas mixtures a constant pressure flow system was used.

The constant pressure apparatus, as illustrated schematically in Fig. 1, permitted a continuous gas flow in order to maintain uniform composition and pressure in the gas phase. After the gas mixture had flowed over the sample for the desired length of time, the pressure and flow being maintained constant by adjustment of the appropriate valves, the contents of the cell were isolated by closing the outlet and inlet valves. The valve from the storage tank was closed one or two seconds before the inlet valve to the cell so that the manometer read the final pressure in the cell. The cell was then heated to 200° to bring about desorption, while the gas was expanded into a calibrated glass measuring system.

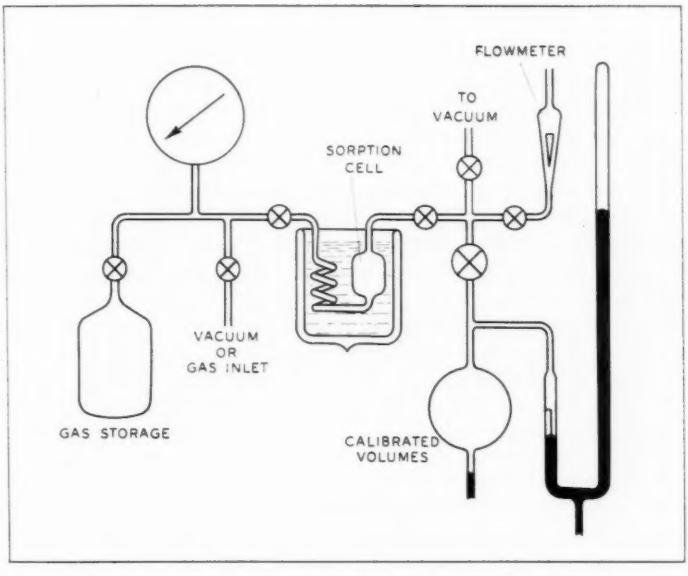

FIG. 1. Constant pressure flow system for sorption measurements.

Analysis of mixtures was by comparison of the thermal conductivity with that of a sample of the original mixture. It was necessary to mix the gas before analysis to ensure uniform composition and this was done by collection in a single bulb on charcoal at liquid air temperature followed by an hour's reheating. The thermal conductivity measurements were made with a Gow-Mac cell in a conventional bridge arrangement. It was found important to maintain the total cell current constant within 0.1% to obtain reproducible results.

A series of such measurements was carried out with different contact times. The dead space was measured both with helium and by extrapolation to zero time of the total gas volume. In calculating the amount of sorbed gas it is necessary to assume that the gas in the free space of the cell is of the same composition as the original gas mixture. A flow rate of about 10 times the average rate of sorption during the first minute appeared sufficient to ensure this, as shown by constancy of composition with varying flow rate. A higher rate would sometimes have been desirable for times less than one minute but it would then be uncertain that the gas had reached bath temperature. Measurements could be made to contact times as low as ten to fifteen seconds.

Two apparatuses of this type were used, one of glass with fritted disks at the inlet and outlet to retain the powdered zeolite and the other of metal for use at higher pressures with the zeolite in pellet form.

Gases

Purified grade nitrogen was passed through a charcoal trap cooled in dry ice – acetone. Some argon remained but this did not appear to collect on the zeolite. Phillips pure grade methane was passed through an ascarite column to remove carbon dioxide and through a charcoal trap cooled in dry ice – acetone to remove ethane.

Zeolite

The Molecular Sieve 4A was obtained as a fine crystalline powder and also in the form of extruded pellets $\frac{1}{16}$ inch diameter by about $\frac{1}{4}$ inch long. The pellets were more convenient for measurements at high pressures but the results cannot be compared with those from the powder because of differences in the total sorptive capacities and rates.

The external area of each form was determined from the B.E.T. adsorption isotherm at 0° for isobutane, which may be assumed not to penetrate the intracrystalline pores. Taking 47.4 Å^2 for the area of the isobutane molecule (4), surface areas of 10.5 and 6.9 m^2/g for pellets and powder respectively were obtained. This gives an average particle diameter for the powder of about 0.5 μ and an average intercrystalline pore diameter for the pellets of 0.1 to 0.5 μ.

The density of the dehydrated zeolite powder was determined with carbon tetrachloride (which is too large to penetrate the intracrystalline channels) to be 1.631 g/cc. The density of the hydrated crystals is given as 1.99 g/cc.

Some of the properties of this synthetic zeolite have been described by Breck *et al.* (5) and the crystal structure has been worked out by Reed and Breck (6).

Activation

The zeolite was received in essentially dehydrated form but all samples were further activated by heating under vacuum for 1 to 3 hours at 300° to 400°. The total water removed was around 1.6% and most of this came off below 300°. (The hydrated crystals contain 22.2% H_2O (5).) Activation to 400° appeared to be more reproducible than to 300°. Both the sorptive activity and the total sorptive capacity appeared to be very

sensitive to the precise degree of dehydration achieved; for example, the diffusion coefficients roughly quadrupled for activation at 400° compared to 300°. This behavior is similar to the findings of others (2, 5, 7, 8) and appears to result from the blocking action of a few residual water molecules which effectively seal off portions of the zeolite crystal. Dehydration at 400° was not sufficiently extreme to cause collapse of the crystal and decrease in adsorptive capacity, such as reported for chabazite at high temperatures (7).

Sudden sharp drops in activity often accompanying a large sorption were sometimes observed for samples with initially rather low diffusivities—e.g. those activated around 300°. A possible explanation is a non-uniform initial activation with a redistribution of the residual water, which was assisted by the local heat of sorption.

Because of this sensitivity of the zeolite and as a result of accidental exposures to air it was not possible to obtain all the information desired from a single sorbent sample. Only those results are included for which periodic repetition of some of the measurements showed the activity to be constant over the series of measurements.

RESULTS

Equilibrium Properties: Isotherms

Sorption isotherms, with one exception, gave good fits to the Langmuir equation. Some of the isotherms are shown in Fig. 2 and the Langmuir constants are given in Table I for measurements on two samples of powder at 0° and −79.4° C and on one

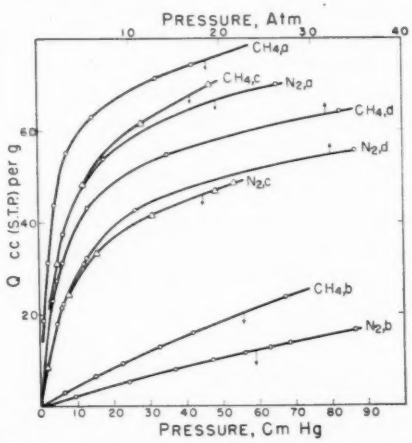

FIG. 2. Sorption isotherms. *a*—powder activated at 400° C, isotherms at 193.7° K; *b*—same sample as *a*, isotherms at 273.1° K; *c*—powder activated at 350° C, isotherms at 193.7° K; *d*—pellets activated at 400° C, isotherms at 273.1° K (upper scale).

sample of pellets at 0°. The nitrogen isotherm for the 350°-activated powder at −79.4° appears anomalous, as do the diffusion properties which were measured at the same time but there was no evident reason for this. The sorption of nitrogen at 700 mm and −78° reported by the Linde workers (5) agrees with the isotherm for the 400°-activated powder.*

**These authors also give a complete isotherm at this temperature which lies considerably above their single value and above our isotherm.*

TABLE I

SORPTION ISOTHERMS AND EQUILIBRIUM SEPARATION FACTORS

Sorbent (temp. of activation)	Temp., °K	Sorbate	Langmuir constants C_m (cc/g)	Langmuir constants b (atm^{-1})	b_{N_2}/b_{CH_4}	α equilibrium (from 10% mixture)
Powder (350°)	273.1	N_2	70.8	0.189		
		CH_4	87.1	0.362	0.52	—
	193.7	N_2	[a]	[a]		
		CH_4	77.6	10.2		—
Powder (400°)	273.1	N_2	86.8	0.210		
		CH_4	104.0	0.336	0.625	0.58[b]
	193.7	N_2	77.2	10.95		
		CH_4	79.5	25.9	0.440	0.52[b]
Pellets (400°)	273.1	N_2	60.5	0.226		
		CH_4	65.5	0.355	0.64	0.60

[a]This isotherm did not fit the Langmuir equation.
[b]The separation factor was determined on a different sample, which gave the same sorption at 1 atm.

The monolayer values are one third to one half the total capacity of the crystal for tightly packed molecules of this size. Determination of such capacity cannot be made directly by sorption of nitrogen at liquid nitrogen temperatures because of the impracticably slow rates but sorption of oxygen, or of nitrogen by the calcium-exchanged form, at liquid nitrogen temperature is around 200 cc per g (5). Since the individual 11.4 Å diameter cavities would each then contain around fifteen molecules, the lower monolayer values at higher temperatures reflect a greater average mobility. The monolayer values decrease between 0° and −79.4°, which must mean that diffusion into parts of the crystal becomes vanishingly slow. In spite of the crystalline nature of this sorbent some inhomogeneities undoubtedly remain.

While complete isotherms for mixtures of nitrogen and methane were not obtained, several individual determinations were made. According to the Langmuir theory, the separation factor for a mixture should be the ratio of the "b" values for the pure gases. This comparison is made in Table I and the agreement is reasonably good. Barrer and Robins likewise found fairly good agreement with the Langmuir theory for pure gases and mixtures in chabazite (2).

Heats of Sorption

Isosteric heats of sorption were calculated from the isotherms at 193.7° and 273.1° K for the 400°-activated powder and these are shown in Fig. 3. For both gases, the heat of sorption appears to be essentially independent of concentration—a result similar to the general conclusions of Barrer and Sutherland (9) from much more extensive work on synthetic faujasite. There is a suggestion of a slight stepwise decrease at intervals of about 12 cc per g corresponding to integral numbers of molecules per cavity. Our value for nitrogen is somewhat lower and less concentration dependent than that given by Breck *et al.* (5).

Lattice Swelling during Sorption

An attempt was made to detect any expansion of the crystal lattice accompanying sorption. Using a Norelco X-ray diffractometer with a Geiger counter scanner the 832 and 910 reflections were examined relative to the 122 quartz line which fell between them. A dehydrated sample of the zeolite was allowed slowly to hydrate in the diffracto-

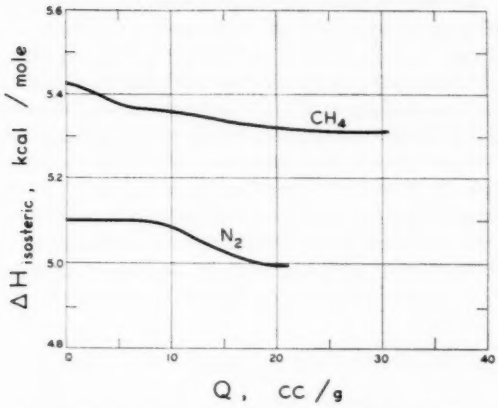

FIG. 3. Isosteric heats of sorption from isotherms at 193.7 and 273.1° K.

meter while the lines were scanned back and forth. The first measurements were taken about two minutes after the sample was opened to the air and from then until complete hydration there was no apparent change (±0.005 Å) in the unit cell spacing. (The value of 12.30 Å compares with 12.32 Å reported by Reed and Breck (6).) Observed expansions accompanying sorption of water on porous glass (10) and on carbon (11) are of the order of 0.2 to 0.3%. Other sorbates at higher pressures give similar expansion. With a maximum change of 0.05%, the crystalline zeolite appears to be more rigid than either of these amorphous materials.

Kinetic Properties—Pure Gases

As Barrer has shown (12), the slow step in these processes may be described as a process of diffusion. The amount of gas sorbed, Q, is found to be proportional to the square root of the time for as much as 50% of the total uptake. From this initial gradient, a diffusion coefficient may be calculated in the usual way according to the following equation:

$$D = \pi\left[\frac{V}{2A\,(C_0-Q_0)}\frac{dQ}{d(t^{\frac{1}{2}})}\right]^2. \qquad [1]$$

D, the diffusion coefficient, is defined by Fick's first law of diffusion

$$J = -D\,(\partial C/\partial x), \qquad [2]$$

where J is the flux of diffusing material and C is the concentration, expressed for the present work in cc (S.T.P.) per g of sorbent. C_0, the concentration at the outer surface, is taken as the equilibrium concentration from the sorption isotherm and Q_0 is the initial uniform concentration which may be zero. A and V are the external area and volume respectively of the sorbent particles. If D varies with concentration equation 1 gives an approximate average value over the concentration interval Q_0 to C_0. Crank (13) has discussed the evaluation of D as a function of C from a series of such measurements.

Obviously, for a given sample of sorbent, relative values of $D^{\frac{1}{2}}$ may be obtained from the ratio between $dQ/d(t^{\frac{1}{2}})$ and (C_0-Q_0).

The variation of D with concentration for each gas alone was examined for both

powder and pellets.* Results for 350°-activated powder at 0° and −79° and for 400°-activated pellets at 0° are shown in Fig. 4. Measurements with the powder were made with constant C_0 and varying Q_0 and the individual measurements are shown as light horizontal lines over the range Q_0 to C_0 together with the fitted curve of D vs. C. Over the shorter concentration ranges at 0° no variation with concentration was found. Measurements with the powder were all made for $Q_0 = 0$ and the curve of D was obtained from the individual measurements according to the method described in Crank (13). Also shown in Fig. 4 are single values at each temperature for a powder sample activated at 400°, which was used for sorption from mixtures. Pellets activated at 300° gave D values about one quarter those for the 400° material and the isotherms were about 10% lower. A similar sensitivity appeared to exist for the powder.

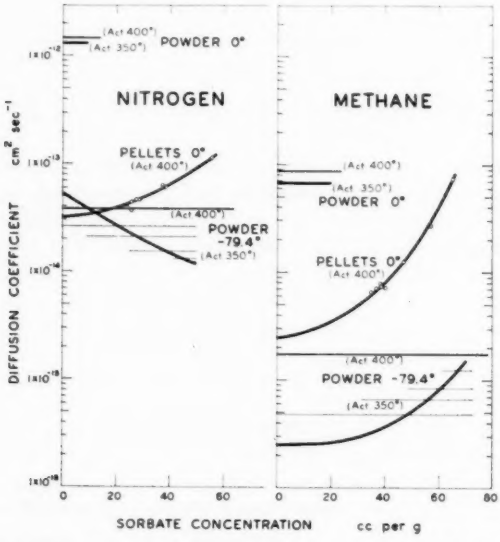

FIG. 4. Diffusion coefficients for pure nitrogen and pure methane. The light horizontal lines show individual measurements over the indicated concentration ranges. The measurements with the pellets were all made between 0 and the concentrations shown by the circles.

Diffusion coefficients for the pellets are seen to be considerably lower than for the powder. It is unlikely at these pressures (2 atmospheres and higher) that there is significant gas phase diffusional resistance in the intercrystalline pores of the pellets. All properties of the pellet form, the larger isobutane surface area, the slower rates of sorption, and the lower capacities, are consistent with the presence of some amorphous, non-sorbing binder, which, while adding to the total external surface, seals off part of the crystal surface through which sorption occurs.

Most of the measurements with the pure gases were made under constant volume conditions where the pressure, and hence C_0, changes with time. As a result, the $Q-t^{\frac{1}{2}}$ plots begin to curve somewhat more quickly than with constant pressure sorption. The initial gradient is still given by equation 1, taking C_0 for zero time, and it can be shown (cf. ref. 13, pp. 31, 86) that the correction term to Q at time t near the beginning is approximately $(\pi t/4C_0)[dQ/d(t^{\frac{1}{2}})]_{t=0}[dC_0/d(t^{\frac{1}{2}})]$. By properly choosing the total volume of the system and the size of the sample, this correction at t = 1 minute can be kept within a few per cents.

In general D increases with sorbate concentration. The one case of decreasing D was associated with an anomalous isotherm so that there is some uncertainty concerning its validity.

Relatively little has been reported previously for the concentration dependence of diffusion coefficients in dehydrated zeolites. Barrer and Brook (14) studying the sorption of several gases by chabazite found all the average diffusion coefficients to decrease with concentration—in some cases by a factor of 100. Barrer and Riley (15) for a synthetic chabazite-like zeolite found D to vary approximately as $(1-\theta)$, where θ is the fractional saturation. Tiselius (16) reported D for water in heulandite to increase rapidly with concentration and for ammonia in analcite (17) to be independent of concentration.

Activation energies for diffusion may be estimated from the diffusion coefficients for zero concentration. For the 350°-activated powder the following expressions are obtained:

$$\text{nitrogen: } D = 2.3\times10^{-9}\exp(-4070/RT),$$
$$\text{methane: } D = 5.8\times10^{-8}\exp(-7420/RT).$$

The D_0 values are of the same order as those reported for diffusion in chabazite (14).

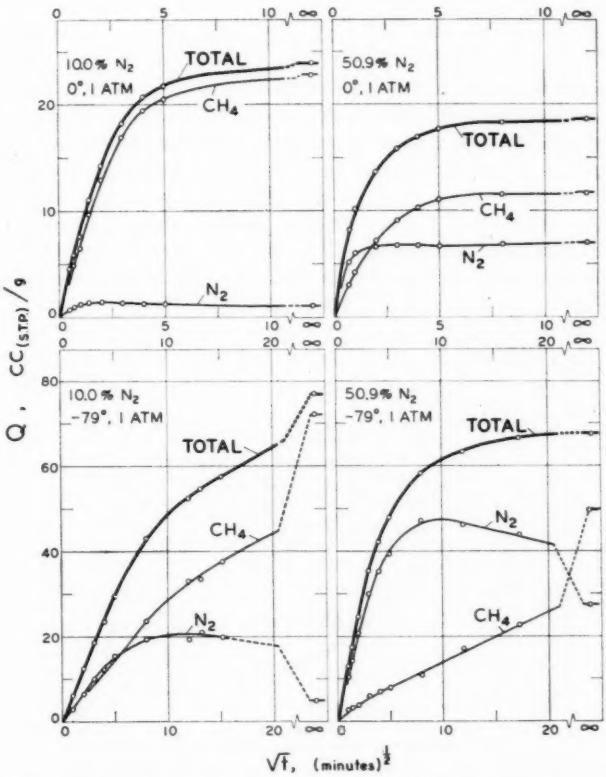

FIG. 5. Sorption from mixtures at 193.7° and 273.1° K. Zeolite powder activated at 400° C.

The activation energies are close to the 3.5 and 7.5 kcal that Kington and Laing (29) calculated as one set of possible values for diffusion in chabazite.

Mixtures

Sorption from mixtures containing 10.0% nitrogen and 50.9% nitrogen at 1 atmosphere and at 0° and −79.4° C is summarized in Figs. 5 and 6. The sample of powdered zeolite was activated at 400° C and gave equilibrium sorptions in agreement with the Langmuir isotherms in Table I. Relative diffusion coefficients for the pure gases were measured only at 1 atmosphere.

The most striking feature of these measurements is the maximum in the total nitrogen sorption, which occurs at a time prior to the establishment of complete equilibrium. This is seen in Fig. 5 only for the lower temperature, it may occur also at 0° but at a very short time where measurements are difficult to get. Measurements with samples of the pelleted zeolite (which had lower diffusion coefficients) did show a distinct maximum in the nitrogen sorption from a 10% mixture at 0°. As can be seen in Fig. 5, the initial sorption of each component is approximately linear in $t^{\frac{1}{2}}$, although less so than for the pure gases.

The degree of separation achieved by sorption from a mixture is often described by a separation factor, α, defined as follows:

$$\alpha_{N_2} = (X_{CH_4}/X_{N_2})\,(Y_{N_2}/Y_{CH_4}), \qquad [3]$$

where X and Y are the mole fractions in the gas and sorbed phases respectively. Y, of course, is an average value over the crystal, which will be uniform only at equilibrium. As shown in Fig. 6, α decreases from an initial value indicating nitrogen enrichment in the sorbed phase to an equilibrium value showing preferential sorption of methane. The value at low times is uncertain; gas diffusion resistances and depletion of the gas phase will tend to make it low; if the individual sorptions from a mixture are each truly initially linear with $t^{\frac{1}{2}}$, α should remain constant.

Fig. 7 shows plots of the variation of α with time for several experiments with the

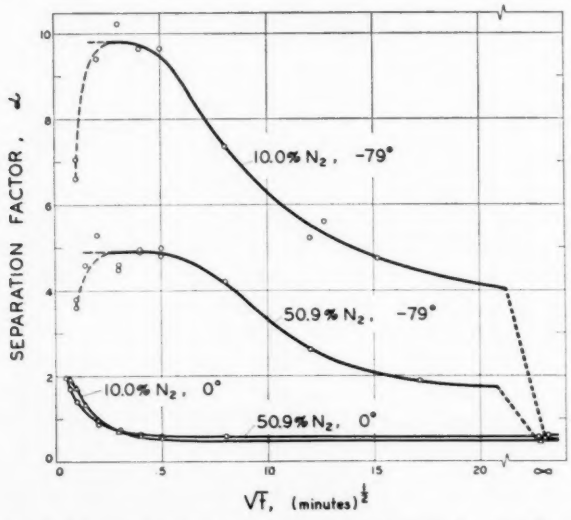

FIG. 6. Separation factors for sorption from mixtures shown in Fig. 5.

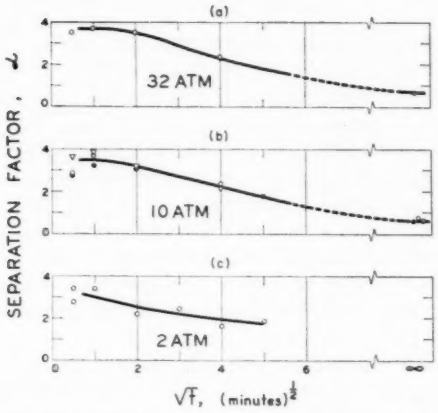

FIG. 7. Separation factors for sorption from 10.0% nitrogen mixture at 273.1° K with zeolite pellets. The different symbols for sorption at 10 atm refer to different sorbent activities.

zeolite pellets. These are very similar to those for the powder, although the actual sorption rates are much lower.

From the initial gradient of each component one may, formally at least, calculate a diffusion coefficient using equation 1 and taking for C_0 the equilibrium sorption for that component. The ratio of diffusion coefficients may also be expressed in terms of the separation factors as follows

$$\alpha_{\text{initial}} = \alpha_{\text{equilibrium}} (D_{N_2}/D_{CH_4})^{\frac{1}{2}}. \qquad [4]$$

Diffusion coefficients thus determined in the mixture are compared with the values for the pure gases in Table II. It can be seen that while methane appears to have the same apparent D in the mixture as alone, nitrogen has a much enhanced value and thus the ratio is also higher. Since the increase in the apparent D for nitrogen is dependent also on the gas phase composition the simple approach of using the pure gas values for D in equation 4 is not satisfactory for predicting the behavior of mixtures.

TABLE II

DIFFUSION OF PURE GASES AND MIXTURES

Sorbent: molecular sieve 4A powder activated at 400° C

Temp., ° K	Gas	$(1/C_0)[dQ/d(t^{\frac{1}{2}})]$ min$^{-\frac{1}{2}}$	$(D_{N_2}/D_{CH_4})^{\frac{1}{2}}$	$\alpha_{\text{initial}}/\alpha_{\text{equilibrium}}$
273.1	N_2 (pure)	1.195		
	CH_4 (pure)	0.295	4.05	—
	N_2 in 10.0% mixture	1.3		
	CH_4 in 10.0% mixture	0.304	4.1	*
	N_2 in 50.9% mixture	1.17		
	CH_4 in 50.9% mixture	0.35	3.34	*
193.7	N_2 (pure)	0.194		
	CH_4 (pure)	0.0417	4.67	—
	N_2 in 10.0% mixture	0.678		
	CH_4 in 10.0% mixture	0.0402	16.9	16.0
	N_2 in 50.9% mixture	0.376		
	CH_4 in 50.9% mixture	0.0368	10.2	9.3

*The initial rates were too high at 273° to give an independent value of the initial separation factor.

DISCUSSION

Diffusion phenomena are usually approached from the point of view of Fick's Law (equation 2) even though in practice the resultant diffusion coefficient is markedly concentration-dependent. As a rule this is not too serious a drawback in view of the extensive experience and mathematical methods which have been accumulated to interpret measurements and to predict diffusion rates for different types of variation of D with concentration. However in the present system the Fick's Law approach is seriously inadequate. Not only are the diffusion coefficients in the mixture different from those for the pure gases but this approach can give no indication that the total sorption of the faster moving component (nitrogen) passes through a maximum before the final equilibrium is reached. The existence of such a maximum means that, in part, diffusion must be occurring under a negative Fick diffusion coefficient—a very uncommon, if not unique, situation.

It is therefore worth while to examine an alternative approach to diffusion. The chemical potential was suggested by Hartley in 1931 (18) as the fundamental driving force for electrolytic diffusion, and other sorts of diffusion have since been considered as flow under a gradient in chemical potential (19, 20, 21, 22). The chemical potential would appear also to be the driving force suggested by the methods of the thermodynamics of irreversible processes (23, 24), although this approach has not been carried through in detail for diffusion of adsorbed films. Babbitt (25, 26, 27) has approached diffusion from a hydrodynamical point of view and considers the surface diffusion of an adsorbed film as due to the gradient in spreading pressure.

The spreading pressure and the chemical potential of an adsorbed film are similar potential functions and are related as follows (28):

$$d\phi = \Gamma_A d\mu_A + \Gamma_B d\mu_B,$$

where ϕ is the spreading pressure, Γ is the concentration of adsorbate in moles per unit area, μ is the chemical potential, and A and B are two adsorbates. For a single adsorbate, the gradient in spreading pressure is therefore equal (apart from a constant factor) to the gradient in chemical potential multiplied by the adsorbate concentration. If, following other authors (18, 19, 20, 21, 22), we assume that the velocity of diffusion is proportional to the gradient in chemical potential, the two approaches are essentially equivalent in taking as the law of diffusion:

$$J = Cv = -CL\,(\partial\mu/\partial x), \qquad [5]$$

where J is the total flux of diffusing material in the x-direction in moles per unit time through unit cross-sectional area, C is the adsorbate concentration in moles per unit volume, v is the average diffusion velocity, and L is a proportionality constant.

For ideal gas diffusion or for diffusion in a mobile monolayer (27) this expression is equivalent to Fick's Law. For an adsorbed film obeying the Langmuir isotherm

$$\partial\mu/\partial x = (\partial\mu/\partial C)(dC/dx) = (RT/p)(dp/dC)(dC/dx),$$

where p is the partial pressure of the gas (assumed ideal) in equilibrium with sorbed phase of concentration C. This gives for the flux of diffusion

$$J = Cv = -[RTL/1-\theta](dC/dx), \qquad [6]$$

where $\theta = C/C_{\text{monolayer}}$. This result is identical with the one Babbitt obtained taking a constant resistive force per molecule. By comparison with equation 2 it is seen that

the Fick diffusion coefficient should accordingly vary as $1/(1-\theta)$, which is roughly what the present results show.

One might expect L to vary with concentration if, for example, there is any change in the openings in the crystal channels accompanying sorption. In view of the X-ray measurements reported above and the calculations of Kington and Laing (29) for chabazite, it is unlikely that the change in activation energy for diffusion would be more than 100 cal, or beyond experiment error. A difficulty remains of explaining the strong decrease in D which Barrer observed. He suggested, in effect, an additional entropy term (30) but this, presumably, is already included in the chemical potential function.

Mixtures

Let us now consider the sorption of a mixture of gases, A and B, as occurring under a gradient in chemical potential. The simplest approach is to assume that the flux of A is still given by equation 5, where the concentration and chemical potential are for A in the mixed sorbed phase. One could allow for an interaction with the other gas by assuming a more general expression:

$$J_A = C_A v = -C_A [L_{AA}(\partial\mu_A/\partial x)+L_{AB}(\partial\mu_B/\partial x)].$$

There is at present no evidence to justify such an extension so L_{AB} will be taken as zero. The presence of B will none the less affect the diffusion of A, since it is included in the mixed Langmuir isotherm

$$p_A = \theta_A/b_A(1-\theta_A-\theta_B).$$

Proceeding as before, using the chemical potential for the gas in equilibrium with C_A and C_B, we obtain

$$J_A = -[RTL_A/(1-\theta_A-\theta_B)]\,[(1-\theta_B)(dC_A/dx)+\theta_A(dC_B/dx)] \qquad [7]$$

with an analogous expression for J_B, the flux of B.

This equation is adequate to explain the observed behavior in a qualitative way. Fig. 8 suggests the distribution of nitrogen and methane with distance from the external crystal surface at different times in the early stages of sorption. The relative amounts of the two substances are proportional to the actual values for a 10% nitrogen mixture at $-79°$ C. Fig. 8 (*a*) is the hypothetical case of methane being unable to penetrate the lattice and θ_B being 0 everywhere but at the outer surface. Figs. (*b*) and (*c*) represent successive stages in the real situation. In region 1 a positive flux of A exists because although $-dC_A/dx$ is negative, $-dC_B/dx$ is strongly positive, and hence the sum of the two terms in equation 7 is positive. In the same region the flux of B will be less than that of pure B because of the negative value of $-dC_A/dx$. In region 2 $-dC_B/dx$ becomes smaller while $-dC_A/dx$ changes from negative to positive and hence a positive flux of A remains. In region 3 the situation is essentially diffusion of a single gas.

An alternative qualitative approach is to consider the equilibrium distribution of A corresponding to any given distribution of B (dashed lines in Fig. 8). The driving force for diffusion of A is a function of the gradient in the difference between this equilibrium concentration and the actual concentration. This gradient is always negative as in ordinary diffusion.

The uptake of A from a mixture is greater than from pure A at a pressure giving the same exterior surface concentration. Because of the high local concentrations the sorption of A may for a time exceed the equilibrium value at the surface, hence the observed

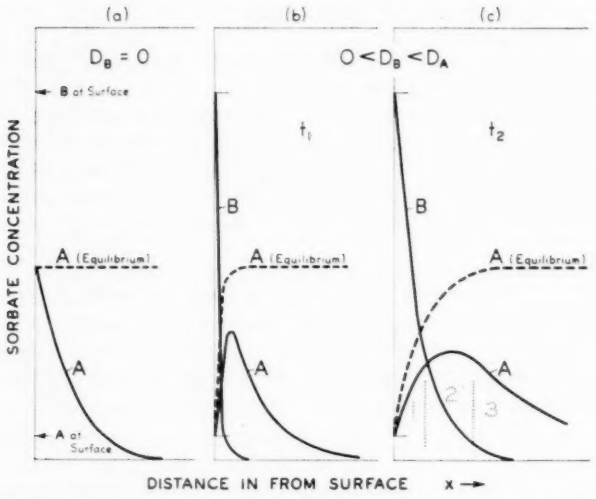

FIG. 8. Sorption from mixtures. Distribution of the sorbates within the crystal. Qualitative curves for 10% nitrogen mixture at 193.7° K. (*a*) Hypothetical case $D_{CH_4} = 0$; (*b*) and (*c*) successive distributions in the actual situation.

maximum. This maximum is more pronounced with the 10% than with the 50% nitrogen mixtures because the curvature of the isotherms gives a greater relative advantage to low partial pressures of nitrogen.

The slower gas, according to equation 7, should be somewhat retarded in the mixture. This appears to be so in the 50% mixture but the evidence is inconclusive.

In view of the complexity of the relationship between the Fick diffusion coefficient and concentration, it is somewhat surprising that the initial sorption-$t^{\frac{1}{2}}$ relationship holds as well as it does. The measurements suggest a somewhat S-shaped plot. An integration of equation 7 for the two species would be necessary to establish the precise shape and hence to quantitatively test this approach.

One may say, in general, that the distinctive feature of the diffusion of a mixture of gases into a porous solid is competition for the limited surface. Consequently, merely specifying the concentration of one sorbate is not a complete description and we may have the apparently anomalous flow of material from regions of low to high concentration. This paper has attempted to show that, qualitatively at least, these anomalies are removed by treating diffusion as flow under a gradient in chemical potential.

ACKNOWLEDGMENTS

I wish to thank R. A. Mooney, E. Dutcher, and G. A. Argue for carrying out much of the experimental work, H. Hansen and Dr. L. B. Halferdahl for assistance with the X-ray diffraction measurements.

REFERENCES

1. BARRER, R. M. Quart. Revs. (London), **3**, 293 (1949); Brennstoff-Chem. **35**, 325 (1954).
2. BARRER, R. M. and ROBINS, A. B. Trans. Faraday Soc. **49**, 807, 929 (1953).
3. HIRCHFELDER, J. O., CURTISS, C. F., and BIRD, R. B. Molecular theory of gases and liquids. John Wiley & Sons, Inc., New York. 1954. p. 1110.
4. NAY, M. A. and MORRISON, J. L. Can. J. Research, B, **27**, 205 (1949).

5. BRECK, D. W., EVERSOLE, W. G., MILTON, R. M., REED, T. B., and THOMAS, T. L. J. Am. Chem. Soc. **78**, 5963 (1956).
6. REED, T. B. and BRECK, D. W. J. Am. Chem. Soc. **78**, 5972 (1956).
7. LAMB, A. B. and WOODHOUSE, J. C. J. Am. Chem. Soc. **58**, 2637 (1936).
8. BARRER, R. M. and REES, L. V. Trans. Faraday Soc. **50**, 852, 989 (1954).
9. BARRER, R. M. and SUTHERLAND, J. W. Proc. Roy. Soc. A, **237**, 439 (1956).
10. AMBERG, C. H. and MCINTOSH, R. Can. J. Chem. **30**, 1012 (1952).
11. FLOOD, E. A. Can. J. Chem. **35**, 48 (1957).
12. BARRER, R. M. Trans. Faraday Soc. **45**, 358 (1949).
13. CRANK, J. The mathematics of diffusion. The Clarendon Press, Oxford. 1956. Chap. XI.
14. BARRER, R. M. and BROOK, D. W. Trans. Faraday Soc. **49**, 1049 (1953).
15. BARRER, R. M. and RILEY, D. W. J. Chem. Soc. 133 (1948).
16. TISELIUS, A. J. Phys. Chem. **40**, 223 (1936).
17. TISELIUS, A. Z. physik. Chem. A, **174**, 401 (1935).
18. HARTLEY, G. S. Phil. Mag. **12**, 473 (1931).
19. HARTLEY, G. D. and CRANK, J. Trans. Faraday Soc. **45**, 801 (1949).
20. HARNED, H. S. Chem. Revs. **40**, 461 (1947).
21. CARMAN, P. C. and STEIN, L. H. Trans. Faraday Soc. **52**, 619 (1956).
22. BOSWORTH, R. C. L. Transport processes in applied chemistry. John Wiley & Sons, Inc., New York. 1956. p. 118.
23. DE GROOT, S. R. Thermodynamics of irreversible processes. North-Holland Pub. Co., Amsterdam. 1951. p. 104.
24. PRIGOGINE, I. Thermodynamics of irreversible processes. Charles C. Thomas, Publisher, Springfield, Ill. 1955. p. 72.
25. BABBITT, J. D. Can. J. Research, A, **28**, 449 (1950).
26. BABBITT, J. D. Can. J. Phys. **29**, 427 (1951).
27. BABBITT, J. D. Can. J. Phys. **29**, 437 (1951).
28. FOWLER, R. and GUGGENHEIM, E. A. Statistical thermodynamics. Cambridge: The University Press, London. 1939. p. 423.
29. KINGTON, G. L. and LAING, W. Trans. Faraday Soc. **51**, 287 (1955).
30. BARRER, R. M. Trans. Faraday Soc. **37**, 590 (1941).

RADIATION CHEMISTRY OF SOLUTIONS

II. DOSE-RATE, ENERGY, AND TEMPERATURE DEPENDENCE OF A LEUCO TRIARYLMETHANE DOSIMETER SOLUTION[1]

W. A. Armstrong and G. A. Grant

ABSTRACT

The dose-rate, energy, and temperature dependence of the system 10^{-4} *M* 4,4′-(5-chloro-2-thenylidene)bis[N,N-dimethylaniline], 10^{-4} *M* ferrous ammonium sulphate, 0.1 *M* sodium chloride, and 7×10^{-3} *M* hydrochloric acid has been investigated. No energy dependence was observed in the range 0.16 to 2.0 Mev and no dose-rate dependence was observed in the range 4 to 230 rads/minute. However, with dose rates of 400 to 1200 rads/minute, postirradiation dye fading was observed. In the dosage range 0 to 1000 rads this fading is not extremely serious. The system is slightly temperature dependent at temperatures lower than 30° C and markedly dependent at higher temperatures. Dye yields of samples irradiated at 30° C were 10% higher than those of samples irradiated at 15° but 33% lower than those of samples irradiated at 45°.

INTRODUCTION

In a previous report (2), the effects of gamma radiation on acidic aqueous solutions of a number of 4,4′-thenylidene bis[N,N-dimethylaniline] compounds were described. Of the systems studied, the one best suited for dosimetric purposes consisted of 10^{-4} *M* 4,4′-(5-chloro-2-thenylidene)bis[N,N-dimethylaniline], 10^{-4} *M* ferrous ammonium sulphate, 0.1 *M* sodium chloride, and 7×10^{-3} *M* hydrochloric acid. With this system, the dye yield, as measured by the optical density at the main absorption peak of 633 mμ, increases linearly with increasing doses from zero to at least two thousand rads.

The common failing of most dosimeters developed for use in the low dosage range is their dose-rate and energy dependence. This is particularly true of systems based on acid formation from the decomposition of chlorinated hydrocarbons (4, 5, 6) where the mechanism involves a chain reaction. With this type of system it is necessary to shield out low-energy radiation and add some chain-breaking inhibitor.

Although the calculated *G* value of approximately one for the aqueous leuco system indicates the absence of chain reactions, the complicated mechanism is such that other factors might lead to dose-rate and energy effects. The present investigation was undertaken to determine the energy, dose-rate, and temperature dependence of the system.

EXPERIMENTAL

The radiation sources used to obtain the desired range of energies and dose rates are listed below:

1 curie of Cs^{137}	300 Kev Muller X-ray machine
150 curies of Co^{60}	2 Mev General Electric X-ray machine
300 curies of Co^{60}	2 curies of Cs^{137}

Procedure

The preparation of the system 10^{-4} *M* 4,4′-(5-chloro-2-thenylidene)bis[N,N-dimethylaniline], 10^{-4} *M* ferrous ammonium sulphate, 0.1 *M* sodium chloride, and 7×10^{-3} *M* hydrochloric acid has been described elsewhere (2). Solutions were found to be slightly

[1]*Manuscript received May 23, 1958.*
Contribution from Defence Research Board, Defence Research Chemical Laboratories, Ottawa, Ontario.
Issued as D.R.C.L. Report No. 257.

light sensitive but blanks showed no change in color during the time required to complete an irradiation (as long as seven hours in a lighted room). Pyrex tubes of 9 mm inside diameter containing 3.3 ml of solution were used throughout. These tubes had a wall thickness of 2 mm, sufficient to ensure that electronic equilibrium was attained during the irradiations.

All dose rates were determined with Fricke ferrous sulphate, 0.8 N sulphuric acid dosimeter solution. The yield of ferric ion was measured spectrophotometrically by its own absorption at 304 mμ. Dose rates were calculated as shown below.

$$\text{Dose rate} = (\eta Fe^{+3}/t) \cdot (100/G) \cdot (1.602\times10^{-12}/100) \text{ rads/minute}$$

where t = irradiation time in minutes,
G = yield of Fe^{+3} = 15.5 molecules per 100 ev,
ηFe^{+3} = number of ferric ions per gram,
$= (6.023\times10^{23}/\epsilon\times1\times1000\times d) \cdot D_s - D_b$ ions/g,

where ϵ = molar extinction coefficient,
1 = path length of spectrophotometer cell,
D_s = optical density of irradiated sample,
D_b = optical density of blank,
d = density of solution.

Thus dose rate $= 9.649\times10^{5} \cdot [(D_s - D_b)/G.\epsilon.1.d.t]$ rads/minute.

The energy absorbed in our system (E_S) can be related to the energy absorbed in the ferrous sulphate dosimeter (E_D) by the following equation:

$$E_S = E_D \cdot \mu_S/\mu_D$$

where μ_S = mass absorption coefficient of the system,
= mass absorption coefficient of 0.1 M sodium chloride.
μ_D = mass absorption coefficient of ferrous sulphate dosimeter,
= mass absorption coefficient of 0.8 N sulphuric acid.

For 160 Kev photons $\mu_S/\mu_D = 0.1479/0.1478 = 1.0007$ and for 1 Mev photons $\mu_S/\mu_D = 0.06336/0.06321 = 1.0024$. Hence for irradiations using the available sources previously mentioned $E_S = E_D$ to within 0.2%.

The housing and use of the 1-curie Cs^{137} source has been previously described (2). Eight sample tubes may be placed around this source and irradiated with gamma rays of 0.66 Mev effective energy at a dose rate of approximately five rads/minute.

The 150-curie Co^{60} source has been described by Aitken, Dyne, and Trapp (1). Three capsules, each containing about fifty curies, form a ring around the sample space. The capsules are attached to adjuster rods and the radiation flux is varied by moving the adjuster rods. Samples to be irradiated are placed on a lead piston and lowered into position. The introduction or removal of a sample requires less than one second. Samples can be irradiated at dose rates of 400 to 2000 rads/minute.

The 300-curie Co^{60} source is designed to give a narrow horizontal beam with a dose rate of 130 rads/minute at the collimator mouth. Because of the narrow field and the uncertain time required to swing the source into position, only one run was made with this source.

The Muller X-ray machine was operated at 300 kv and 10 ma. The beam was filtered to give radiation of 160 Kev effective energy, as measured in copper. With this arrangement samples can be irradiated at a maximum dose rate of 235 rads/minute.

The General Electric machine was operated at 2 Mev and 1.5 ma and the unfiltered radiation used. The dose rate from this machine is very high, being 1000 rads/minute at a distance of 45 cm from the target. As it took approximately five seconds for the machine to reach operating conditions, doses of the desired magnitude (0 to 2000 rads) could not be measured as accurately as with the other radiation sources.

The temperature-dependence studies were performed using a 2-curie Cs^{137} source. The source is placed in the center post of a lucite box. Eight sample tubes may be placed in the box around the source each tube being $1\frac{3}{4}$ in. from it. Water from a constant-temperature bath is pumped through the box during irradiation. With this arrangement samples are irradiated at a rate of approximately 250 rads per hour.

RESULTS

1. Dose-Rate Dependence

Samples were irradiated with 160 Kev X-rays at dose rates of 6, 20, 90, and 235 rads per minute. The results plotted in Fig. 1 as dye yields recorded as optical densities measured at 633 mμ against dose in rads show no dose-rate dependence in this range.

Higher dose rates were obtained with the 150-curie Co^{60} source. Irradiations were made using dose rates of 400, 790, and 1200 rads/minute. Optical densities were measured 15 minutes after irradiation and again $\frac{3}{4}$ hour later. As illustrated in Fig. 2, there is a considerable postirradiation dye fading at these dose rates. However the degree of fading is the same, within the range of experimental error, for each of these dose rates. Results obtained with a dose rate of 4 rads/minute using the 300-curie Co^{60} source are also included in Fig. 2. No dye fading was observed at this dose rate. Optical densities measured 15 minutes after irradiation at dose rates of 400 rads/minute or greater are about 8% higher than those measured after irradiation at dose rates of 4 rads/minute, while optical densities measured 1 hour after irradiation at dose rates of 400 rads/minute or greater are about 8% lower than those measured after irradiation at dose rates of 4 rads/minute. The results of a further study of postirradiation dye fading are given in Table I.

TABLE I

EFFECT OF TIME OF MEASUREMENT AND DOSE ON OPTICAL DENSITY
(Dose rate = 1200 rads/minute)

Time after irradiation, hr	Optical density, rads							
	302	604	906	1208	1510	1812	2114	2416
0.08	0.030	0.066	0.094	0.120	0.134	0.164	0.196	0.220
0.25	0.029	0.058	0.090	0.114	0.143	0.168	0.199	0.227
0.50	0.029	0.055	0.084	0.107	0.133	0.161	0.187	0.209
1.00	0.028	0.055	0.079	0.098	0.122	0.138	0.168	0.193
1.50	0.030	0.050	0.076	0.094	0.113	0.132	0.159	0.184
2.00	0.030	0.052	0.072	0.093	0.114	0.132	—	—
3.00	0.032	0.052	0.072	0.093	0.116	0.133	—	—
20.0	0.032	0.052	0.072	0.090	0.108	0.123	0.143	0.163

These results indicate that the dye concentration reaches a maximum prior to 15 minutes after irradiation, decreases for the next one to two hours, after which it changes only slightly.

A number of changes in the system were made in an attempt to decrease the after reaction. Increasing the leuco concentration from 10^{-4} M to 5×10^{-3} M increased the

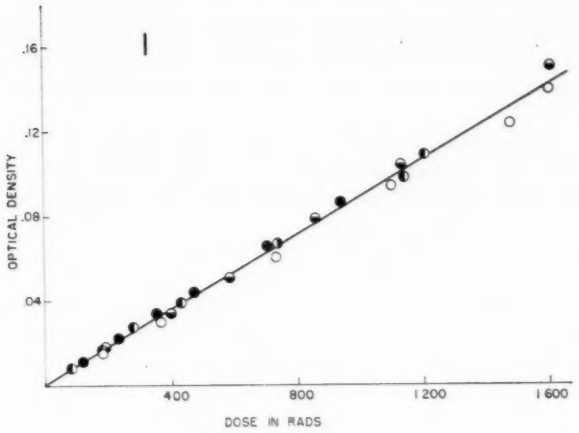

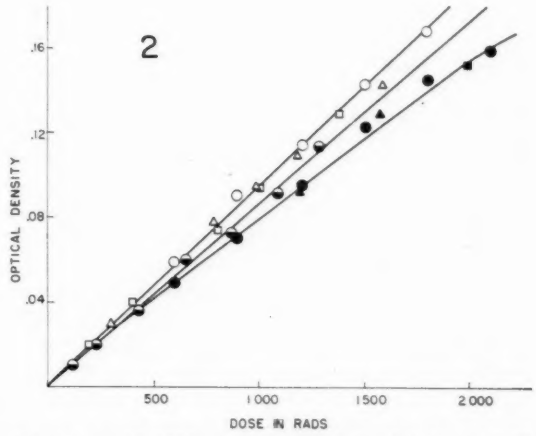

FIG. 1. Effect of dose rate with 160 kev irradiation: ○ 6 rads/minute, ◒ 20 rads/minute, ◐ 90 rads/minute, ● 235 rads/minute.

FIG. 2. Effect of dose rate with 1.25 Mev irradiation: ◒ 4 rads/minute, □ 400 rads/minute, △ 790 rads/minute, ○ 1200 rads/minute. Open symbols indicate measurements made 15 minutes after irradiation, darkened symbols 1 hour after irradiation.

amount of dye fading. With this system, the optical density of a sample which received a dose of 1000 rads at a dose rate of 1200 rads/minute decreased by 30% during the first hour following irradiation. Decreasing the sodium chloride concentration decreased greatly the sensitivity of the system and did not eliminate fading.

The effect of high dose rates on the corresponding trifluoroacetic acid system was also investigated. The system consisted of 10^{-4} M 4,4′-(5-chloro-2-thenylidene)bis[N,N-dimethylaniline], 10^{-4} M ferrous ammonium sulphate, 0.1 M sodium chloride, and 5×10^{-3} M trifluoroacetic acid. Dose-rate effects are shown in Fig. 3. As well as showing postirradiation fading, dye yields for doses received at 1200 rads/minute were about 18% lower than for doses received at 5 rads/minute.

2. Energy Dependence

In Fig. 4, dye yields recorded as optical densities are plotted against dose in rads for primary energies of 0.160, 0.660, and 1.25 Mev. Dose rates were approximately five rads/minute in each case. There is no detectable energy dependence in the range 0.160 to 1.25 Mev.

Because of the machine design, irradiation with 2 Mev X-rays at this low dose rate was not possible and dye fading at high dose rates made it difficult to compare yields with those obtained using lower-energy radiations. However, as shown in Fig. 5, optical

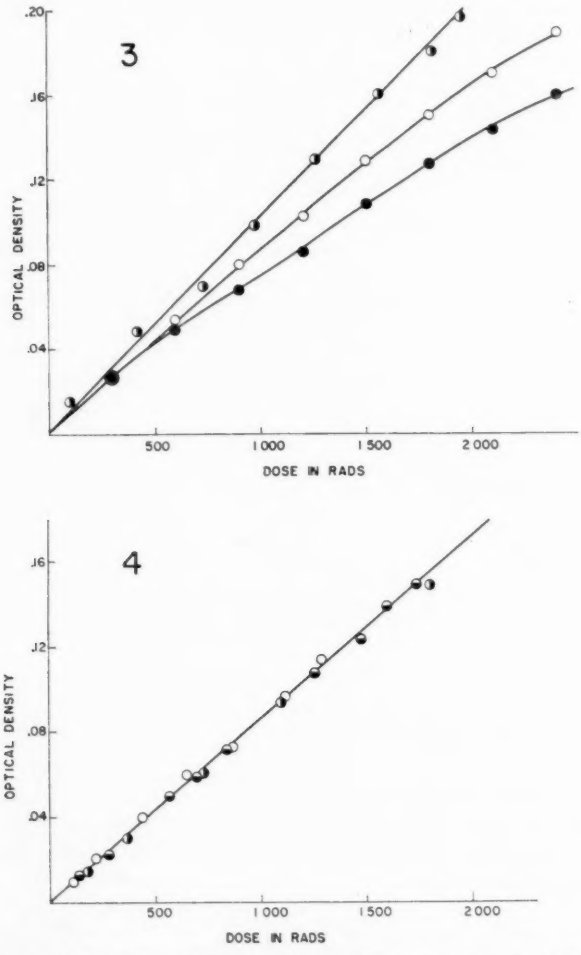

FIG. 3. Effect of high dose rate on the postirradiation stability of trifluoroacetic acid dosimeter solution: ◑ 5 rads/minute (Cs^{137} γ-rays), ○ 1200 rads/minute (Co^{60} γ-rays) (measurements made 15 minutes after irradiation), ● 1200 rads/minute (measurements made 3 hours after irradiation).

FIG. 4. Effect of energy at low dose rates (5 rads/minute): ◑ 0.16 Mev X-rays, ◒ 0.66 Mev γ-rays (Cs^{137}), ○ 1.25 Mev γ-rays (Co^{60}).

densities of solutions irradiated in one case with 1.25-Mev γ-rays at 1200 rads/minute and in the other with 2-Mev X-rays at 920 rads/minute, when remeasured at corresponding times after irradiation, show no variation attributable to energy effects.

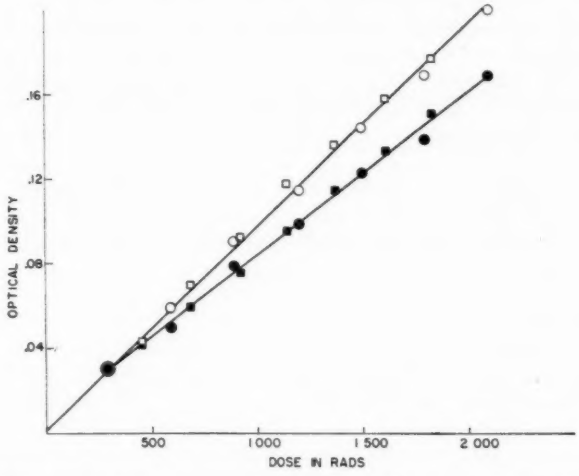

FIG. 5. Effect of energy at high dose rates (1000 rads/minute): ○ 1.25 Mev γ-rays (1200 rads/minute), □ 2 Mev X-rays (920 rads/minute). Open symbols indicate measurements made 15 minutes after irradiation, darkened symbols 1 hour after irradiation.

3. Temperature Dependence

Samples thermostated at temperatures from 15° to 45° C were irradiated with Cs^{137} γ-rays and optical densities measured after samples had been brought to room temperature. The optical densities of samples at various temperatures receiving given doses are listed in Table II. The slope of a plot of optical density vs. dose for each temperature is also given. The system is slightly temperature dependent at temperatures lower than 30° C and markedly dependent at higher temperatures. Raising the temperature from 20° to 30° C increases the dye yield per rad approximately 6%. However raising the temperature from 30° to 45° C increases the dye yield per rad approximately 22%.

TABLE II

EFFECT OF TEMPERATURE ON DYE YIELDS

Dose, rads	Optical density						
	15°	20°	25°	30°	35°	40°	45°
141	0.014		0.016	0.014	0.014	0.019	0.020
280	0.020	0.022	0.024	0.024	0.026	0.030	0.036
548	0.038	0.047	0.049	0.052	0.051	0.060	0.073
765	0.061	0.063	0.069	0.065	0.073	0.082	0.100
1002	0.079	0.085	0.091	0.090	0.098	0.110	0.134
1335	0.106	0.108	0.116	0.117	0.125	0.135	0.170
1639	0.128	0.133	0.138	0.142	0.152	0.170	0.213
1832	0.143	0.152	—	0.157	0.176	0.190	0.232
1919	0.153	0.155	0.169	0.165	0.182	0.194	0.236
Slope	7.85	8.15	8.63	8.63	9.40	10.55	12.87

DISCUSSION

As the mechanism of this system is not completely clear, the postirradiation fading at dose rates higher than 200 rads/minute cannot be wholly explained. Studies of the oxidation potential of the leuco compound (3) indicate that destructive oxidation of the dye occurs near the oxidation potential of the leuco compounds. Hence species formed during radiolysis which will oxidize the leuco compound may also be capable of destroying the dye. The dye fading at high dose rates is then probably due to the build-up in concentration of a dye-destroying species of relatively long life. The temperature dependence also supports the suggestion of the presence of a long-lived reactive species.

The postirradiation fading is not too serious in the range 0–1000 rads. Optical densities measured 15 minutes to 24 hours after irradiation at dose rates of 400–1200 rads/minute are within 8% of values obtained after irradiation at dose rates of 5–230 rads/minute. Optical densities measured at times greater than $1\frac{1}{2}$ hours after irradiation at high dose rates are within 2% of each other and are 6% to 8% lower than values obtained with low dose-rate exposures.

Although no temperature effects were observed when the dosimeter solution was being used at room temperature, thermostating the samples revealed a slight temperature dependence at temperatures lower than 30° and a considerable dependence at higher temperatures. A number of runs were carried out at 25° and 30° C. In all cases, dye yields for a given dose were the same. Hence only slight errors are introduced when working at room temperatures.

The system described in this report has been examined spectrophotometrically to determine the linearity of response, accuracy, reproducibility, dose-rate, energy, and temperature dependence. The results show that, in the energy range 160 kev to 2 Mev and with dose rates of 4 rads/minute to 1200 rads/minute, doses of 140 to 1000 rads absorbed at room temperature can be measured spectrophotometrically with 1-cm cells to within ±8%. With dose rates of 4 rads/minute to 200 rads/minute, doses in this range can be measured more accurately as there are no postirradiation effects. At temperatures higher than 30° C there is a marked temperature dependence. The system should prove useful as a laboratory chemical dosimeter when employed within the limits outlined above.

ACKNOWLEDGMENTS

The authors wish to express their thanks to Dr. W. F. Baldwin and Dr. P. J. Dyne of Atomic Energy of Canada Limited for making available the 2 Mev X-ray machine and the 150-curie cobalt source as well as for valuable assistance and discussion. The authors would also like to thank Dr. J. A. Carruthers of these laboratories for the use of radiation sources.

REFERENCES

1. AITKEN, P. B., DYNE, P. J., and TRAPP, E. C. Nucleonics, **15** (1), 100 (1957).
2. ARMSTRONG, W. A. and GRANT, G. A. Radiation Research, **8**, 375 (1958).
3. GRANT, G. A., BLANCHFIELD, R., and SMITH, D. M. Can. J. Chem. **35**, 40 (1957).
4. TAPLIN, G. V. The University of California School of Medicine, Atomic Energy Project Report No. UCLA 304.
5. TAPLIN, G. V. and DOUGLAS, C. H. Nucleonics, **6** (6), 66 (1950).
6. TAPLIN, G. V., DOUGLAS, C. H., and SANDEZ, B. Nucleonics, **9** (2), 73 (1951).

SYNTHESIS OF N-SUBSTITUTED DIISOPROPANOLAMINES, THEIR SEBACATE POLYESTERS AND POLYURETHANE ELASTOMERS[1]

JEAN L. BOIVIN

ABSTRACT

Several N-substituted diisopropanolamines were prepared by reacting aqueous solutions of amines with excess propylene oxide at ordinary pressure but higher N-substituted diisopropanolamines had to be prepared in an autoclave at 200° C. The ionization constants of these bases were measured and recorded as pK_a values. Their infrared absorption spectra gave bands common to all diisopropanolamines mainly at 3.04, 7.14, 7.55, 7.85, 9.45, 10.6, and 11.95 microns. Their condensation with sebacic acid gave the corresponding polyesters, which were soluble in strong acids and had molecular weights of about 1500. The hydroxyl-terminated polyesters were cured with a slight excess of 2,4-tolylene diisocyanate at 100° C for 2 days to yield elastomers of brittle temperatures in the region of −50° C.

INTRODUCTION

During the course of a research project, there were indications that elastomers containing tertiary amino derivatives in the recurring unit of the chain would be valuable elastomers with respect to their low-temperature properties and toughness. Our attention was drawn to the N-substituted diisopropanolamines[2] as starting diols in the condensation with dibasic acids. It seemed that the N-substituted diisopropanolamines have not been described in the literature, but diisopropanolamine itself has been prepared by allowing aqueous ammonia to react with propylene oxide.

Preparation of N-Substituted Diisopropanolamines

The diisopropanolamines were prepared by adding propylene oxide in excess to aqueous solutions of various primary amines. The reaction is shown by the following equation:

$$RNH_2 + 2CH_3CH\!-\!\!-\!CH_2 \longrightarrow RN\left[CH_2CH(CH_3)OH\right]_2.$$

It is believed that secondary diols were formed, since their condensation with diacids was rather slow and the reaction of their polyesters with diisocyanate required 2 days for completion. The concentration of the aqueous amine solution varying from 25 to 95% as the molecular weight of the amine increased. Reactivity with propylene oxide was observed to decrease with increasing molecular weight. The condensation was usually carried out at 60–80° C by adding propylene oxide to the amine solution. The reaction was exothermic and cooling was necessary up to amylamine, but from amylamine to decylamine the mixture had to be heated and the addition of propylene oxide was slower. From dodecylamine to octadecylamine, the reaction had to be carried out in an autoclave at 200° C. Table I shows the diisopropanolamines prepared together with their physical properties and purity as based on their acid equivalent.

Tertiary butylamine yielded the monoisopropanolamine derivative only when the reaction was run at normal pressure. The yields ranged from 90 to 100% when the amine and propylene oxide were used in the respective molar ratios of 1:2.5. The water

[1]*Manuscript received June 10, 1958.*

Contribution from the Polymer Research Group of the Canadian Armament Research and Development Establishment, Valcartier, Quebec.

This article is based on a paper presented at the 41st Annual Conference and Exhibition of the Chemical Institute of Canada, Toronto, May 26–28, 1958.

[2]*These compounds would be correctly named as N-substituted bis-(2-hydroxypropyl)-amines and for convenience the diisopropanolamine designation will be retained.*

TABLE I

N-SUBSTITUTED DIISOPROPANOLAMINES $RN\left[\begin{array}{c}CH_2CH-OH\\|\\CH_3\end{array}\right]_2$

R	B.p. (mm Hg)	Analysis* % purity	Method of preparation
Propyl	104–105 (2.0)	99.1	‖
Butyl	111–112 (1.5)	99.4	‖
Amyl	127–128 (3.0)	99.9	‖
Hexyl	144 (3.5)	98.5	‖
Octyl	144 (0.7)	99.7	‖
Decyl	152 (0.8)	99.4	‖
Dodecyl	172–174 (1.0)	96.4§	¶
Tetradecyl	185–190 (1.2)	101§	¶
Hexadecyl	205–208 (1.2)†	100§	¶
Octadecyl	210–213 (0.5)‡	102§	¶
Allyl	101–103 (0.5)	98.0	‖
Isobutyl	98–100 (1.5)	99.8	‖
tert-Butyl	122 (3.0)	99.7	¶
Benzyl	148–149 (0.5)	99.4	‖
2-Ethylhexyloxypropyl	162–164 (1.0)	99.7	‖
Dimethylaminopropyl	145 (2.8)	—§	‖
Morpholinoethyl	154–155 (0.5)	—§	‖
Morpholinopropyl	163–165 (0.5)	—§	‖

*By titration with 0.1 *N* HCl using methyl red as indicator.
†M.p. 39–40° C.
‡M.p. 38–39° C.
§Poor end point.
‖Ordinary pressure at 60–80° C.
¶In an autoclave at 200° C.

solubility of the diisopropanolamines decreased in ascending the homologue series, reaching nearly complete insolubility with the N-octadecyl compound.

Condensation products were also obtained by reacting propylene oxide with various amines; details are recorded in Table II.

Basicity of the N-Substituted Diisopropanolamines

Since the diisopropanolamines contain a tertiary nitrogen atom, they should be quite basic and have a high ionization constant (K_b). It was noticed that the determination of the purity of the base by titration with standard acid using methyl red as indicator

TABLE II

OTHER AMINE CONDENSATION PRODUCTS WITH PROPYLENE OXIDE

Compound	B.p. (mm Hg)	Analysis* % purity	Method of preparation
2-Hydroxyethyl-2-hydroxypropylmethylamine	103 (1.5)	99.0	‖
N,N′-Bis-(2-hydroxypropyl)-piperazine	130 (1.5)†	—‡	¶
tert-Butylamino-2-propanol	58 (2.5)§	99.7	‖

*By titration with 0.1 *N* HCl using methyl red as indicator.
†M.p. 70–75° C.
‡Poor end point.
§M.p. 26–27° C.
‖Ordinary pressure at 60–80° C.
¶In an autoclave at 200° C.

was erratic with the high molecular weight N-alkylated diisopropanolamines. The ionization constant of the diisopropanolamines was therefore measured by dissolving the diisopropanolamines in standard acid and back-titrating with a standard base while recording the pH.

The pK_a was given by the middle of the flat portion of the titration curve and the ionization constants are recorded for these amines using the normal acidity scale (pK_a). The results given in Table II show that the first members of the series from C_3 to C_6 inclusive have strengths similar to that of ammonium hydroxide; the higher homologues are less basic until they reach a pK_a on the acid side. It is worth while to note that

TABLE III

ELEMENTAL ANALYSIS AND pK_a VALUES OF N-SUBSTITUTED DIISOPROPANOLAMINES AND RELATED COMPOUNDS

R	pK_a*	Found for:†			Calculated for:		
		C, %	H, %	N, %	C, %	H, %	N, %
Propyl	8.9	61.0	11.9	7.56	61.7	12.0	8.00
Butyl	9.3	63.6	11.7	6.98	63.5	12.2	7.40
Amyl	9.0	64.6	12.3	6.54	65.0	12.3	6.90
Hexyl	8.5	66.4	12.5	6.27	66.5	12.4	6.48
Octyl	8.3	69.0	12.9	5.84	68.6	12.6	5.72
Decyl	7.6	69.9	12.8	5.35	70.5	12.7	5.13
Dodecyl	6.2	72.0	12.9	4.81	72.0	12.9	4.65
Tetradecyl	5.6	72.6	13.0	4.52	73.1	13.1	4.25
Hexadecyl	4.8	74.2	13.0	4.09	73.8	12.5	3.93
Octadecyl	4.6	74.6	13.2	3.89	74.9	13.2	3.64
Allyl	8.2	62.1	10.9	7.33	62.5	11.0	8.11
Isobutyl	8.8	59.9	11.9	12.5	60.5	11.9	12.7
tert-Butyl	9.4	60.0	11.9	12.6	60.5	11.9	12.7
Benzyl	7.5	69.8	9.48	6.43	70.0	9.40	6.98
2-Ethylhexyloxypropyl	7.7	67.5	11.8	4.54	67.4	12.2	4.63
Dimethylaminopropyl	6.5, 9.2	59.9	11.9	12.5	60.5	11.9	12.7
Morpholinoethyl	7.9	57.8	10.6	11.5	57.0	10.4	11.3
Morpholinopropyl	5.5, 8.4	59.8	10.6	10.5	60.0	10.7	10.7
2-Hydroxyethyl-2-hydroxypropyl methylamine	8.7	54.9	11.2	9.98	54.1	11.1	10.5
tert-Butylamino-2-propanol	10.0	63.6	13.1	10.7	64.2	13.0	10.7
N,N′-Bis-(2-hydroxypropyl)-piperazine	7.1	58.4	11.9	13.3	58.6	12.1	13.6

*Determined graphically from the titration curves.
†Analysis by Micro-Tech Laboratories, Skokie, Illinois.

N-substituted monoisopropanolamines such as the N-methyl derivative are more basic than diisopropanolamine itself. Where two tertiary nitrogen atoms are present in the same molecule, two pK_a values were recorded indicating different degrees of ionization. Highly symmetrical molecules such as N,N′-bis-(2-hydroxypropyl)-piperazine exhibited only one ionization constant (pK_a of 7.1). In the case of N-morpholinoethyl diisopropanolamine the single pK_a obtained indicated that the two nitrogen atoms are equally electronegative.

Infrared Spectra

The infrared absorption spectra of all the N-substituted diisopropanolamines prepared were determined on a double beam Perkin–Elmer spectrophotometer between sodium chloride plates. They all exhibit similar absorption bands at 3.04, 7.14, 7.55, 8.85, 9.45, 10.6, and 11.95 microns excepting the CH bands.

The diisopropanolamines, which are probably associated hydroxylated compounds, exhibit an intense absorption band in the region of 3.0 to 3.04 microns which can be

attributed to the OH vibration. Most of the other bands are practically common to all the compounds studied and the N-substituents have no effect on the spectra at least for the N-alkyl derivatives. Substituents containing nitrogen or oxygen influenced the spectra in the region of 8.5 to 10 microns.

Polyesters from N-Substituted Diisopropanolamines and Sebacic Acid

The N-substituted diisopropanolamines were condensed with sebacic acid using a molar ratio of 1.1 to 1.0 at a temperature of 210–220° C for 20 hours, during which time water was eliminated. Nitrogen was passed through the melt to provide stirring and prevent oxidation. After heating for a further hour at 220° C under vacuum, the polyesters of sebacic acid were obtained and their molecular weight estimated by the hydroxyl end-group analysis after making a correction for the acidity number. Table IV shows the molecular weight, acidity number, and viscosity of the polyesters prepared. Determination of the pK_a values showed that they were weakly basic. The pK_a values range from 3 to 5.

TABLE IV

POLYESTERS OF N-SUBSTITUTED DIISOPROPANOLAMINES AND SEBACIC ACID AND THEIR 2,4-TOLYLENE DIISOCYANATE (TDI) POLYURETHANE ELASTOMERS

	Polyesters of sebacic acid and N-substituted diisopropanolamines			Polyurethanes	
N-Substituents	Mol. wt.	Viscosity at 20° C, centostokes	Acid No.*	TDI†	Gehman freeze point, ° C
Propyl	1880	—	19.6	2	−42
Butyl	1090	5450	58.8	3	−46
Amyl	1450	—	6.1	2	−51
Hexyl	1410	13400	3.4	3	−60
Octyl	1600	5580	4.5	3	−45
Decyl	2010	7690	4.0	2	−55
Dodecyl	1960	—	2.5	2	−55
Tetradecyl	1520	3000	2.8	4	−40
Hexadecyl	2450	7700	1.7	2	−40
Octadecyl	1530	2470	2.6	3	−30
Allyl	1230	—	6.2	3	−58
Isobutyl	1230	—	13.0	4	−49
Benzyl	1430	—	6.4	3	−16
tert-Butyl	1400	—	5.2	3	−42
Morpholinopropyl	1910	—	10.8	2	−32
Morpholinoethyl	1820	—	21.2	3	−28
Dimethylaminopropyl	1420	—	12.3	3	−40
2-Ethylhexyloxypropyl	1920	4200	3.5	2	−50

*Milligrams of KOH per gram of prepolymer.
†Grams per 20 grams of prepolymer.

Polyurethane Elastomers

The hydroxyl-terminated polyesters of N-substituted diisopropanolamines and sebacic acid were treated with various quantities of 2,4-tolylene diisocyanate, mixed thoroughly, and cured 48 hours at 100° C. The low-temperature brittleness of the elastomers was measured by determining the Gehman freeze point. Table IV shows the results. In most cases, the brittle point of the best specimen of elastomer was in the region of −50° C. The elastomers obtained from low molecular-weight-substituted diisopropanolamines were tough but the strength decreased in ascending the series. Owing to the high acid numbers of most polyesters prepared the elastomers were not free of bubbles.

CONCLUSION

There is an indication that N-substituted diisopropanolamine containing elastomers are slightly better at low temperature than those made from non-basic polyesters. However, these diols will be valuable intermediates to terminate any polymeric chain by secondary hydroxyl groups which are less reactive toward diisocyanates than the primary functions.

THE SPONTANEOUS PRECIPITATION OF HYDRATED ALUMINA FROM ALUMINATE SOLUTIONS[1]

T. VRBAŠKI,[2] H. IVEKOVIĆ,[3] AND D. PAVLOVIĆ[4]

ABSTRACT

The rates of spontaneous precipitation of hydrated alumina from unseeded and metastable sodium aluminate solutions of a molar relation for Na_2O/Al_2O_3 (α) ranging from 1.15 to 1.60 have been investigated. All precipitation curves showed autocatalytic characteristics with a pronounced induction period, during which no precipitation occurred, a steady state period, and a period of delayed precipitation. Empirical equations for calculating the maximum precipitation rate, for the time when this precipitation takes place, and for the amount of the precipitate at equilibrium for any of these aluminate solutions have been developed.

INTRODUCTION

The precipitation of hydrated alumina from metastable sodium aluminate solutions represents the basic reaction in the formation of alumina by the Bayer process.

This reaction has been the subject of extensive investigation using mainly hydrargillite as a seed substance (1, 2, 3, 4). Spontaneous process was also studied by Calvet *et al.* (5) and by Sato (6).

The experiments described below were carried out in order to obtain a closer insight into the kinetics of the spontaneous precipitation of hydrated alumina from unseeded aluminate solutions. The time after which first nuclei of hydrated alumina (hydrargillite) are formed in a clear solution is of greatest significance as the crystallites once formed act as seed substance (7). It is of great interest, therefore, to investigate the dependence of the induction period (6) on the molar relation (α), where $\alpha = Na_2O/Al_2O_3$, of the aluminate solution used.

As no crystallites are present in the clear solution at the beginning of the reaction, and since the precipitate formed will cause a considerable promotion of the precipitation rate, the precipitation would be expected to show autocatalytic characteristics (cf. 7). In the Bayer process such autocatalytic characteristics are masked by the action of the high concentration of seed material.

EXPERIMENTAL

Preparation of Sodium Aluminate Solutions

The solution of sodium aluminate was prepared in the way described in our previous paper (8). The aluminate solutions used were prepared by dilution of the stock solution with distilled water to a concentration of approximately one mole Al_2O_3 and 1.15 to 1.60 mole Na_2O.

The content of Al_2O_3 and Na_2O in the solution was determined by titration with 1 *N* HCl using tropeolin 00 and phenolphthalein respectively as indicators (9). The aluminate solutions were shaken continuously in stoppered Erlenmeyer flasks in a water bath at 30.0±0.1° C. When the agitation was discontinued the precipitate settled down quickly and the sample for analysis was taken from the supernatant liquid.

[1]*Manuscript received June 9, 1958.*
Contribution from the Department of Inorganic, Analytic, and Physical Chemistry, Faculty of Pharmacy, University of Zagreb, Yugoslavia.
[2]*National Research Council of Canada Postdoctorate Fellow, 1957–1959. Present address: National Research Council, Applied Chemistry, M-12.*
[3]*Professor, Department of Inorganic, Analytic, and Physical Chemistry, Faculty of Pharmacy, University of Zagreb, Yugoslavia.*
[4]*Department of Inorganic, Analytic, and Physical Chemistry, Faculty of Pharmacy, University of Zagreb, Yugoslavia.*

RESULTS

Each experiment was carried out using six different aluminate solutions. Their compositions are given in Table I.

TABLE I

THE COMPOSITION OF ALUMINATE SOLUTIONS

Solution	Al_2O_3, mole	Na_2O, mole	Initial molar relation for Na_2O/Al_2O_3 (α)	Molar relation for Na_2O/Al_2O_3 at equilibrium (α_e)
1	0.95	1.10	1.15	5.00
2	1.00	1.22	1.22	5.00
3	0.98	1.29	1.32	5.00
4	1.00	1.39	1.39	5.00
5	1.01	1.50	1.50	5.00
6	1.00	1.60	1.60	5.00

The solutions were prepared by diluting 100 ml samples of the freshly prepared stock solution to a volume of 150 ml. The molar percentage of the precipitated hydrated alumina was plotted against time. A family of curves was obtained as the molar relation for Na_2O/Al_2O_3 was varied. These are shown in Fig. 1. It was not found profitable to plot molar relation for Na_2O/Al_2O_3 against time because its values, depending on the initial molar relation, changed in a different way for each solution during the reaction.

All precipitation curves showed an autocatalytic trend with a characteristic induction period, during which no precipitation occurred, a steady state period, and a period of delayed precipitation.

(*a*) *The Induction Period*

It is evident from the Fig. 1 that the precipitation of hydrated alumina takes place

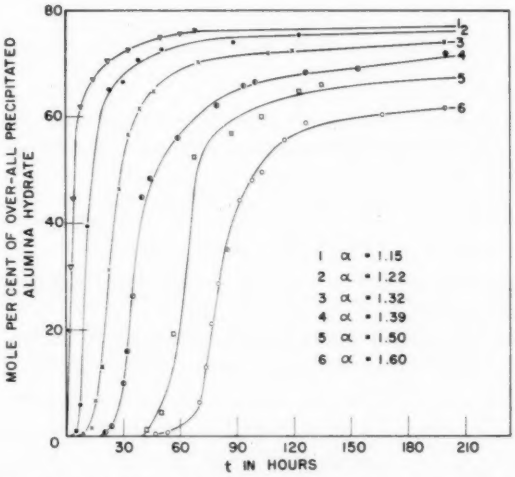

FIG. 1. Spontaneous precipitation of hydrated alumina from aluminate solutions of different molar relation for Na_2O/Al_2O_3. The volume of solutions was 150 ml, and the temperature 30.0±0.1° C.

only after an induction period, which becomes longer as the initial molar relation for Na_2O/Al_2O_3 is increased. This dependence of the induction period upon the initial molar relation is shown in Fig. 2.

The ratio of the induction period to the initial molar relation is not steady along the whole of the investigated region. The experimental curve (in Fig. 2) could be composed of two straight lines with an intersection point in *S* corresponding to a solution of a molar relation $\alpha = 1.385$ and an induction period of 685 minutes. Calvet *et al.* (10) found by thermochemical method of measuring the stability of solutions of sodium aluminate an instability ceiling at the same molar relation for Na_2O/Al_2O_3. This phenomenon might possibly be caused by a structural change of the aluminate solution (11) at this point. In the low molar relation region ($\alpha = 1.15$ to $\alpha = 1.40$) the increase of the induction period is slow, the slope being 62.0, i.e. only about a quarter of the succeeding slope over the region $\alpha = 1.40$ to $\alpha = 1.60$.

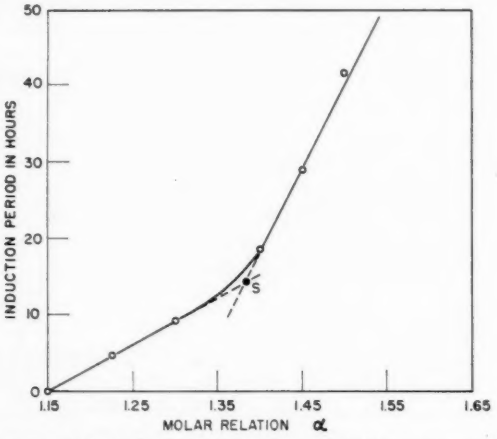

FIG. 2. The dependence of the induction period upon the initial molar relation for Na_2O/Al_2O_3.

(*b*) *The Equilibrium State*

In order to obtain data on the equilibrium state, the precipitation from solutions with higher molar relation had to be followed for up to sixty days. The amount of hydrated alumina precipitated at equilibrium was plotted against the initial molar relation. A straight line was obtained and could be expressed fairly well by the equation

$$C = 100 - 20\,\alpha, \qquad [1]$$

in which *C* is the molar percentage of over-all precipitated hydrated alumina and α the initial molar relation.

The molar relations established at equilibrium were found to be identical for all solutions and did not depend upon the initial molar relations used.

(*c*) *The Precipitation Rate*

The precipitation rate is higher if the initial molar relation of the aluminate solution is lower, as shown in Fig. 1. The amount of hydrated alumina precipitated in 100 minutes (ϕ) can be taken as a measure of the precipitation rate. Plotting the rates so obtained (ϕ) against time (t) we obtain a family of curves shown in Fig. 3.

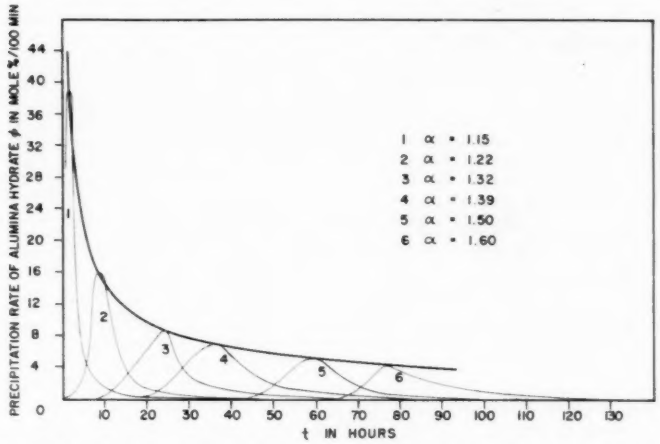

FIG. 3. Precipitation rates of hydrated alumina precipitated from aluminate solutions of various molar relations for Na_2O/Al_2O_3.

The maximum precipitation rate (ϕ_m) is higher if the initial molar relation (α) is lower. This relationship can be expressed by the equation

$$\log \phi_m = k(1/\log \alpha)^n, \qquad [2]$$

where α is the initial molar relation, and n and k are constants. The average values of n and k are 0.761 ± 0.001 and 0.188 ± 0.001 respectively. They have been calculated from the equation [2] using pairs of corresponding values of α and ϕ_m. They could also be obtained graphically from a diagram in which log log ϕ_m versus log $1/(\log \alpha)$ was plotted. In the straight line so obtained n was the slope and log k the segment of the ordinate.

The maximum precipitation rate of any sodium aluminate solution of known initial molar relation can thus be readily calculated from the equation [2].

(d) The Time of the Maximum Precipitation Rate

Relationship between the maximum precipitation rate (ϕ_m) and the time of the maximum precipitation rate (t_{ϕ_m}) is obtained by connecting the peaks of the velocity curves in Fig. 3. This relationship can be expressed by the equation

$$\phi_m = k'(1/t_{\phi_m})^{n'}, \qquad [3]$$

where n' and k' are constants. The average n' and k' values calculated from the above equation or determined graphically, similarly as n and k values, are 0.610 ± 0.001 and 60.26 ± 0.15 respectively.

Combining [2] and [3] and eliminating ϕ_m the expression

$$t_{\phi_m} = (\log k'/n') - (k/n')(1/\log \alpha)^n \qquad [4]$$

is obtained.

Inserting numerical values of the constants into equation [4] we obtain

$$\log t_{\phi_m} = 2.92 - 0.308(1/\log \alpha)^{0.761}. \qquad [5]$$

The time of the maximum precipitation rate can thus be calculated directly from the initial molar relation for Na_2O/Al_2O_3.

Comparison of the calculated and observed values of ϕ_m and t_{ϕ_m} is given in Table II. The differences are within $\pm 1.15\%$.*

TABLE II

COMPARISON OF CALCULATED AND OBSERVED VALUES OF ϕ_m AND t_{ϕ_m}

Initial molar relation for Na_2O/Al_2O_3 (α)	ϕ_m		t_{ϕ_m}	
	Calculated by eq. 2	Observed	Calculated by eq. 4	Observed
1.15	38.9	39.0	2.0	2.0
1.22	16.2	16.1	8.6	8.8
1.32	8.7	8.7	24.0	24.0
1.39	6.7	6.8	36.3	36.3
1.50	5.0	5.0	59.0	59.2
1.60	4.3	4.3	77.6	77.8

On the Kinetics of Precipitation of the Hydrated Alumina

The family of curves in Fig. 1 indicates that the precipitation reaction behaves more like an autocatalytic reaction at higher molar relations and less so at lower molar relations when it seems to follow a simple logarithmic law.

This phenomenon can be readily explained on the basis of the expression for the autocatalytic reaction rate†

$$+dx/dt = (k_1+k_2x)(a-x), \qquad [6]$$

where k_1 is the first-order reaction rate constant, k_2 the constant of the autocatalysis, a the initial concentration of sodium aluminate, and x the concentration of hydrated alumina, i.e. of the catalyst produced at the time t. The use of this expression is only tentative. Attributing the discussed precipitation a reaction type of a definite order is not possible at present because of lack of information.

Since the precipitation does not start if crystallization nuclei are not present, k_1 is very probably small. As soon as the reaction initiates k_1 can be neglected compared to k_2x because x increases rapidly; x and thus (k_1+k_2x) tend to reach soon a final value and the precipitation reaction seems to behave like a first-order reaction. The same conclusion will be reached if we take into consideration similar expressions proposed by other authors (13).

In the solutions of low molar relation, crystallization nuclei are rapidly formed at the very beginning of the reaction and the entire course of precipitation seems to follow the first-order reaction law. In the solutions of higher molar relation similar behavior is observed after the initial autocatalytic period.

However, if an excess of seed material is added at the beginning of the reaction the precipitation reaction is expected to behave in the same way as that in the solutions of lower molar relation. This assumption has been confirmed by recent investigations of Herrmann *et al.* (7). The authors, however, pointed out that their empirically found expression should not be considered as a simple equation for a first-order reaction rate, although this expression showed some similarity with it.

**In conclusion it should be emphasized that for generalization of equations obtained the temperature dependence of the reaction should be determined. This will be the subject of a further study.*

†This expression can be deduced from the Ostwald's expression for the first-order reaction rate if the product formed acts as a negative catalyst (12).

REFERENCES

1. Vol'f, F. F., Kuznetsov, S. S., and Serebrennikova, O. V. J. Appl. Chem. U.S.S.R. (English translation) **23**, 57 (1950). Zhur. Priklad. Khim. **23**, 60 (1950).
2. Sato, T. J. Chem. Soc. Japan, Ind. Chem. Sect. **55**, 66, 192 (1952); **56**, 399, 743, 840 (1953); **57**, 20, 111, 355, 540, 805 (1954); **58**, 325, 556 (1955).
3. Herrmann, E. Z. anorg. u. allgem. Chem. **274**, 81 (1953).
4. Marićić, S. and Markovčić, I. Arhiv Kem. **27**, 41 (1955). Z. anorg. u. allgem. Chem. **276**, 193 (1955). Bogdanović, P., Marićić, S., and Vidan, M. Croat. Chem. Acta, **28**, 155 (1956).
5. Calvet, É., Thibon, H., Maillard, A., and Boivinet, P. Bull. soc. chim. France, 130 (1950); 402 (1951).
6. Sato, T. J. Chem. Soc. Japan, Ind. Chem. Sect. **54**, 755 (1951).
7. Herrmann, E. and Stipetić, J. Z. anorg. Chem. **262**, 258 (1950).
8. Iveković, H., Vrbaški, T., and Pavlović, D. Croat. Chem. Acta, **28**, 41 (1956).
9. Herrmann, E. Arhiv kem. **21**, 218 (1949).
10. Calvet, É., Thibon, H., and Maillard, A. Compt. rend. **228**, 928 (1949).
11. Iveković, H. and Bačić, I. Chemiker-Ztg. **55**, 255 (1954).
12. Ostwald, W. Allgem. Chem. **2**, II, 270 (1902). Verlag von W. Engelmann, Leipzig.
13. Adam, N. K. Physical chemistry. Oxford University Press, London. 1956. p. 448.

AN INTERPRETATION OF THE MOISTURE DESORPTION ISOTHERM OF WHEAT[1]

H. A. BECKER

ABSTRACT

It is shown that the moisture desorption isotherm of wheat can be interpreted in harmony with Cassie's theoretical assumptions regarding adsorption on localized sites by the equation

$$\frac{N}{S} = (1+K'f^n)\left(\frac{Kf}{1+Kf}\right),$$

where N is the number of adsorbed molecules per gram of wheat and S is the number of localized sites. $Kf/(1+Kf)$ is a Langmuir-type factor for adsorption of the low energy fraction of molecules, and $K'f^n$ is a factor for adsorption of the normally condensed fraction of molecules. In agreement with theory K', n, and S are independent of temperature. The dependence of K on temperature gives a value of -6.27 kcal/mole for the partial molal enthalpy of dilution of the low energy fraction of molecules, which is in the order of magnitude of a hydrogen bond. The analysis also illuminates the practice of the drying of wheat. An exact correspondence appears to exist between the calculated values of S and the apparent surface (or equilibrium) moistures observed in studying the diffusion of moisture out of wheat. The theoretical relation

$$m_s = 0.1157\ K/(1+K)$$

is therefore given for predicting apparent surface moisture contents in the vacuum drying of wheat, where

$$K = 3.05\times10^{-4}\exp(6270/RT).$$

Becker and Sallans (1) have made a comprehensive study of the moisture desorption isotherm of wheat. The isotherm was found to be sigmoid in shape and was described mathematically in three sections: at low relative vapor pressures, by the B.E.T. equation (2)

$$\frac{m}{m_L} = \frac{Kf}{1-f}\left(\frac{1}{1+(K-1)f}\right), \qquad [1]$$

where m is the moisture content, g/g dry basis, f is the relative vapor pressure, and m_L and K are constants; at intermediate relative vapor pressures, by the linear relation

$$m-m_0 = af, \qquad [2]$$

where m_0 and a are constants; and at high relative vapor pressures, by Smith's equation (3)

$$\frac{w-w_b}{w'} = \ln\frac{1}{1-f}, \qquad [3]$$

where w is the moisture content, g/g wet basis, and w_b and w' are constants. The use of the last two equations for accurate description of the isotherm was necessitated by the usual failure of the B.E.T. equation at intermediate and high relative vapor pressures. Even if put in the form for limited adsorption,

$$\frac{m}{m_L} = \frac{Kf}{1-f}\left(\frac{1-(n+1)f^n+f^{n+1}}{1+(K-1)f-Kf^{n+1}}\right), \qquad [4]$$

where n is the limiting number of layers of molecules, the B.E.T. equation will not accurately fit the data. However, the inexactness of the B.E.T. equation at all but

[1]*Manuscript received July 18, 1958.*
Contribution from the National Research Council, Prairie Regional Laboratory, Saskatoon, Saskatchewan. Issued as N.R.C. No. 4890.

low relative vapor pressures is of little consequence theoretically. The really irregular features of the data are (i) that the calculated moisture contents corresponding to a B.E.T. molecular monolayer, $m_L = 0.078$ g/g at 25° C and 0.060 g/g at 50° C, are markedly functions of temperature; and (ii) that there is no apparent relation between any of the constants in equations 1, 2, and 3 and the dynamic equilibrium moistures observed by the author (4) and by Becker and Sallans (5) in studying moisture diffusion out of the wheat kernel. It is the purpose of the present paper, therefore, to explain or eliminate these discrepancies.

THE ISOTHERM EQUATION

The B.E.T. equation was derived by Brunauer *et al.* (2) on the basis of a somewhat dubious evaporation–condensation mechanism. Cassie (6) has given the equation thermodynamic credence by derivation from statistical–thermodynamical arguments. In Cassie's view the equation is applicable to adsorption on localized sites, such as polar groups on a polymer molecule, rather than to adsorption on an unspecified surface. He postulated that the first molecule associated with each localized site is strongly adsorbed, while subsequently attached molecules are at the same energy level as in the normal liquid state. Adsorption of an essentially liquid fraction at vapor pressures below saturation is made possible by mixing with the low energy fraction. His version of the B.E.T. equation is written

$$\frac{N}{S} = \frac{Kf}{(1-f)}\left(\frac{1}{1+(K-1)f}\right), \qquad [5]$$

where N is the number of adsorbed molecules per gram of adsorbent and S is the number of localized sites. In the statistical–thermodynamical definition $K = (j_S/j_L) \exp(-\Delta\bar{H}_S/RT)$, which differs from Brunauer *et al.*'s definition by prefixing the ratio j_S/j_L where j_S and j_L are respectively the partition functions for molecules in the low energy state and in the normal liquid state; $\Delta\bar{H}_S$ is the partial molal enthalpy of dilution of the low energy (X) fraction of molecules; and R and T are respectively the gas constant and the absolute temperature. It appears that Cassie's arguments provide a reasonable and simple basis for interpretation of the moisture sorption isotherms of materials such as wheat. However, it can be expected that the course of multimolecular adsorption will rarely follow equations 1 or 4 exactly. If it is desired to obtain an accurate description of the adsorption isotherm with values of the B.E.T. constants which are consistent with their assumed behavior, then equation 4 should be written in a form which allows greater variation between the paths of adsorption of the "normally condensed" and the low energy fractions of molecules. A simple equation with flexible parameters for multimolecular adsorption, which still retains the theoretical skeleton of equation 5, can be formulated as follows.

Consider the adsorption of N molecules on X sites in a material which contains S localized sites. Following Cassie (6), we assume that X molecules are singly adsorbed, one to a site, with a constant, negative partial molal enthalpy of dilution, $\Delta\bar{H}_S$, in the order of several kilocalories. These X molecules provide the sites for adsorption of the remaining N–X molecules, which are assumed to be condensed with a zero partial molal enthalpy change. The adsorption of the X low energy molecules can reasonably be assumed, on the basis of Cassie's (6) and Enderby's (7) statistical–thermodynamical analyses, to be governed by the Langmuir form of equation 5

$$X/S = Kf/(1+Kf). \qquad [6]$$

In Cassie's argument the adsorption of the N–X condensed molecules derives from random mixing with the X low energy molecules. It is obvious, however, that this process will be complicated by various influences resulting from the physical and chemical characteristics of both adsorbate and adsorbent. Even so, it appears that the state of the normally condensed molecules should be similar in some ways to a gaseous film in which the molecules are associated, on the average, in groups of n molecules each. The equation of state of such a film is (8)

$$\pi(n\sigma) = kT, \qquad [7]$$

where π is the film pressure, $\sigma = \Sigma/N$ is the area per molecule, Σ is the area of the film, and k is Boltzmann's constant. Conjunction with Gibb's equation

$$\pi = \frac{kT}{\Sigma}\int_0^f \frac{N}{f}\,df \qquad [8]$$

gives Freundlich's isotherm (1)

$$N = K'f^n. \qquad [9]$$

We shall therefore assume that the adsorption of the N–X normally condensed molecules on X available sites can be expressed by

$$(N-X)/X = K'f^n. \qquad [10]$$

Eliminating X between equations 6 and 10 we find for the adsorption isotherm

$$\frac{N}{S} = (1+K'f^n)\left(\frac{Kf}{1+Kf}\right). \qquad [11]$$

A definite physical significance can be attached to the parameters K and K' in this equation: at saturation the Langmuir part reduces to

$$X_1/S = K/(1-K) \qquad \text{or} \qquad K = X_1/(S-X_1), \qquad [12]$$

where X_1 is the number of occupied sites. Hence K is the numerical ratio of the occupied sites to the vacant ones at the saturation vapor pressure. Putting $S = X_1(1+K)/K$, equation 11 becomes

$$\frac{N}{X_1} = (1+K'f^n)\left(\frac{(1+K)f}{1+Kf}\right) \qquad [13]$$

and at $f = 1$, $N/X_1 = 1+K'$. Therefore K' can be thought of as the average number of normally condensed molecules per occupied site toward which adsorption tends at saturation.

THE EVALUATION OF THE ISOTHERM PARAMETERS

Before discussing the evaluation of the parameters S, K, K', and n, we shall summarize the assumptions to be made as to their behavior. The following assumptions are fundamental to equation 11:

(i) The number of localized sites, S, is a constant characteristic of the adsorbent.

(ii) The parameter K is independent of concentration but is dependent on temperature. The temperature dependency should be very nearly given by

$$\frac{\partial \ln K}{\partial\, 1/T} = -\frac{\Delta H_s}{R}. \qquad [14]$$

(iii) The parameter K' and the exponent n are independent of temperature but may be dependent on concentration.

The evaluation of the parameters may be carried out by trial and error treatment of data. A solution is obtained when the properties of the parameters are in accord with their assumed behavior. Eventually the exponent n will need to be considered as a function of the relative vapor pressure. The following cases may occur:

(i) $n = 0$. When n is equal to zero, K' will also be equal to zero, and the isotherm equation reduces to Langmuir's equation.

(ii) $n, K' =$ constants. The trial and error method should quickly yield a solution if n and K' can be treated as constants.

(iii) $K'f^n \ll 1$. In this case equation 11 reduces to Langmuir's equation.

(iv) K' and/or n are functions of relative vapor pressure. This most general case can be treated by writing equation 11 in the form

$$\frac{f(1+\phi(f))}{N} = \frac{1}{KS}+\frac{f}{S}, \qquad [15]$$

where $\phi(f) = K'f^n$. The problem then is to find a value of $\phi(f)$ which gives a linear relation between $f(1+\phi(f))/N$ and f, and a constant, temperature-independent value of S.

The general technique is illustrated by the following analyses of Bull's data (9) on the adsorption of water vapor by proteins or protein-like polymers. Figure 1 shows that a reasonably good correlation of the data on silk, wool, and gelatin is obtained by putting $1+K'f^n = 1+f+f^2$. (This substitution produces an approximation to the B.E.T. equation, since $1+f+f^2$ is an approximation to $1/1-f$.) The curves are linear in a wide region of relative vapor pressures, and the slopes of the linear regions are substantially independent of temperature. The moisture contents, m_L, corresponding to the number of localized sites, S, (m_L is given by the reciprocals of the slopes) are about 30% higher than predicted by the B.E.T. equation 1. A somewhat different relation is shown by nylon, Fig. 2, for which trial and error treatment of the data for 25° C gives

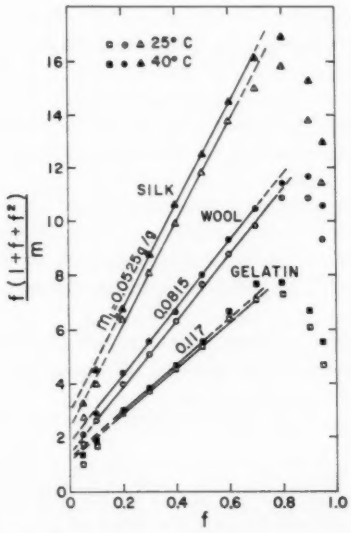

FIG. 1. Correlation of Bull's data on the adsorption of water vapor by silk, wool, and gelatin.

$K' = 5$ and $n = 2$. The data for 40° C show rather peculiar behavior at low relative vapor pressures. It may be noted that the B.E.T. equation does not fit the data on nylon at all.

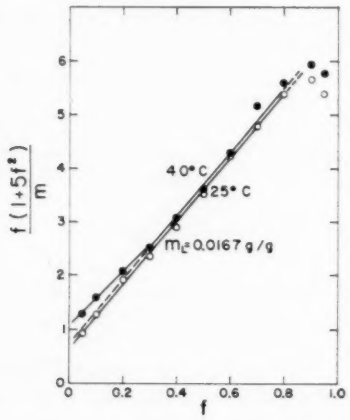

FIG. 2. Correlation of Bull's data on the adsorption of water vapor by nylon.

THE ANALYSIS OF THE MOISTURE DESORPTION ISOTHERM OF WHEAT

Becker and Sallans (1) determined the moisture desorption isotherm of wheat at temperatures of 25° and 50° C. As already noted in the introduction, the B.E.T. equation for $n = \infty$ was found to fit the data at low relative vapor pressures but gave values of the B.E.T. monolayer moisture content, m_L, which decreased markedly with increasing temperature. This discrepancy with Cassie's interpretation of m_L can be explained, most obviously, by hypothesizing an actual decrease in the number of localized sites available for adsorption. However, although the adsorptive capacity might diminish with rising temperature, owing to the exposure of non-polar areas, it is difficult to conceive of an over-all reaction which would cause a diminution of the number of polar groups exposed for water adsorption. We shall therefore accept the alternative explanation that the B.E.T. equation gives erroneous values of the parameters K and S, and assume that some form of equation 11 is applicable.

Trial and error examination of the data showed that the Langmuir form of the equation gives an excellent fit at low relative vapor pressures, Fig. 3. The values of the Langmuir parameters were thus found to be $K = 12.14$ and $m_L = 0.1157$ g/g at 25° C, and $K = 5.17$ and $m_L = 0.1178$ g/g at 50° C. As required, m_L so evaluated is constant within experimental error.

The data were subsequently analyzed to find empirical expressions for $K'f^n$. For this purpose the isotherm equation was arranged in the form

$$\frac{N}{S}\frac{1+Kf}{Kf}-1 = K'f^n \qquad [16]$$

where $N/S = m/m_L$. Values of K' were calculated for integer values of n, and were found to have a minimum which moved toward higher vapor pressures with increasing value of n and reached the immediate neighborhood of $f = 1$ at $n = 4$. The minimum near $f = 1$, in value $K' = 2.2$, was then used to calculate values of n for a constant

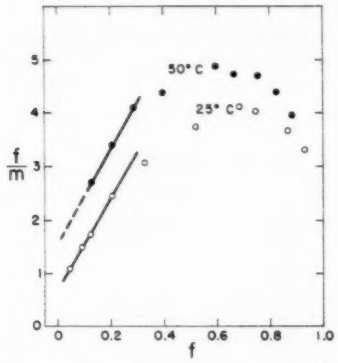

FIG. 3. Langmuir plot of moisture desorption equilibrium data on wheat.

K'. Figure 4 shows these values as a function of the relative vapor pressure. The relation is seen to be substantially independent of temperature, as it should be if the assumption of normal condensation of the multimolecularly adsorbed molecules has any truth. The calculations leading to Fig. 4 are summarized in Table I. It must be assumed that n becomes large at relative vapor pressures below 0.3 or, more likely, that K' becomes small, if the applicability of the Langmuir equation is to be retained.

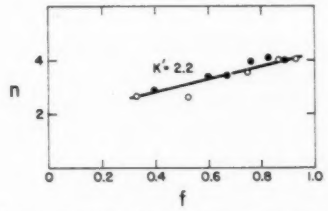

FIG. 4. Correlation of the exponent n with relative vapor pressure for $K' = 2.2$.

The rationale underlying the foregoing treatment of K' and n is as follows. The exponent n can be interpreted as being proportional to the number of normally condensed molecules on an average site. If so, it appears that n must increase with increasing relative vapor pressure and, for limited adsorption, approach constancy in the immediate neighborhood of $f = 1$. The parameter K' is in essence an equilibrium "constant", and if adsorption tends to a finite limit it is reasonable to assume that K' tends toward constancy at high relative vapor pressures. The analysis which has been given meets all of these conditions. K' is treated as a constant, and n increases with increasing relative vapor pressure and approaches constancy at $f = 1$. However, it may be seen from Table I that the assumption that K' and n are independent of temperature is fulfilled in any case, regardless of whether K' or n is treated as a constant, provided that reasonable values of K' or n are assumed.

The values found for the Langmuir constants K and S can be used directly to estimate some of the thermodynamic magnitudes involved in desorption. Equation 14 gives for K

$$K = 3.05 \times 10^{-4} \exp(6270/RT). \qquad [17]$$

TABLE I

ANALYSIS OF THE MOISTURE DESORPTION ISOTHERM OF WHEAT

				$\left(\frac{N}{S}\frac{1+Kf}{Kf}\right)-1 = K'f^n$		
				K'		n
f	m	$N/S = m/m_L$	$Kf/(1+Kf)$	$n = 3$	$n = 4$	$K' = 2.2$
			A: 25° C			
0.045	0.0421	0.364	0.353	—	—	—
0.090	0.0602	0.520	0.523	—	—	—
0.111	0.0646	0.559	0.574	—	—	—
0.203	0.0830	0.717	0.711	—	—	—
0.328	0.1068	0.924	0.799	4.41	13.40	2.64
0.520	0.1395	1.206	0.863	2.83	5.43	2.62
0.683	0.1660	1.433	0.893	1.91	2.79	3.38
0.747	0.1852	1.602	0.900	1.88	2.51	3.54
0.863	0.2351	2.03	0.913	1.89	2.19	4.00
0.930	0.2810	2.43	0.920	2.03	2.18	4.03
			B: 50° C			
0.127	0.0471	0.407	0.405	—	—	—
0.206	0.0609	0.526	0.525	—	—	—
0.286	0.0698	0.603	0.603	—	—	—
0.396	0.0907	0.785	0.690	2.44	6.15	2.89
0.596	0.1222	1.056	0.763	1.81	3.04	3.38
0.669	0.1411	1.220	0.782	1.88	2.81	3.40
0.757	0.1610	1.391	0.803	1.70	2.23	3.96
0.823	0.1878	1.623	0.815	1.78	2.17	4.09
0.884	0.2238	1.935	0.825	1.95	2.21	3.99

Hence the partial molal enthalpy of dilution of the low energy fraction of the molecules is (for desorption equilibrium) $\Delta\bar{H}_s = -6.27$ kcal/mole. This is a reasonable value for one hydrogen bond. Multiplication by the number of moles of low energy molecules adsorbed at saturation then gives an estimate of the net heat of dehydration. Equation 12 gives for the pertinent moisture content

$$m_1 = m_L\{K/(1+K)\}, \qquad [18]$$

whence $m_1 = 0.1069$ g/g at 25° C, and 0.0989 g/g at 50° C. The corresponding net heats of dehydration $(-m_1\Delta\bar{H}_s/18)$ are respectively 37.2 cal and 34.5 cal per gram of moisture-free wheat. A value of 43 cal/g was previously estimated (1) for 25° C.

The values of K' in Table I indicate that adsorption tends toward a limit of about 3.2 molecules per occupied site, or toward a moisture content of about 3.2 m_1. This gives a value of 0.34 g/g for 25° C, which is in good agreement with the previous estimate (3) of 0.37 g/g.

The results of the analysis of the desorption isotherm may now be compared with previous data (4, 5) on moisture equilibria in the diffusion of moisture out of the wheat kernel. The diffusion data were correlated by application of non-stationary state, integral diffusion equations with constant diffusion coefficients. The author in his recent study has shown that the form of the equation for vacuum drying in the range of initial moistures 0.13–0.25 g/g is

$$\bar{M} = 1-(2/\sqrt{\pi})X+0.326M^*X^2 \qquad [19]$$

where

$$\bar{M} = (\bar{m}-m_{s0})/(m_0-m_{s0}),$$
$$M^* = (m_0-m_{s\infty})/(m_0-m_{s0}),$$
$$X^2 = Dt/r^2,$$

$\bar{m}$ is the average moisture content of a drying wheat kernel at time t; m_0 is the initial, uniform moisture content at time zero; r is the volume to surface ratio of the wheat kernel; and D is the diffusion coefficient. m_{s0} and $m_{s\infty}$ are the dynamic, equilibrium moistures which we wish to explain; m_{s0} is the apparent value at time zero of the moisture content, m_s, at the surface of a drying wheat kernel, and $m_{s\infty}$ is the limiting value to which m_s tends with time.

The values found for m_{s0} and $m_{s\infty}$ in vacuum drying (4) are given in Table II, and are compared with the values found in this paper for the Langmuir parameters m_L and m_1. The similarities are clear: the apparent surface moisture content (m_{s0}) at time zero

TABLE II

COMPARISON OF THE ISOTHERM PARAMETERS m_L AND m_1 WITH THE DYNAMIC EQUILIBRIUM MOISTURES IN VACUUM DRYING m_{s0} AND $m_{s\infty}$

	m_L	$m_{s\infty}$	m_1	m_{s0}
25° C	0.1157	0.1159	0.1044	0.1069
50° C	0.1178	0.1153	0.0989	0.0989

appears to be identical with the moisture content (m_1) which corresponds to the number (X_1) of sites occupied at saturation, and the value ($m_{s\infty}$) toward which the surface moisture tends with time is evidently identical with the moisture content (m_L) which corresponds to the number (S) of localized sites. It can therefore be assumed that the apparent surface moisture content for the vacuum drying of wheat in the neighborhood of time zero is given by the relation (after equation 12)

$$m_s = 0.1157K/(1+K), \qquad [20]$$

where 0.1157 g/g is the average value found by the author (2) for $m_{s\infty}$. This interpretation also provides a qualitative explanation of the observed behavior (4, 5) of the diffusion coefficient. Clearly, molecules of the low energy fraction must be much less mobile than the normally condensed ones, and hence the diffusion coefficient should decrease markedly with decreasing concentration in the neighborhood of m_1 and m_L.

REFERENCES

1. BECKER, H. A. and SALLANS, H. R. Cereal Chem. **33**, 79 (1956).
2. BRUNAUER, S., EMMETT, P. H., and TELLER, E. J. Am. Chem. Soc. **60**, 309 (1938).
3. SMITH, S. E. J. Am. Chem. Soc. **69**, 646 (1947).
4. BECKER, H. A. A general mathematical derivation of the integral diffusion equations for non-stationary state diffusion with a constant diffusion coefficient, and its application to the vacuum drying of the wheat kernel. Forthcoming publication.
5. BECKER, H. A. and SALLANS, H. R. Cereal Chem. **32**, 212 (1955).
6. CASSIE, A. B. D. Trans. Faraday Soc. **43**, 615 (1947).
7. ENDERBY, J. A. Trans. Faraday Soc. **51**, 106 (1955).
8. ADAM, N. K. The physics and chemistry of surfaces. 3rd ed. Oxford University Press, London. 1941.
9. BULL, H. J. Am. Chem. Soc. **66**, 1499 (1944).

NEUTRON CAPTURE CROSS SECTION OF I^{129} AND I^{130} [1]

J. C. Roy and D. Wuschke

ABSTRACT

The capture cross section of I^{129} for 2200 m/sec neutrons and its resonance capture integral were determined by counting the beta rays emitted by the 12.5-hour I^{130} formed by an (n, γ) reaction on I^{129}. The σ_{2200} was found to be 26.7 ± 2.0 barns and the resonance capture integral 36 ± 4.0 barns. The effective capture cross section of I^{130} for reactor neutrons was measured to be 18.0 ± 3.0 barns by counting the beta rays emitted by the 8.1-day I^{131} produced by successive neutron capture in I^{129}. The neutron fluxes were measured with cobalt monitors; the thermal cross section and the resonance capture integral of Co^{59} were taken to be 36.5 and 48.6 barns.

INTRODUCTION

This paper describes measurements of the effective capture cross section of the 12.5-hour I^{130} for reactor neutrons. An activation method has been used which depends on successive neutron capture in the long-lived radionuclide I^{129} ($t_{\frac{1}{2}} = 1.7 \times 10^7$ years (1)). Obviously, the cross section for I^{130} obtained by this technique depends on that of I^{129} for which two different values have been reported in the literature. A value of 11 ± 4 barns, an unpublished measurement credited to Oak Ridge, is found in the compilation of neutron cross sections of Hughes and Harvey (2). Purkayastha and Martin (3), as an incidental experiment to their work on the yields of I^{129} in natural and neutron induced fission of uranium, found a value of 35 barns. They do not give the errors involved in the measurement. Since it is difficult to assess which of the two values is better and furthermore considering the large discrepancy between them, it seemed necessary to re-evaluate the thermal cross section of I^{129}. The resonance capture integral of I^{129} was also measured.

Both determinations were done by counting directly the beta rays emitted by the 12.5-hour I^{130} and 8.1-day I^{131} formed respectively by single and double neutron capture in I^{129} according to the following nuclear reactions:

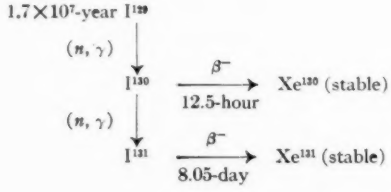

EXPERIMENTAL

(a) *Irradiation*

The I^{129} used for the irradiations was obtained from the Oak Ridge National Laboratory. A mass spectrometer analysis supplied with the material gave the following composition: 51.3% I^{129} and 48.7% I^{127}.

The samples were prepared for irradiations by precipitating the iodide as palladous iodide by the addition of 0.05 molar solution of palladous chloride to a NaI solution (3). The precipitate was washed, dried at 60° C, and transferred to one arm of a U-tube in a vacuum line. The tube was evacuated and closed off from the rest of the line. The

[1]*Manuscript received June 13, 1958.*
Contribution from Research Chemistry Branch, Atomic Energy of Canada Limited, Chalk River, Ontario. Issued as A.E.C.L. No. 679.

palladous iodide was heated to liberate the iodine and distill it into the other arm of the tube, which was made of quartz. The tube was sealed off at a constriction to form a quartz ampoule containing the elementary iodine. It was irradiated in an aluminum capsule in the NRX reactor at Chalk River.

For the measurement of the resonance capture integral the quartz ampoules were wrapped with 0.028 in. thick cadmium sheet.

To obtain the neutron flux, a piece of cobalt wire was irradiated in each capsule; the details are described in section (*e*).

(*b*) *Chemical Purification*

After the irradiation, the quartz tube was crushed under a solution of sodium bisulphite. The solution was boiled to desorb the iodine on the quartz walls. No iodine carrier was added. The iodide was oxidized with nitrous acid (4) and the iodine extracted with carbon tetrachloride. The cycle of oxidation, reduction, and extraction was repeated several times. The final iodine extract in carbon tetrachloride was washed thoroughly with water and dried with magnesium sulphate. The concentration of iodine was then measured with a Beckman spectrophotometer. The details of the method used are given in section (*d*).

The iodine was then reduced and extracted from CCl_4 with water and the resulting solution made up to a known volume. Separate experiments showed that there is a loss of $7\pm3\%$ in the reduction and extraction step following the yield determination, and the yield was corrected accordingly. The preparation of the sample for counting depended on which radioactive species was to be counted.

(*c*) *Counting Techniques*

The activities of I^{130} and I^{131} were measured with a methane-flow proportional counter having a window thickness of 2.74 mg/cm^2.

Iodine-130 was measured by taking an aliquot from the standard solution and precipitating PdI_2 on an aluminum tray. The efficiency of the detector for I^{130} was determined in one experiment by measuring an aliquot from a standard solution (5) with a 4π counter. The estimated accuracy is $\pm3\%$.

In order to measure the I^{131}, the total iodide in the standard solution was precipitated as PdI_2, filtered on a "Millipore" paper, dried, and counted as such. The yield in the precipitation had to be determined because a fraction ($\sim20\%$) of the I^{131} activity was not carried with PdI_2. It was done by the addition of iodide carrier to the filtrate, reprecipitation, filtration, and counting. This procedure was repeated until no activity was left in the filtrate.

The efficiency of the detector for I^{131} was determined in an auxiliary experiment. A source of I^{131} was obtained from the Isotope Product Division, A.E.C.L.; aliquots were measured simultaneously in the 4π and proportional counter. The accuracy of the counting of I^{131} was estimated to be $\pm5\%$.

(*d*) *Yield Determination of* I^{129}

The amounts of iodine were of the order of 0.1 mg for the measurements of the I^{129} cross section and 0.5 mg for the measurements of I^{130} cross section. They were determined at the end of the chemical purification from the measurement of the optical density of iodine in carbon tetrachloride at 516 mμ with a Beckman spectrophotometer. The instrument was calibrated with carbon tetrachloride solutions of iodine standardized with arsenious acid. The solvent used for every optical measurement was passed through a silica gel column to remove traces of unsaturated compounds which could have reacted

with iodine. No change in concentration of iodine was observed in the solutions prepared in this way over a period of several weeks. The errors were considered to be ±2% and ±5% for amounts of 0.5 and 0.1 mg of iodine respectively.

(*e*) *Neutron Flux Monitoring*

The neutron fluxes were determined by the cobalt monitoring technique developed by Jervis (6). Weighed pieces of pure cobalt wire 0.005 in. in diameter and 0.4 in. in length, wrapped in aluminum foil, were placed in each capsule for all irradiations except for those done under cadmium. In these the wire was 4 in. in length and it was coiled around the quartz ampoule. The observed activity was corrected for self-shielding in the wire. The self-shielding correction for 0.005 in. Co wire is 2.1% and 5.5% for thermal and epicadmium neutrons, respectively (7). The accuracy of the flux determination is estimated to be ±2% (6).

A value of 36.5 barns (2) was used for the thermal neutron capture cross section of Co^{59} and 48.6 barns (8) for the resonance integral. The half-life of Co^{60} was taken to be 5.28 years (2).

The thermal neutron flux $(nv_0)_{th}$ was determined from the difference in activity of the monitors irradiated with and without cadmium covers. The resonance neutron flux $(nv)_{res}$ was obtained from the activity of the monitor irradiated with cadmium covers. Thus the fluxes are defined in the way described by Cabell *et al.* (9, 10).

(*f*) *Errors*

The errors involved in the operations and measurements just described are summarized in Table I. The total error resulting from the combination of each individual error is expressed as the square root of the sum of the squares of each error.

TABLE I

SUMMARY OF THE ERRORS INVOLVED IN THE MEASUREMENTS

Radionuclide	Loss in chemical purification (%)	Counting (%)	Yield determination (%)	Neutron flux (%)	Total (%)
I^{130}	±3	±3	±5	±2	±7
I^{131}	±3	±5	±2	±2	±6.5

RESULTS

(*a*) *Cross Section of* I^{129}

The counting of I^{130} was started about 30 hours after the end of the irradiation. This delay was necessary to allow for the decay of the 25-minute I^{128}, produced by the (n, γ) reaction in I^{127}. The average of six determinations of the half-life, each followed for 10 half-lives, was 12.5±0.1 hours, in agreement with the value of 12.6 hours given in the Table of Isotopes of Hollander *et al.* (11).

The effective cross section of I^{129}, σ_{eff}, for reactor neutrons is calculated from the equation

$$[1] \qquad A = N(nv_0)_{th}\sigma_{eff}(1-e^{-\lambda t}),$$

where A is the activity of I^{130} at the end of the irradiation of an unshielded sample,
N is the number of I^{129} atoms present during the irradiation,
$(nv_0)_{th}$ is the thermal neutron flux as defined in section (*e*) of Experimental,
λ is the disintegration constant of I^{130}, and
t is the time of irradiation.

The details of the four irradiations without cadmium shielding are given in Table II. An effective cross section under cadmium, $\sigma_{\text{eff, Cd}}$, is calculated from eq. [1] in a manner similar to σ_{eff}; A is now the I^{130} activity found under cadmium. The results of irradiations under cadmium are given in Table III.

TABLE II

EFFECTIVE CAPTURE CROSS SECTION OF I^{129} FOR REACTOR NEUTRONS

Experiment	I^{129} atoms	Time of irradiation, hours	$(nv_0)_{th}$	Activity, dis/sec	σ_{eff}, barns
1	1.53×10^{15}	26.0	1.06×10^{13}	3.49×10^{5}	28.3
2	1.08×10^{15}	32.0	0.79×10^{13}	1.93×10^{5}	27.1
3	0.42×10^{15}	42.2	4.64×10^{13}	4.74×10^{5}	26.9
4	0.79×10^{15}	42.2	6.10×10^{13}	12.4×10^{5}	28.5
Mean	—	—	—	—	27.7

TABLE III

EFFECTIVE CAPTURE CROSS SECTION UNDER CADMIUM FOR I^{129}

Experiment	I^{129} atoms	Time of irradiation, hours	$(nv_0)_{th}$	Activity, dis/sec	$\sigma_{eff, Cd}$, barns
5	2.72×10^{15}	7.33	1.56×10^{13}	1.23×10^{4}	0.9
6	0.96×10^{15}	13.66	1.48×10^{13}	0.81×10^{4}	1.1
Mean	—	—	—	—	1.0

The σ_{2200} m/sec neutron cross section for I^{129} is obtained by the subtraction of the effective cross section under cadmium from the effective cross section for reactor neutrons and is found to be 26.7 ± 2.0 barns.

The resonance capture integral of I^{129} is related to its cadmium ratio, R_{Cd}, by the following relationship,

$$[2] \qquad \int_{0.5}^{\infty} \sigma_c \frac{dE}{E} = \frac{(nv_0)_{th}}{(nv)_{res}} \cdot \frac{\sigma_{2200}}{(R_{Cd}-1)}$$

where $(nv_0)_{th}/(nv)_{res}$ is the ratio of the thermal flux to the resonance flux per unit interval of ln E, calculated to be 36 ± 4 from the activities of cobalt monitors inside and outside cadmium. From a Cd ratio of 28 ± 3 for I^{129}, the resonance capture integral

$$\int_{0.5}^{\infty} \sigma_c \frac{dE}{E}$$

is found to be 36 ± 4. There is therefore very little resonance capture in I^{129}.

(*b*) *Cross Section of* I^{130}

The counting of I^{131} started about 15 days after the end of the irradiation in order to allow the 12.5-hour I^{130} to decay. Iodine-131 was identified by its half-life and gamma-ray spectrum. The average of two determinations of the decay period, each followed for five half-lives, was 8.1 ± 0.1 days after the subtraction of a long-lived residual activity of 1000 counts/minute. This background represents less than 1% of the initially observed I^{131} activity and most of it can be accounted for by the radiations of I^{129}. Values of 8.04 to 8.16 days are given for the half-life of I^{131} in Hollander *et al.* (11). A decay curve of one of the two samples is given in Fig. 1.

Some I^{126} (13.3 days) is produced by the reaction $I^{127}(n, 2n)I^{126}$ during the long

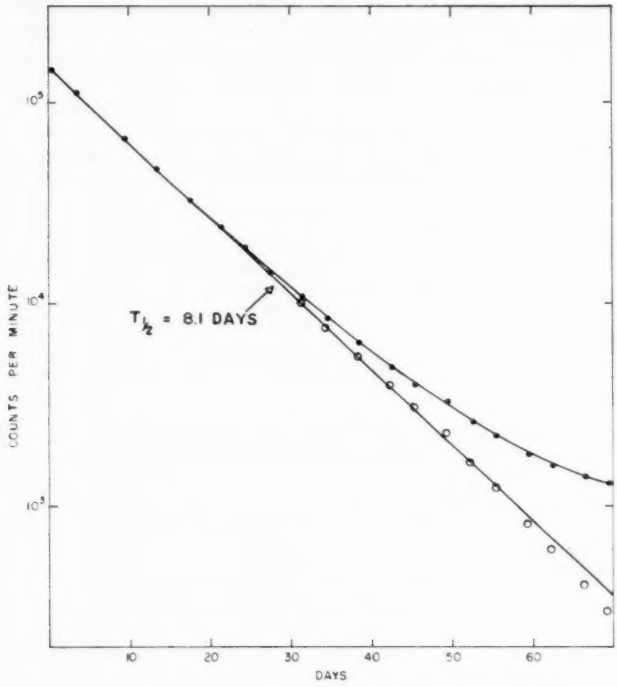

FIG. 1. Decay curve of I^{131}. A residual activity of 1000 counts/minute attributed to the radiations of I^{129} has been subtracted from the observed activity.

irradiation required to measure the I^{130} cross section. It does not interfere with the determination of the yield of I^{131}; its contribution was of the order of 2% when the counting of the samples was begun. This was shown by irradiating a known amount of natural iodine in a separate ampoule with the I^{129}. The I^{126} formed was counted under conditions identical with those used for I^{131}.

Since there were four shutdowns, each one of several hours, while the target material

TABLE IV

DETAILS OF THE IRRADIATION FOR THE FORMATION OF I^{131}

Segments x	Duration of a segment t_x (hours)	State of the reactor	Length of time from the end of segment to the end of the whole irradiation t'_x (hours)
1	26.33	On	536.3
2	7.67	Off	
3	54.75	On	473.9
4	22.65	Off	
5	248.1	On	203.2
6	22.73	Off	
7	129.4	On	51.1
8	17.5	Off	
9	33.6	On	0

was in the reactor, the calculation of σ_{eff} for I^{130} from the observed I^{131} activity becomes involved. The effect of these shutdowns on the formation of I^{131} was taken into account by assuming that the whole irradiation consisted of nine segments, the details of which are given in Table IV. The five segments characterized by the operation of the reactor are considered as separate irradiations. Then the activity of I^{131}, B, at the end of the irradiation is the sum of the activities produced during each one of these segments, namely 1, 3, 5, 7, and 9. Each activity is multiplied by a factor $e^{-\lambda_B t'}$ to take into account the decay from the end of the segment to the end of the irradiation.

[3] $$B = B_9 + B_7 e^{-\lambda_B t'_7} + B_5 e^{-\lambda_B t'_5} + B_3 e^{-\lambda_B t'_3} + B_1 e^{-\lambda_B t'_1}.$$

The I^{131} activity, B_x, formed during each segment is

[4] $$B_x = \frac{N\sigma\sigma_A (nv_0)^2_{th} T_A}{0.693(T_A - T_B)} [T_A(1-e^{-\lambda_A t_x}) - T_B(1-e^{-\lambda_B t_x})] + P,$$

$$P = \frac{N_{A(x-1)} T_A \sigma_A (nv_0)_{th}}{(T_B - T_A)} (e^{-\lambda_A t_x} - e^{-\lambda_B t_x}).$$

The first term in eq. [4] represents the formation of I^{131} by successive neutron capture in I^{129}; the second term, P, represents the formation of I^{131} by neutron capture in I^{130} formed in the previous segments of the irradiation.

N is the number of I^{129} atoms present during the irradiation,

σ is the effective cross section of I^{129} for reactor neutrons, 27.7 barns,

σ_A is the effective cross section of I^{130} for reactor neutrons to be measured,

T_A is the half-life of I^{130}, taken to be 12.5 hours,

T_B is the half-life of I^{131}, taken to be 8.1 days,

λ_A and λ_B are the disintegration constants of I^{130} and I^{131} respectively,

t_x is the duration of a segment as given in Table IV,

t'_x is the time elapsed from the end of the final irradiation to the end of a segment, x,

N_{Ax} is the number of I^{130} atoms present at the end of the 2nd, 4th, 6th, and 8th segments and is equal to

[5] $$N_{Ax} = \left[\frac{N\sigma (nv_0)_{th}}{\lambda_A} (1-e^{-\lambda_A t_{(x-1)}}) + N_{A(x-2)} e^{-\lambda_A t_{(x-1)}} \right] e^{-\lambda_A t_x}.$$

Initially $N_A = 0$.

The experimental details and the results are given in Table V.

TABLE V

EFFECTIVE CAPTURE CROSS SECTION OF I^{130} FOR REACTOR NEUTRONS

Experiment No.	I^{129} atoms	$(nv_0)_{th}$	Activity, dis/sec	σ_{eff} (I^{130}), barns
1	7.5×10^{17}	4.76×10^{13}	3.51×10^{4}	17.1
2	8.1×10^{17}	6.30×10^{13}	7.45×10^{4}	19.2
Mean	—	—	—	18.1

The value 18.0±3.0 barns is for a typical reactor neutron spectrum in a vacant fuel rod position near the center of the NRX reactor. In the two positions used in these experiments, the epicadmium neutrons are 3.5% and 4% of the thermal flux. The assigned error includes the uncertainty in the value of the cross section of I^{129}.

ACKNOWLEDGMENTS

The authors wish to thank Dr. T. A. Eastwood for helpful discussions, Mrs. J. S. Merritt and Dr. P. J. Campion for doing the 4π β-counting.

REFERENCES

1. KATCOFF, S., SCHAEFFER, O. A., and HASTINGS, J. M. Phys. Rev. **82**, 688 (1951).
2. HUGHES, D. J. and HARVEY, J. A. Brookhaven Natl. Lab. Rept. BNL-325 (1955).
3. PURKAYASTHA, B. C. and MARTIN, G. R. Can. J. Chem. **34**, 293 (1956).
4. TURK, E. H. Argonne Natl. Lab. Rept. ANL-5271 (1954).
5. PATE, B. D. and YAFFE, L. Can. J. Chem. **33**, 15, 610, 929, 1656 (1955).
6. JERVIS, R. E. Atomic Energy of Canada Limited, Rept. CRDC-730 (1957).
7. BUTLER, J. P., LOUNSBURY, M., and MERRITT, J. S. Can. J. Phys. **35**, 147 (1957).
8. MACKLIN, R. L. and POMERANCE, H. S. International conference on the peaceful uses of atomic energy. Vol. 5. United Nations, New York. 1956. p. 96.
9. CABELL, M. J., EASTWOOD, T. A., and CAMPION, P. J. Nuclear energy. (In press).
10. CABELL, M. J., EASTWOOD, T. A., and CAMPION, P. J. Atomic Energy of Canada Limited, Rept. CRC-738 (1958).
11. HOLLANDER, J. M., PERLMAN, I., and SEABORG, G. T. Revs. Modern Phys. **25**, 469 (1953).

STEREOCHEMISTRY OF REDUCTION OF KETONES BY COMPLEX METAL HYDRIDES[1]

OWEN H. WHEELER[2] AND JOSÉ L. MATEOS[3]

ABSTRACT

The stereochemistry of the reduction of a number of cyclic ketones with complex metal hydrides has been determined. In the absence of any large steric effect in the ketones, the reduction is essentially stereospecific, giving the more stable alcohol.

INTRODUCTION

The reduction of a carbonyl group by a simple metal hydride must proceed by four successive stages (1), utilizing each of the four available hydrogen atoms. Each stage probably involves two reaction steps, the initial reversible formation of a complex of the hydride ion and the carbon atom of the carbonyl group (I) and the irreversible transfer of hydrogen to this carbon atom (II).

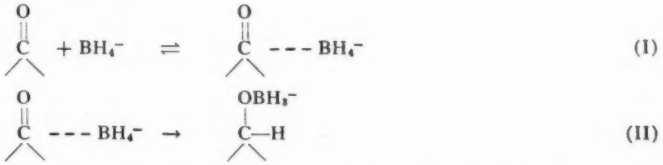

(I)

(II)

In the case of a cyclic ketone there are two possible directions of attack, pseudo equatorial and pseudo axial, giving the axial or equatorial alcohol. Dauben and co-workers (2, 3) have discussed the stereochemistry of reduction of cyclic ketones in terms of "steric approach control" to the attack of the hydride upon the ketone (stage I), and "product development control", determined by the relative thermodynamic stabilities of the two alcohols formed (and governing the relative stabilities of the two possible transition states in stage II). For a complex metal hydride substituted with bulky substituents, approach to the carbon atom of the carbonyl group, in stage I, will take place from the less hindered side. In stage II the large steric size of the reagent will favor the formation of the transition state leading to the more stable of the two products, since a bulky group is more stable in this the equatorial position. Reduction of an unhindered ketone should thus give the equatorial alcohol, whereas a sterically hindered ketone could give either isomer depending on the direction of steric hindrance.

A number of complex metal hydrides have recently been prepared and the simplest is sodium trimethoxyborohydride. However, this undergoes disproportionation in solution (4) and the reduction of 2-methylcyclohexanone with this reagent gives the same ratio of isomers as does sodium borohydride (2). Recently H. C. Brown and McFarlin (5) have developed a simple preparation of lithium tri-*tert*-butoxyaluminum hydride and we have investigated the stereochemistry of the reduction of a number of cyclic ketones (Table I) with this reagent. In all cases this reagent is considerably more stereospecific than either lithium aluminum hydride or sodium borohydride.

[1]*Manuscript received March 10, 1958.*
Contribution from the Instituto de Quimica, Universidad Nacional Autonoma de Mexico, Mexico 20, D.F. Part VI of Reactivity Studies on Natural Products. Part V, Can. J. Chem. **36**, *1049 (1958). A preliminary communication of part of this work appeared in Chem. & Ind. 395 (1957).*
[2]*Present address: Department of Chemistry, Dalhousie University, Halifax, N.S.*
[3]*Present address: Department of Chemistry, University of California, at Los Angeles.*

TABLE I

PERCENTAGE OF EQUATORIAL ISOMER*

	$LiAlH_4$	$NaBH_4$	$LiAlH(t\text{-}BuO)_3$‡	$LiAlH_4/AlCl_3$‡
Cholestan-3-one	88†	85‖	98.5	100
Coprostan-3-one	93†	87‖	96.5	94
Cholest-4-en-3-one	74†	95‖	100	—**
Cholest-5-en-3-one	87†	83‖	100	—††
Cholestan-7-one	—	58‖	86	—
Δ^5-Androsten-17-one-3β-acetate	—	—	100	—
Δ^8-Lanostenone	100‡	—	100	—
Camphor	90§	—	25	—
4-Methylcyclohexanone	81§	85¶	84	—

*Percentages normalized to 100%. †Ref. 16. ‡Present work. §Ref. 17. ‖Ref. 6. ¶Ref. 2. **Cholest-4-ene-(80%) + cholestane. ††Cholest-4-en-3-one (83%) + alcohols.

DISCUSSION

The keto group of cholestan-3-one (III*a*) is unhindered to attack from either an axial or equatorial direction (3, 6). In the transition state, however, the bulky alkoxide group could not occupy a pseudo-axial position, since it would be sterically hindered by the axial hydrogen atoms on carbon atoms 1 and 5. Moreover in such a position it is also sterically hindered to solvation (7), which would help to stabilize the ion. Thus the preferred transition state will be that with the alkoxy group in a pseudo-equatorial position, and the product observed is essentially that (β-cholestanol) which arises from this. Similarly coprostan-3-one (IV) is not subject to steric hindrance from either direction (6) and the equatorial (α) isomer is largely formed. A double bond at the union of rings A and B as in Δ^4- and Δ^5-cholesten-3-one will lead to a general flattening of the rings. The steric repulsion to a 3-α group will be less, since there is now no α-hydrogen at carbon-5 and the flattening of the rings moves the 3-position away from the 1-α hydrogen atom. However, electronic interaction (6) between the double bond and the pseudo-equatorial alkoxy group will greatly stabilize the transition state for formation of the equatorial alcohol, and this is formed exclusively in both cases.

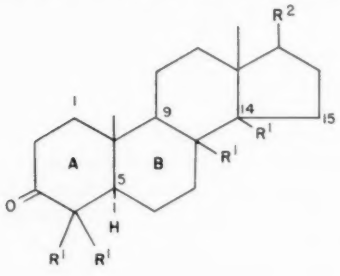

III a R^1 = H
R^2 = Isohexyl

b R^1 = Me
R^2 = Isohexyl

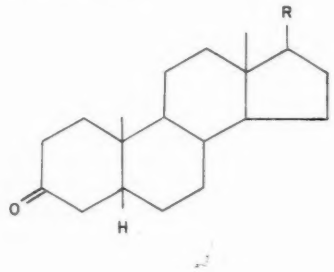

IV R = Isohexyl

The attack on the ketone group of cholestan-7-one from an axial direction will be hindered by the axial hydrogen atoms at C-5, C-9, and C-14. However, approach to the keto group from a pseudo-equatorial direction is highly hindered by the axial methyl groups at C-10 and C-13 and by the eclipsing effect of the 15-α hydrogen atom (6), and cholestan-7α-ol is only formed in 6% yield. This same eclipsing effect will tend to expel the bulky alkoxy transition complex from the 7-β position, and 57% of cholestane is formed (cf. 6).

Approach to the 17-keto steroid group from the topside of the molecule is hindered by the axial methyl group on C-18. However, approach from the underside is free and the resulting pseudo-equatorial transition complex will not be hindered by the methyl group on C-18, since the *trans*-fusion of rings C and D bends the 17-position down away from this group. Thus, Δ^5-androsten-17-one-3β-acetate gives exclusively Δ^5-androsten-3β,17β-diol.

In the case of Δ^8-lanosten-3-one (III*b*) approach to the ketone group from the upper pseudo-equatorial direction is also hindered by the axial methyl group on C-4. However, again approach from the underside is unhindered and the pseudo-equatorial transition complex (stage II) is not very hindered by either methyl group. Accordingly the β-alcohol is the sole product.

The camphor molecule (V) presents an interesting case, since one of the *gem*-dimethyl groups on the bridgehead is placed nearly above the ketone group (8). Approach from the exo (equatorial) direction is hindered and, although there is little hindrance to approach from the *endo* (axial) direction, the resulting pseudo-exo transition complex will be highly hindered. The net result of these opposing factors is that only 25% of the exo product (isoborneol) is formed.

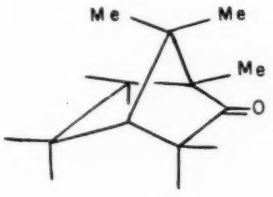

V

In the transition state of reduction of 4-methylcyclohexanone, the methyl group is free to take up either an axial or equatorial position (9), with the large alkoxy group remaining in the preferred equatorial position. Consequently lithium tri-*tert*-butoxyaluminum hydride gives nearly the same isomer distribution as lithium aluminum hydride and sodium borohydride.

The complex of lithium aluminum hydride and excess aluminum chloride was first used for reduction by B. R. Brown (10). Aluminum hydride is formed as an intermediate (11), but the active reducing species may be AlH_2Cl (12). In the cases of the two saturated ketones, cholestan-3-one and coprostan-3-one, reduction was essentially stereospecific giving predominately the β-alcohols. Cholest-4-en-3-one, however, gave no alcohol. The product, previously reported as Δ^4-cholestene (13), was shown to be a mixture of cholestene with about 10% cholestane. Hydrogenolysis has been observed in the reduction of other compounds by this reagent (14, 15). Cholest-5-en-3-one gave a mixture which contained

cholest-4-en-3-one as well as alcohols. Because of these unfavorable observations and the uncertainty of the nature of the reducing reagent, no further work was carried out with this complex.

EXPERIMENTAL

Tetrahydrofuran and *t*-butanol were dried by refluxing with and distilling from lithium aluminum hydride and sodium, respectively. Lithium aluminum hydride and aluminum chloride were commercial samples which were finely ground. The ketones used were all analytically pure samples.

Reductions with lithium tri-tert-butoxy aluminum hydride.—In a typical experiment *t*-butanol (2 ml) was added slowly to a solution of lithium aluminum hydride (400 mg) in tetrahydrofuran (30 ml) at 0° (5). Cholestanone (1.0 g) in tetrahydrofuran (30 ml) was then added and the mixture allowed to stand at 0° for ½ hour and at room temperature for 1 hour. The mixture was then poured into excess dilute hydrochloric acid and the product extracted in the usual way. In this case the crude product was chromatographed on alumina and eluted with hexane–benzene giving α-cholestanol (14 mg), m.p. 182°–185°, and β-cholestanol (937 mg), m.p. 143°–146°. Both alcohols gave no depression on mixed melting-point determinations with authentic samples.

Coprostanone.—The product from coprostanone (200 mg) gave a precipitate with digitonin (50 mg) from which β-coprostanol (7 mg) was liberated with pyridine. α-Coprostanol (185 mg), m.p. 115°, was recovered by evaporation of the mother liquors (6).

Cholest-4-en-3-one.—Cholest-4-en-3-one (1.0 g) gave a crude product (1.0 g), m.p. 121°, which on chromatography using hexane–benzene as eluent (50 fractions) gave only cholest-4-en-3β-ol, m.p. 127°–131°, recrystallized from ether–methanol to m.p. 132°, $[\alpha]_D^{CHCl_3}$ +44°.

Cholest-5-en-3-one.—Cholest-5-en-3-one (500 mg) gave cholesterol, m.p. and mixed m.p. 148°, $[\alpha]_D^{CHCl_3}$ −42° (lit. $[\alpha]_D$ −39°, m.p. 149° (18)).

Cholestan-7-one.—Cholestan-7-one (500 mg) gave a product separated by chromatography into a fraction (243 mg) eluted with hexane, m.p. 65°–70°, recrystallized from hexane to m.p. 80°, $[\alpha]_D$ +30°. The infrared absorption showed no carbonyl or hydroxyl groups or double bond. Further elution with hexane–benzene gave 7α-cholestanol (27 mg), m.p. 92°–98° (lit. m.p. 94°–97° (19)), and 7β-cholestanol (168 mg), m.p. 103°–109° (lit. m.p. 108°–112° (19)).

Δ⁵-Androsten-17-one-3β-acetate.—Reduction in like manner of Δ⁵-androsten-17-one-3β-acetate gave a product, m.p. 183°–184°, $[\alpha]_D$ −54°. Reported for Δ⁵-3β,17β-androstendiol, m.p. 182°–183°, $[\alpha]_D$ −55° (20).

Δ⁸-Lanosten-3-one.—Δ⁸-Lanosten-3-one (500 mg) gave a product, m.p. 142°–146°, recrystallized to m.p. 146°–148° and undepressed on admixture with lanostenol.

Camphor.—Two grams of this gave a product, m.p. 85°–110°, which could not be separated by chromatography on alumina (cf. 22). The mixture (500 mg) in pyridine (2 ml) was treated with *o*-nitrobenzoyl chloride and allowed to stand overnight. The pyridine was removed in vacuum and the isoborneol (106 mg), m.p. 210° from petroleum ether, separated by steam distillation (23). The residual borneol *o*-nitrobenzoate (618 mg) corresponded to borneol (322 mg).

4-Methylcyclohexanone.—Ten grams of 4-methylcyclohexanone gave a product n_D^{20} 1.4560, d_4^{30} 0.9061, which showed a small infrared ketone peak. After washing with sodium bisulphite solution the values were n_D^{20} 1.4569 and d_4^{30} 0.9063, and the compound showed no infrared carbonyl absorption. *Cis*- and *trans*-4-methylcyclohexanol have

respectively n_D^{20} 1.4614, 1.4561, and d_4^{30} 0.9173 and 0.9040 (24). The isolated product therefore contains 15% (from n_D^{20}) or 17% (from d_4^{30}) of the *cis*-isomer.

Reductions with lithium aluminum hydride – aluminum chloride.—In a typical experiment aluminum chloride (600 mg) was added to lithium aluminum hydride (135 mg) dissolved in ether (50 ml).

Cholestanone.—One gram of this ketone in ether (20 ml) was then added and the mixture allowed to stand at room temperature for at least four hours. The product (m.p. 141°–143°) was isolated by pouring the mixture into dilute hydrochloric acid. Recrystallization from ether–methanol gave β-cholestanol, m.p. 141°–142°, undepressed on admixture with an authentic sample.

Coprostanone.—Coprostanone (200 mg) gave a product from which β-coprostanol (12 mg) was isolated by digitonin separation. α-Coprostanol (180 mg) was isolated from the mother liquors, as before.

Cholest-4-en-3-one.—This gave a product, readily eluted from alumina with hexane, m.p. 65°, $[\alpha]_D^{CHCl_3}$ +56°. This rotation corresponds to Δ^4-cholestene ($[\alpha]_D$ +65°) 78% and cholestane ($[\alpha]_D$ +24°) 22%. Bromine titration showed the presence of about 85% olefin.

Cholest-5-en-3-one.—Five hundred milligrams gave a product (450 mg), which had λ_{max} 240 mμ, ε 15,700 corresponding to cholest-4-en-3-one 87%. Infrared spectra showed the presence of alcohols. No attempt was made to separate the mixture.

ACKNOWLEDGMENTS

The authors are grateful to Professor D. H. R. Barton for a gift of lanosterol and to the Rockefeller Foundation, New York, for financial assistance.

REFERENCES

1. Brown, H. C., Wheeler, O. H., and Ichikawa, K. Tetrahedron, **1**, 214 (1957).
2. Dauben, W. G., Fonken, G. J., and Noyce, D. S. J. Am. Chem. Soc. **78**, 2579 (1956).
3. Dauben, W. G., Blanz, E. J., Jiu, J., and Micheli, R. A. J. Am. Chem. Soc. **78**, 3752 (1956).
4. Brown, H. C., Mead, E. J., and Shoaf, C. J. J. Am. Chem. Soc. **78**, 3616 (1956).
5. Brown, H. C. and McFarlin, R. F. J. Am. Chem. Soc. **78**, 252 (1956).
6. Wheeler, O. H. and Mateos, J. L. Can. J. Chem. **36**, 1049 (1958).
7. Bird, C. W. and Cookson, R. C. Chem. & Ind. 1479 (1955).
8. Wheeler, O. H., Cetina, R., and Zabicky, J. Z. J. Org. Chem. **22**, 1153 (1957).
9. Winstein, S. and Holness, N. J. J. Am. Chem. Soc. **77**, 5562 (1955).
10. Brown, B. R. J. Chem. Soc. 2756 (1952).
11. Finholt, A. E., Bond, A. C., and Schlesinger, H. I. J. Am. Chem. Soc. **69**, 1199 (1947).
12. Wiberg, E. and Schmidt, M. Z. Naturforsch. **6b**, 460 (1951).
13. Broome, J. and Brown, B. R. Chem. & Ind. 1307 (1956).
14. Birch, A. J. and Slaytor, M. Chem. & Ind. 1524 (1956).
15. Brown, B. R. and White, A. M. S. J. Chem. Soc. 3755 (1957).
16. Dauben, W. G., Micheli, R. A., and Eastham, J. F. J. Am. Chem. Soc. **74**, 3852 (1952).
17. Noyce, D. S. and Denney, D. B. J. Am. Chem. Soc. **72**, 5743 (1950).
18. Fieser, L. F. and Fieser, M. Natural products related to phenanthrene. Reinhold Publishing Corp., New York. 1949. p. 95.
19. Cremlyn, R. J. W. and Shoppee, C. W. J. Chem. Soc. 3515 (1954).
20. Ruzicka, L. and Kägi, H. Helv. Chim. Acta, **18**, 1481 (1935).
21. Ruzicka, L., Denss, R., and Jeger, O. Helv. Chim. Acta, **27**, 759 (1944).
22. Vavon, G. and Gastambide, B. Compt. rend. **226**, 1201 (1948).
23. Jackman, L. M., Macbeth, A. K., and Mills, J. A. J. Chem. Soc. 2641 (1949).
24. Jackman, L. M., Macbeth, A. K., and Mills, J. A. J. Chem. Soc. 1717 (1949).

SYNTHESES OF SUBSTITUTED GUANIDINES[1]

PAUL E. GAGNON, JEAN L. BOIVIN,[2] AND JOSEPH ZAUHAR[3]

ABSTRACT

Ethyl-, propyl-, and benzyl-guanidine nitrates were prepared from amine nitrates and calcium cyanamide or dicyandiamide. Carboxyalkylguanidines were made by condensing the corresponding amino acids with guanidine carbonate in aqueous medium. All the guanidine nitrates, except the benzyl derivative, were converted into the corresponding nitroguanidines by treatment with concentrated sulphuric acid. Esters and metal salts of 1-(α-carboxyalkyl)-2-nitroguanidines were also prepared.

INTRODUCTION

Guanidine nitrate is prepared by heating ammonium nitrate with calcium cyanamide in aqueous solution (1, 2) or in the presence of urea (3), or with dicyandiamide (4, 5). Carboxyalkylguanidines have been previously made from amino acids and cyanamide in aqueous solution (6, 7) and by the action of haloaliphatic acids on guanidine (8). A more recent method for the preparation of carboxyalkylguanidines involves the use of methylisothiourea in an ammoniacal medium (9, 10). Carboxymethylguanidine was synthesized by the direct condensation of guanidine carbonate and glycine in aqueous medium (11).

RESULTS

Alkylguanidines

The methods of preparation of guanidine nitrate were extended to the syntheses of substituted guanidine nitrates in view of their nitration into the corresponding 1-substituted 2-nitroguanidines. The reaction of aqueous solutions of amine nitrates with calcium cyanamide gave the corresponding guanidine nitrates in yields ranging from 35 to 41%, as recorded in Table I.

TABLE I

ALKYLGUANIDINE NITRATES AND 1-ALKYL-2-NITROGUANIDINES

	Alkyl substituent		
	Ethyl	Propyl	Benzyl
	Nitrates		
M.p. °C	108–109	93–94	164–165
Yield, %: 1	41	38	35
2	86	67	51
3	41	41	40
4	88	67	45
	Nitroguanidines		
M.p. °C	147–148	99–100	—
Yield, %	30	57	—

1. Calcium cyanamide and amine nitrates in aqueous solution.
2. Dry mixtures of calcium cyanamide and amine nitrates.
3. Dry mixtures of calcium cyanamide, amine nitrates, and urea.
4. Dicyandiamide and amine nitrates.

[1]*Manuscript received June 2, 1958.*
Contribution from the Department of Chemistry, Laval University, Quebec, Que., with financial assistance from the Defence Research Board of Canada in 1955–56. This paper constitutes part of a thesis submitted to the Graduate School, Laval University, in partial fulfillment of the requirements for the degree of Doctor of Science.
[2]*Defence Research Board, C.A.R.D.E., Valcartier, Que.*
[3]*Graduate Student, holder of National Research Council of Canada Studentships in 1956–58.*

$$3RNH_2.HNO_3 + CaCN_2 \longrightarrow RHNC(=NH)NH_2.HNO_3 + 2RNH_2 + Ca(NO_3)_2$$

R = C_2H_5, C_3H_7, and $C_6H_5CH_2$

By heating the reactants in the solid state, instead of in aqueous solution, an increased yield was observed, namely, 86% for ethylguanidine nitrate, 67% for propylguanidine nitrate, and 51% for benzylguanidine nitrate. By adding urea to the dry reagents to depress the melting point of the mixtures, yields of about 40% were obtained. This behavior was unexpected because Wright obtained increased yields of guanidine nitrate from cyanamide (3) by using urea.

Ethyl-, propyl-, and benzyl-guanidine nitrates were also successfully synthesized by heating the amine nitrates with dicyandiamide. The over-all reaction can be expressed by the equation:

$$NCNHC(=NH)NH_2 + 2RNH_2.HNO_3 \longrightarrow 2RHNC(=NH)NH_2.HNO_3.$$

The latter method of preparation of ethyl-, propyl-, and benzyl-guanidine nitrates from amine nitrates and dicyandiamide gave yields up to 88% in some cases. In the preparation of guanidine hydrochloride from dicyandiamide and ammonium chloride (5), a biguanide hydrochloride is formed and ammonolyzed. A similar mechanism applies to the preparation of substituted guanidine nitrates from amine nitrates and dicyandiamide in which a substituted biguanide nitrate is the intermediate.

Carboxyalkylguanidines

Carboxyethylguanidine and carboxypropylguanidine were prepared from the corresponding amino acids and guanidine carbonate.

$$2H_2NCHRCOOH + [H_2NC(=NH)NH_2]_2.2H_2CO_3 \longrightarrow 2H_2NC(=NH)NHRCOOH + 2NH_3 + CO_2 + H_2O.$$

Cyclization of carboxyalkylguanidines can also take place (7, 12) in aqueous medium to form anhydro compounds.

$$2C_6H_5CH_2CH(NH_2)COOH + [H_2NC(=NH)NH_2]_2.H_2CO_3 \longrightarrow 2C_6H_5CH_2CH\text{—}C{=}O \quad (HN\text{—}C(=NH)\text{—}NH) + CO_2 + 3H_2O + 2NH_3$$

Carboxyalkylguanidines when treated with a slight excess of dilute nitric acid gave the corresponding carboxyalkylguanidine nitrates. The nitrates slowly decomposed on heating in aqueous solution at temperatures above 100° C. Anhydrocarboxyphenylethylguanidine nitrate was obtained in the same manner.

Substituted Nitroguanidines

Ethyl- and propyl-nitroguanidines were obtained by a method similar to the production of nitroguanidine from guanidine nitrate using sulphuric acid (13, 14) but benzylnitroguanidine could not be obtained by this method, which confirms the results of other investigators (15). The results are shown in Table I.

Nitroguanidines substituted with an acid function were obtained by treating the corresponding carboxyalkylguanidine nitrates with concentrated sulphuric acid. The results are shown in Table II. To obtain 1-(α-carboxypropyl)-2-nitroguanidine, which was soluble in dilute sulphuric acid, the sulphate ions were eliminated and the compound was isolated as the dihydrate of the barium salt.

$$HNO_3.H_2NC(=NH)NHRCOOH \longrightarrow H_2NC(=NNO_2)NHCHRCOOH + H_2O$$

1-(α-Carboxymethyl)-2-nitroguanidine was also identified by its lead salt; it was prepared by treating an aqueous solution of the nitroguanidine with lead oxide.

The esters of 1-(α-carboxyalkyl)-2-nitroguanidines were prepared by esterification with absolute ethanol in the presence of dry hydrogen chloride. The results are shown in Table II.

TABLE II

CARBOXYALKYLGUANIDINES, NITRATES, AND NITRO DERIVATIVES

Compound	Formula	M.p., °C	Yield, %	Calculated C	Calculated H	Calculated N	Found C	Found H	Found N
Carboxyalkylguanidines									
Ethyl	$C_4H_9O_2N_3$	225–226	31	36.64	6.87	32.06	36.9	7.0	32.1
Anhydro β-phenylethyl	$C_{10}H_{11}O_1N_3$	234–235	28	63.44	5.82	22.22	63.2	5.6	21.8
Propyl	$C_5H_{11}O_2N_3$	234–235	29	41.45	7.59	28.95	41.6	7.6	29.2
Carboxyalkylguanidine nitrates									
Methyl	$C_3H_8O_5N_4$	180–181	52 (Calc. for HNO_3: 34.42. Found for HNO_3: 34.8)						
Ethyl	$C_4H_{10}O_5N_4$	149–150	51 [Ramsay, H. Ber. **41**, 4385 (1908).]						
Anhydro β-phenylethyl	$C_{10}H_{12}O_4N_4$	134–135	65	47.61	4.76	22.22	47.8	4.8	22.4
Propyl	$C_5H_{12}O_5N_4$	146–147	58	28.81	5.77	26.92	28.8	5.7	27.0
1-(α-Carboxyalkyl)-2-nitroguanidines									
1-(α-Carboxymethyl)	$C_3H_6O_4N_4$	166–167	60	22.42	3.70	34.60	22.4	3.6	34.7
1-(α-Carboxyethyl)	$C_4H_8O_4N_4$	155–157	55	27.22	4.54	31.80	27.1	4.6	31.6
Ethyl esters of 1-(α-carboxyalkyl)-2-nitroguanidines									
1-(α-Carbethoxymethyl)	$C_5H_{10}O_4N_4$	149–150	29	31.58	5.26	29.47	31.8	5.3	29.2
1-(α-Carbethoxyethyl)	$C_6H_{12}O_4N_4$	175–176	32	35.30	5.88	27.40	35.2	6.0	27.6

DISCUSSION

The present study has shown that the methods of syntheses of guanidine nitrate apply as well to the substituted guanidine nitrates with the difference that lower yields resulted with the use of amine nitrates. Guanidines substituted by a carboxylic group are monobasic in character and form the lead and barium salts. The solubilities of the nitro derivatives were greater than that of nitroguanidine itself or of the alkyl nitroguanidines. The esterification of 1-(α-carboxyalkyl)-2-nitroguanidines in the presence of hydrogen chloride did not yield the corresponding hydrochloride salts, which supports the view that acids combine with the free amino group to form salts.

EXPERIMENTAL PART

Alkylguanidine Nitrates

1. Syntheses from calcium cyanamide and amine nitrates in aqueous solution.—The amine nitrate (0.29 mole) was dissolved in water (100 ml) and the resulting solution was evaporated until it reached a boiling point of 100° C. Calcium cyanamide (55%, 0.05 mole) was added slowly while stirring and at that temperature the reaction occurred with frothing while some free amine was evolved. The guanidine nitrate salt crystallized from the solution on cooling. The results are shown in Table I.

2. Syntheses from amine nitrates and calcium cyanamide in the dry state.—Dry solid mixtures of amine nitrates (0.21 mole) and calcium cyanamide were heated at 110° C for 1 hour (55%, 0.05 mole), during which time free amine was liberated. The fluid

reaction products were diluted with hot water (40 ml) and the mixtures filtered while hot. On cooling, the guanidine nitrate salts crystallized and were separated by filtration. The experimental results obtained are given in Table I.

3. Syntheses from calcium cyanamide, amine nitrates, and urea.—Calcium cyanamide (55%, 0.05 mole), amine nitrates (0.21 mole), and urea (0.13 mole) were heated at 90° C for 1 hour, during which time some free amine was evolved. Hot distilled water (40 ml) was added and the mixtures were filtered while hot. The guanidine nitrate salts crystallized from the cooled filtrate and were isolated by filtration. The results are listed in Table I.

4. Syntheses from amine nitrates and dicyandiamide.—Mixtures of dicyandiamide (0.22 mole) and amine nitrates (0.44 mole) were heated in an oil bath. Fusion began at 70° C, was complete at 130–133° C, and the temperature was gradually raised to 170° C and kept there for 3 hours. Upon cooling, the crude guanidine nitrate salts crystallized from the solution and were recrystallized from water. The results obtained are given in Table I.

Alkylnitroguanidines

The substituted guanidine nitrate (0.46 mole) was slowly added to sulphuric acid (98%, 2.1 mole) and cooled to 5° C. After all the solid was added, the mixture was stirred at that temperature for 3 hours, and afterwards poured over cracked ice. A small amount of the product precipitated from the solution. The compound was separated by filtration, the filtrate neutralized with barium hydroxide, and the barium sulphate formed was filtered through charcoal. The resulting filtrate was evaporated under vacuum and a second crop of crystals was obtained. The compound was then recrystallized from ethanol. The results obtained are shown in Table I.

Carboxyalkylguanidines

An aqueous solution of guanidine carbonate (0.06 mole) was added to an aqueous solution of amino acid (0.12 mole) and the reaction vessel was heated on a sand bath for 24 hours, during which time ammonia was liberated. Upon cooling, the resulting liquid was filtered, and the filtrate evaporated under reduced pressure until a yellow viscous product remained. A mixture of absolute alcohol (50 ml) and acetone (50 ml) was added, with stirring, and the resulting solution was stored in a cool place for several hours. The carboxyalkylguanidine soon separated from the solution and after filtration and washing with ethanol, the crude product was recrystallized from water. The results are given in Table II.

Carboxyalkylguanidine Nitrates

Dilute nitric acid (0.06 mole) was added slowly to an aqueous solution of the carboxyalkylguanidine (0.05 mole) while it was being cooled and stirred, and the resulting solution was evaporated to dryness under vacuum. The product was recrystallized from water. The results are listed in Table II.

1-(α-Carboxyalkyl)-2-nitroguanidines

Concentrated sulphuric acid (98%, 0.06 mole) was cooled to 5° C and the carboxyalkylguanidine nitrate (0.01 mole) was added in small portions with continuous stirring and cooling whenever necessary. After all the nitrate salt was added, the mixture was further stirred for 15 minutes at the above temperature and then allowed to reach 20° C, where the mass was stirred for 3 hours. The sulphuric acid solution was then

poured over cracked ice, which effected precipitation, after 15 minutes, of the crude product, which separated by filtration and was recrystallized from water. The compounds prepared are shown in Table II.

Salts of 1-(α-Carboxyalkyl)-2-nitroguanidines

1-(α-Carboxymethyl)-2-nitroguanidine was also identified by its dihydrate lead salt obtained by treating 1-(α-carboxymethyl)-2-nitroguanidine with an excess of lead oxide (litharge). The compound had no melting point but decomposed above 300° C. Calc. for $C_6H_{14}O_{10}N_6Pb$: Pb, 38.50%. Found: 38.8%. 1-(α-Carboxypropyl)-2-nitroguanidine, which was soluble in sulphuric acid, was isolated by precipitating the sulphate with barium hydroxide, filtering off the barium sulphate, and evaporating the resulting filtrate under reduced pressure. The dihydrate barium salt of 1-(α-carboxypropyl)-2-nitroguanidine crystallized from the concentrated solution in colorless needles: m.p. 183–184° C. Yield, 27%. Calc. for $C_{10}H_{22}O_{10}N_8Ba$: C, 21.76; H, 4.00; N, 20.31%. Found: C, 22.2; H, 4.2; N, 19.9%.

Esters of 1-(α-Carboxyalkyl)-2-nitroguanidines

Pulverized samples of 1-(α-carboxyalkyl)-2-nitroguanidines (0.06 mole) were added to absolute ethanol (70 ml), and dry hydrogen chloride was added until the solution was saturated. The mixtures were then refluxed for 1 hour, filtered, and left to stand in a cool place. The crude esters which separated from the filtrates were recrystallized from ethanol. The compounds obtained were slightly soluble in water. The results are given in Table II.

REFERENCES

1. Burns, R. and Gay, P. F. Brit. Patent No. 507,498 (1939).
2. Dhommee, R. Compt. rend. **134**, 1313 (1902).
3. Wright, G. F. U.S. Patent No. 2,431,301 (1947).
4. Werner, F. A. and Bell, J. J. Chem. Soc. **117**, 1133 (1920); **121**, 1790 (1922).
5. Blair, J. S. and Braham, J. M. J. Am. Chem. Soc. **44**, 2342 (1922).
6. Strecker, A. Compt. rend. **52**, 1212 (1861).
7. Duvillier, E. Compt. rend. **91**, 171 (1880).
8. Ramsay, H. Ber. **41**, 4385 (1908).
9. Mourque, M. Bull. soc. chim. France, 181 (1948).
10. Bengerlsdorf, I. S. J. Am. Chem. Soc. **75**, 3138 (1953).
11. Nencki, M. and Seiber, N. J. prakt. Chem. **17**, 478 (1878).
12. Abderhalden, E. and Sickel, H. Z. physiol. Chem. **173**, 51 (1928).
13. Thiele, J. Ann. **270**, 1 (1892).
14. Ewan, T. and Young, J. H. J. Chem. Ind. **40**, 109 (1921).
15. Davis, T. L. and Elderfield, R. C. J. Am. Chem. Soc. **55**, 731, 735 (1933).

THE ULTRAVIOLET AND INFRARED SPECTRA OF VICINAL-TRIAZOLE DERIVATIVES

E. LIEBER,[1] C. N. R. RAO,[2] T. S. CHAO,[3] AND H. RUBINSTEIN[4]

Unlike tetrazole (1, 2) vicinal-triazole absorbs in the ultraviolet region (3). Ramart-Lucas and Hoch (4) have observed that the ultraviolet spectra of the phenyltriazoles (I, $R_1 = C_6H_5$) vary according to the nature of the groups R_4 and R_5. However, they

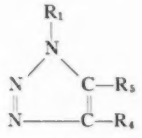

I

found that phenyltriazoles do not exhibit any absorption in the near ultraviolet region, when R_5 is H, CH_3, C_6H_5, or COOH, and R_4 is H or COOH. This appeared rather unusual because alkyl and aryl groups in 4-position have been found (3) to produce bathochromic shifts. Also, the ultraviolet spectrum of 4-phenyltriazole (I, $R_1 = R_5 = H$ and $R_4 = C_6H_5$) has been compared to that of biphenyl (3). Lieber, Rao, and Chao (5) have studied the near-ultraviolet absorption spectra of substituted aminotriazoles and have discussed the results in terms of the resonance interaction of R_1, R_4, and R_5 with triazole nucleus. We have now studied the ultraviolet spectra of a few other derivatives of vicinal-triazole. The results are summarized in Table I.

TABLE I

ULTRAVIOLET ABSORPTION SPECTRA OF VICINAL-TRIAZOLE DERIVATIVES (I)

R_1	R_4	R_5	λ_{max} (mμ)	log ϵ_{max}
C_6H_5	H	OH	235	4.03
C_6H_5	H	Cl	228	4.03
C_6H_5	COOH	Cl	231	4.03
C_6H_5	$COOCH_3$	Cl	218	4.24

The infrared spectral data on the vicinal-triazoles derivatives are limited (3, 6). We have now studied the infrared spectra of several derivatives of vicinal-triazole. All the important absorption frequencies that are common to most of the derivatives in the region 900–1310 cm^{-1} are shown in Table II. The intensities are indicated by the symbols: (s) strong; (m) medium; (w) weak; and (vw) very weak.

The syntheses of the compounds used in this study have been reported (7). The ultraviolet absorption spectra were recorded in 95% ethanol using a Cary recording

[1]*Department of Chemistry, DePaul University, Chicago 14, Illinois, U.S.A., the author to whom all correspondence should be addressed.*
[2]*Department of Chemistry, Purdue University, Lafayette, Ind., U.S.A.*
[3]*Archer-Daniels-Midland Co., Minneapolis, Minn., U.S.A.*
[4]*Wyandotte Chemical Co., Wyandotte, Mich., U.S.A.*

TABLE II

INFRARED SPECTRA OF VICINAL-TRIAZOLE DERIVATIVE (I)

R_1	R_4	R_5	Triazole vibrations (cm^{-1})			
C_6H_5	H	OH	1290(w)			
			1264(s)	1111(m)	1093(w)	990(m)
			1202(vw)		1068(w)	
C_6H_5	COOH	Cl	1277(m)	1105(w)	1081(s)	984(m)
			1230(m)			901(m)
			1198(m)			
C_6H_5	H	Cl	1290(m)	1111(m)	1053(w)	1000(m)
			1230(s)		1029(vw)	956(m)
			1203(m)			
H	H	NHC_6H_5	1302(m)			
			1236(m)	1129(w)	1081(m)	990(s)
			1176(w)		1018(s)	964(w)
			1151(w)			
C_6H_5	C_6H_5	NH_2	1297(w)	1101(w)	1067(w)	968(m)
			1235(w)		1013(w)	
p-BrC_6H_4	C_6H_5	NH_2	1280(w)	1111(w)	1082(w)	1003(m)
			1242(w)		1062(m)	974(s)
			1217(w)			
$CH_2C_6H_5$	C_6H_5	NH_2	1299(w)	1104(w)	1067(m)	999(w)
			1239(w)		1022(w)	990(w)
			1218(w)			
H	C_6H_5	NH-(*p*-$CH_3C_6H_4$)	1289(m)	1121(w)	1070(w)	996(w)
			1241(m)		1045(w)	969(m)
			1195(m)		1020(w)	911(w)
			1181(w)			

spectrophotometer. The infrared spectra were recorded using a Perkin–Elmer spectrometer (Model 21). The samples were prepared in Nujol mulls or KBr pellets.

From the results in Table I and the earlier observations (3, 5), it is found that the triazole derivatives, I, absorb in the near-ultraviolet region immaterial of the substituents in 1-, 4-, and 5-positions. These results are in variance with the earlier work of Ramart-Lucas and Hoch (4). Further, it is hard to generalize that the influence of the substituents is greater in 5- than in the 4-position (4). From the spectra of 1-substituted 4-phenyl-1,2,3-triazoles (5) it appears that the 1-(4-phenyl-5-amino)-triazolyl group is not capable of strong resonance interaction, since the effect of the substituents on the 1-phenyl group on the spectra of these derivatives is of the same magnitude as that on benzene alone. It is interesting to see that 1-phenylaminotetrazole absorbs at 225 mμ (2) compared to 221 mμ of 1-phenyl-5-amino-1,2,3-triazole (5). This difference is explained on the basis of the difference in electronegativities of the triazole and the tetrazole ring systems. Tetrazole is more electronegative than triazole, because of the greater electronegativity of nitrogen compared to carbon.

Since all the triazole derivatives had phenyl groups attached to them, it was hard to assign infrared frequencies for the N=N and the C=C links of the triazole nucleus. Some of the weak intensity bands listed in Table II may be due to the substituted aromatic groups. It is interesting to see that all the vicinal-triazole derivatives, just like the thiatriazole and tetrazole derivatives (8), exhibit a medium or weak intensity band in the region 1277–1302 cm^{-1}. This band cannot be ascribed to C—N or C_6H_4—NH or C_6H_5N< linkages. It may be due to the cyclic —N—N=N— configuration (8).

From Table II it can be seen that there are at least three bands in the regions 968–1003 cm^{-1}, 1101–1129 cm^{-1}, and 1045–1093 cm^{-1} which are characteristic of the vicinal-triazole ring system. However, the possibility of one of these bands in the region 1020–1220 cm^{-1} being the C—N vibration frequency is not completely eliminated. The

characteristic frequencies for vicinal-triazoles assigned by us agree with the observation of Hartzel and Benson (3), who assigned two bands between 1136–1087 cm^{-1} and 1020–971 cm^{-1} as characteristic of *v*-triazole.

ACKNOWLEDGMENTS

The authors' thanks are due to the U. S. Office of Naval Research and the Research Corporation, New York, N.Y., U.S.A., for research grants which made this study possible.

1. SCHUELER, F. S., WANG, S. C., FEATHERSTONE, R. M., and GROSS, E. G. J. Pharmacol. Exptl. Therap. **97**, 266 (1949).
2. LIEBER, E., RAO, C. N. R., and PILLAI, C. N. Current Sci. (India), **26**, 167 (1957).
3. HARTZEL, L. W. and BENSON, F. R. J. Am. Chem. Soc. **76**, 667 (1954).
4. RAMART-LUCAS, P. and HOCH, J. Bull soc. chim. France, 451 (1949).
5. LIEBER, E., RAO, C. N. R., and CHAO, T. S. Spectrochim. Acta, **10**, 250 (1950).
6. BENSON, F. R. and SAVELL, W. L. Chem. Revs. **46**, 1 (1950).
7. LIEBER, E., CHAO, T. S., and RAO, C. N. R. J. Org. Chem. **22**, 654 (1957).
8. LIEBER, E., RAO, C. N. R., PILLAI, C. N., RAMACHANDRAN, J., and HITES, R. D. Can. J. Chem. **36**, 801 (1958).

RECEIVED JUNE 23, 1958.
DEPARTMENT OF CHEMISTRY,
DEPAUL UNIVERSITY,
CHICAGO 14, ILLINOIS.

ON THE PREPARATION AND SINTERING OF CLOUD PRECIPITATING AGENTS. LEAD DI-IODIDE MICROCRYSTALS

HENRY M. PAPÉE[1]

Lead iodide of relatively large and controlled specific surface areas had to be prepared in this laboratory in connection with a microcalorimetric study of heats of adsorption of water vapor on lead iodide surfaces (1).

EXPERIMENTAL

Attempts to prepare finely subdivided lead iodide by electrostatic precipitation of a smoke (2) failed because of considerable contamination of the product by elementary iodine, and because of low specific areas obtained. No significant improvement could be attained by varying the flow of the dry nitrogen carrying gas, the temperatures of the melt, and the potentials applied.

An entirely different method was therefore tried, and the pattern outlined by Marshall (3) was followed with some modifications. Twenty-five grams of ammonium iodide was dissolved in 700 cc of absolute ethanol, and cooled to −20° C. A boiling solution of 50 g of lead iodide in 50 cc of water was added with vigorous stirring. The resulting slurry was quickly centrifuged in a low-temperature centrifuge maintained at −15° C. The precipitate was decanted and repulped several times by means of an electromagnetic vibrator with water at 0° C and then with absolute ethanol which has been chilled to −20° C. This was followed by several repulpings with anhydrous ether at low temperatures.

The precipitate obtained was then placed in a desiccator and evacuated for 48 hours to a vacuum obtained by a 2-stage Edwards diffusion pump. The agglomerated product was ground in a mortar in an atmosphere of dry nitrogen and sieved through a 200-mesh screen. The compound was then placed again in a desiccator and again evacuated for 48

[1]*Present address: Division of Applied Chemistry, National Research Council of Canada, Ottawa, Canada.*

hours. Analysis of the product showed it to be 99.8% pure, and BET surface determinations led to values of 2.05 m^2/g. The stock was then stored in a desiccator at 25.0° C, and all further manipulations of samples were done under nitrogen of a humidity below 1%, in a dry box.

Sintering by Heating

Quantities of about 8 g of lead iodide were sintered under vacuum in a glass cell of the type represented in Fig. 1. The cell was fitted directly onto the BET apparatus, and a heating unit which could be controlled within 1° C was placed around it. It was seen that the same final results were obtained at a temperature of 100° C, whether the process of heating lasted for 6 or for 48 hours. The samples were heated therefore for 24-hour periods, BET measurements taken subsequently, and the relative change between

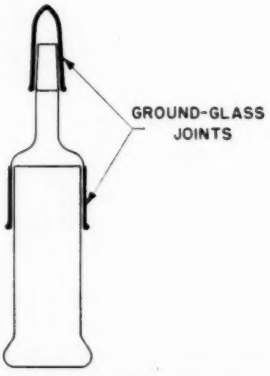

FIG. 1. Cell for storage, sintering, dispensing, and surface measurements of the product.

specific surface areas before (S_0) and after sintering (S) was plotted against the temperature of heating. Figure 2 gives the results obtained on samples originating from different batches of various initial specific areas. Each point represents a measurement taken on a different sample. It was noticed that, while salts whose area was reduced by sintering by exposure to saturated water vapor at 25° C follow the pattern of Fig. 2, samples which were presintered by heating give completely random results. The plot therefore represents measurements on crystals originating from one particular batch, and some others that were presintered by exposure to water vapor, and subsequently evacuated for long time periods.

The curve represented by Fig. 2 can be split in three parts:

(i) The ascending part, in which small variations of temperature seem to provoke considerable changes in the function and where, because of this, the error is considerable. This part has therefore been dotted.

(ii) The fairly rectilinear descending part of the curve.

(iii) The extrapolated part of the line, where there is a considerable scattering of the experimental values.

The parameters of the line in part (ii) are:

$$\text{Slope: } -0.003_2 \pm 0.0005 \ (^\circ \text{C})^{-1}$$

$$\text{Intercept: } 0.50 \pm 0.06 \text{ units.}$$

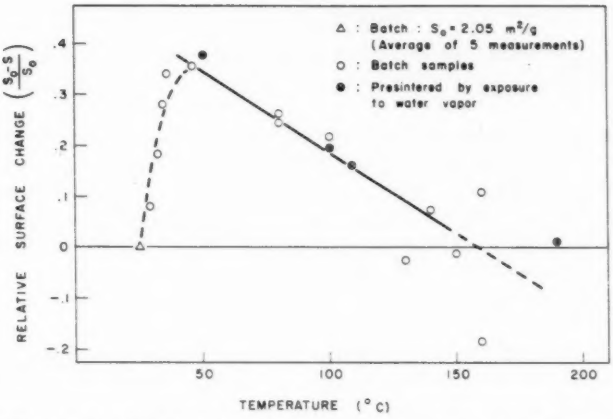

FIG. 2. Effect of sintering of lead iodide with temperature: plot of relative surface change against temperature of sintering, in degrees Centigrade.

The plot indicates a decrease of specific surface below 160° C and suggests a possible increase above that temperature of sintering.

Elementary iodine was observed in the traps during experiments which were performed in the higher temperature range. Since it was not expected that at these temperatures decomposition would set in, a separate experiment was performed at 240° C. Lead di-iodide of a specific surface of 1.5 m²/g was placed in a long glass tube surrounded by a heating element, and was heated for 24 hours under an atmosphere of dry nitrogen at room pressure. During this time period, the salt underwent a process of stoichiometric decomposition into lead mono-iodide and elementary iodine, with the latter condensing on the colder part of the tube which protruded from the heater.

Sintering by Exposure to Water Vapor

Microcrystals of lead di-iodide, contained in the type of cell previously described, were evacuated for 12 hours by pumping with a diffusion pump. Water vapor was subsequently admitted from a cell containing distilled water at saturated vapor pressure. The cells were kept in communication for the required period of time. The cell containing the water was closed a few seconds before the end of the treatment, and, at the required time, the salt container was connected with the high-vacuum manifold. The latter was kept under vacuum by a 2-stage silicon oil diffusion pump, which was backed by a high-speed rotary mechanical pump and by a 24-liter flask branched in parallel. This was followed by 12 hours of evacuation. The whole operation was performed at 25.0° C. The surface area was then determined by BET nitrogen adsorption. Salt of an initial specific surface of 1.5_1 m²/g was used for all of those experiments.

The results are given in Fig. 3. Two extra runs were performed with hydration times of 24 and 48 hours, and areas of 0.60_0 m²/g were obtained in both cases. It was therefore assumed that the specific surface reached an asymptotic value of 0.60_0 m²/g, and it was seen that under this condition the phenomenon follows first-order kinetics with respect to surface, as shown in Fig. 4. The parameters of the line are found to be:

$$\text{Slope: } -0.245 \pm 0.007 \text{ hours}^{-1}$$

$$\text{Intercept: } -0.04 \pm 0.03$$

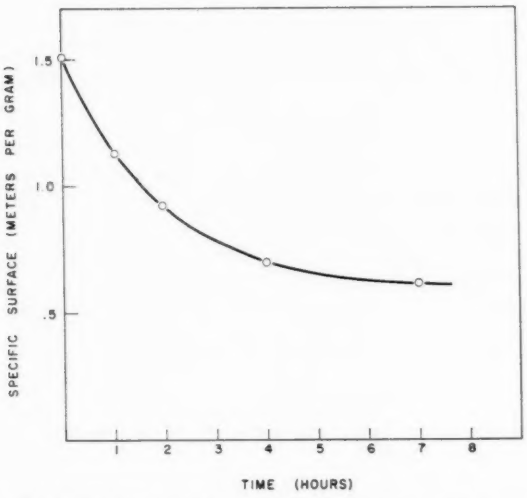

FIG. 3. Sintering of lead iodide particles with time of exposure to water vapor, at 25° C, and unit relative vapor pressure: plot of specific surface against time of exposure.

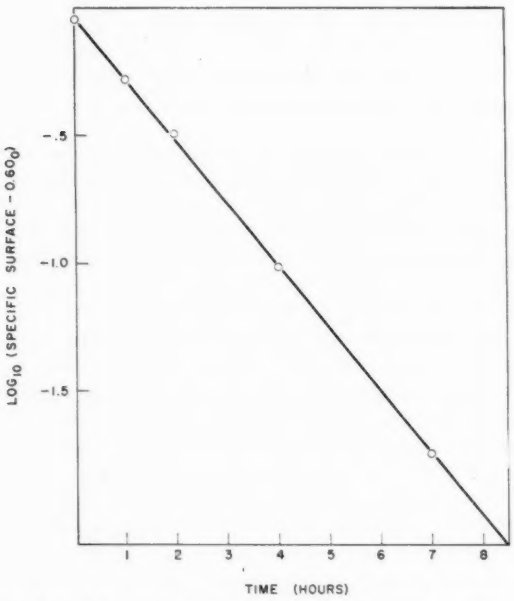

Fig. 4. Sintering of lead iodide particles with time of exposure to water vapor: plot of the decimal logarithm of the difference between the specific surface at time 't' and the asymptotic experimental value, against time of exposure.

DISCUSSION

The activity of lead iodide particles as condensation nuclei (4) and their properties toward ice nucleation (5, 6, 7) have recently resulted in investigations of the surface properties of these crystals (1, 8).

Sintering of the surface of lead di-iodide under exposure to water vapor is a slow process leading to asymptotic values. This can be visualized in terms of homogenization of initial imperfections on the surface and the absence of agglomeration between original particles. The curve of Fig. 3 follows a pattern similar to that of the curves obtained by Moffat and McIntosh (9), who studied the sintering of sodium chloride microcrystals under exposure to low partial pressures of water vapor. The pattern is, however, different from the one obtained recently by Papée (10), where sodium chloride microcrystals were sintered under exposure to water vapor at saturated vapor pressure at 25° C, and where no asymptotic values could be detected in the fast first-order process.

Experiments reported in this note indicate that the process of decrease of surface by heating under vacuum is accompanied by a contrary process of increase, and that the latter effect becomes prevalent at higher temperatures. Since no evidence indicating transition between phases, below 250°, could be found in the literature, it is assumed that the increase is due to thermal decomposition. This explains the controversial results obtained in measuring the melting point of the product (11, 12, 13). This controversy is not eliminated by data obtained by various workers who worked with purified products and knew that decomposition occurs (14), and by those who worked under inert atmospheres (15, 16) to eliminate the action of water vapor and oxygen. Similarly, measurements of vapor pressures of lead di-iodide at various temperatures seem to have led so far to controversial statements (17, 18) mainly because of misinterpretations of the experimental values and failure to analyze the final products.

The controversy noted above and the evidence of the present investigation points, however, to the conclusion that the crystals responsible for the condensation of water or for ice nucleation will have a strongly distorted lattice because of the nature of their preparation, and that this factor will possibly favor their action (19, 20). Since, furthermore, the compound can be decomposed by light (21, 22), and its over-all surface will sinter and homogenize only slowly under exposure to water vapor, as shown by experiments reported previously, a PbI_2 nucleus will probably remain active for long periods of time; even seasoned and originally inactive particles may eventually be activated photochemically.

Another surface-dependent factor that might favor condensation of water on lead iodide nuclei ought to be considered at the same time, since lead iodide gives rise to the photoelectric effect in the visible spectrum (23). It is to be expected that the nucleus will become electrically charged when illuminated, and will therefore bind water molecules by a sort of electrostriction, which, under suitable conditions, may promote coalescence (cf. ref. 24). The fact that freshly prepared lead iodide 'tires' with time towards its photoelectric properties, whether kept in moderate light or in darkness (25), may well be partly explained by the sintering of its surface when exposed to the water vapor in the atmosphere.

ACKNOWLEDGMENTS

Thanks are due to Messrs. T. W. Zawidzki and S. Tong for their help in preparing the lead iodide, and to Drs. G. C. Benson and K. J. Laidler and Mr. S. J. Birstein for many helpful discussions.

This work was performed under Contract No. A.F. 19(604)-2026 between the U.S. Air Force Cambridge Research Center and the University of Ottawa.

REFERENCES

1. PAPÉE, H. M. To be published.
2. YOUNG, D. M. and MORRISON, J. A. J. Sci. Instr. **31**, 90 (1954).
3. MARSHALL, F. H. Phys. Rev. **58**, 642 (1940).
4. SCHAEFER, V. J. J. Meteorol. **11**, 417 (1954).
5. HOSLER, C. L. and SPALDING, G. R. Artificial stimulation of rain (Symposium). Pergamon Press Ltd., New York. 1957. p. 369.
6. BIRSTEIN, S. J. and ANDERSON, C. E. J. Meteorol. **12**, 68 (1954).
7. PRUPPACHER, H. R. and SÄNGER, R. Z. angew. Math. u. Phys. **6**, 407 (1955).
8. BIRSTEIN, S. J. Geophys. Research, Paper No. 32. (1954).
9. CARNELLY, T. J. Chem. Soc. **33**, 273 (1878).
10. MOFFAT, J. B. and MCINTOSH, R. Can. J. Chem. **35**, 1511 (1957).
11. PAPÉE, H. M. J. Meteorol. To be published.
12. EHRHARDT, O. Ann. Rev. Phys. Chem. **24**, 215 (1885).
13. RAMSAY, W. and ENMORPOPULOS, M. Phil. Mag. **41**, 460 (1896).
14. CZEPINSKY, V. Z. anorg. Chem. **19**, 257 (1899).
15. SANDONINI, C. Gazz. chim. ital. **41**, II, 145 (1911).
16. TUBANDT, C. and EGGERT, S. Z. anorg. Chem. **110**, 218 (1920).
17. VON WORTENBERG, H. and BOSSES, O. Z. Elektrochem. **28**, 384 (1922).
18. JELLINEK, K. and RUDAT, A. Z. physik. Chem. A, **143**, 55 (1929).
19. TURNBULL, D. Artificial stimulation of rain (Symposium). Pergamon Press Ltd., New York. 1957. p. 356.
20. MANSON, J. E. Artificial stimulation of rain (Symposium). Pergamon Press Ltd., New York. 1957. p. 367.
21. ROUSSIEU, M. Ann. chim. et phys. **47**, 154 (1856).
22. SANYAL, A. K. and DHAR, N. R. Z. anorg. Chem. **128**, 212 (1923).
23. COBLENTZ, W. W. and ECKFORD, J. F. Sci. Papers, U.S. Bureau of Standards, 18/456.489. (1922).
24. MARSHALL, J. S. and GUNN, K. L. S. Artificial stimulation of rain, (Symposium). Pergamon Press Ltd., New York. 1957. p. 345.
25. DIMA, M. B. A. Compt. rend. **157**, 592 (1913).

RECEIVED MAY 22, 1958.
DEPARTMENT OF CHEMISTRY,
UNIVERSITY OF OTTAWA,
OTTAWA, CANADA.

CANADIAN JOURNAL OF CHEMISTRY

Notes to Contributors

Manuscripts

(i) ***General.*** Manuscripts, in English or French, should be typewritten, double spaced, on paper 8½×11 in. **The original and one copy are to be submitted.** Tables and captions for the figures should be placed at the end of the manuscript. Every sheet of the manuscript should be numbered.

Style, arrangement, spelling, and abbreviations should conform to the usage of recent numbers of this journal. Names of all simple compounds, rather than their formulas, should be used in the text. Greek letters or unusual signs should be written plainly or explained by marginal notes. Superscripts and subscripts must be legible and carefully placed.

Manuscripts and illustrations should be carefully checked before they are submitted. Authors will be charged for unnecessary deviations from the usual format and for changes made in the proof that are considered excessive or unnecessary.

(ii) ***Abstract.*** An abstract of not more than about 200 words, indicating the scope of the work and the principal findings, is required, except in Notes.

(iii) ***References.*** These should be designated in the text by a key number and listed at the end of the paper, with the number, in the order in which they are cited. The form of the citations should be that used in this journal; in references to papers in periodicals, titles should not be given and only initial page numbers are required. The names of periodicals should be abbreviated in the form given in the most recent *List of Periodicals Abstracted by Chemical Abstracts*. All citations should be checked with the original articles and each one referred to in the text by the key number.

(iv) ***Tables.*** Tables should be numbered in roman numerals and each table referred to in the text. Titles should always be given but should be brief; column headings should be brief and descriptive matter in the tables confined to a minimum. Vertical rules should not be used. Numerous small tables should be avoided.

Illustrations

(i) ***General.*** All figures (including each figure of the plates) should be numbered consecutively from 1 up, in arabic numerals, and each figure referred to in the text. The author's name, title of the paper, and figure number should be written in the lower left corner of the sheets on which the illustrations appear. Captions should not be written on the illustrations (see Manuscripts (i)).

(ii) ***Line Drawings.*** Drawings should be carefully made with India ink on white drawing paper, blue tracing linen, or co-ordinate paper ruled in blue only; any co-ordinate lines that are to appear in the reproduction should be ruled in black ink. Paper ruled in green, yellow, or red should not be used. All lines should be of sufficient thickness to reproduce well. Decimal points, periods, and stippled dots should be solid black circles large enough to be reduced if necessary. Letters and numerals should be neatly made, preferably with a stencil (**do NOT use typewriting**), and be of such size that the smallest lettering will not be less than 1 mm high when reproduced in a cut of suitable size.

Many drawings are made too large; originals should not be more than 2 or 3 times the size of the desired reproduction. Wherever possible two or more drawings should be grouped to reduce the number of cuts required. In such groups of drawings, or in large drawings, full use of the space available should be made; the ratio of height to width should conform to that of a journal page (5¼×7¼ in.) but allowance must be made for the captions.

The original drawings and one set of clear copies (e.g. small photographs) are to be submitted.

(iii) ***Photographs.*** Prints should be made on glossy paper, with strong contrasts. They should be trimmed so that essential features only are shown and mounted carefully, with rubber cement, on white cardboard, with no space between them. In mounting, full use of the space available should be made to reduce the number of cuts required (see Illustrations (ii)). Photographs or groups of photographs should not be more than 2 or 3 times the size of the desired reproduction.

Photographs are to be submitted in duplicate; if they are to be reproduced in groups one set should be mounted, the duplicate set unmounted.

Reprints

A total of 50 reprints of each paper, without covers, are supplied free. Additional reprints, with or without covers, may be purchased at the time of publication.

Charges for reprints are based on the number of printed pages, which may be calculated approximately by multiplying by 0.5 the number of manuscript pages (double-space typewritten sheets, 8½×11 in.) and including the space occupied by illustrations. An additional charge is made for illustrations that appear as coated inserts. Prices and instructions for ordinary reprints are sent out with the galley proof.

Any reprints required in addition to those requested on the author's reprint requisition form must be ordered officially as soon as the paper has been accepted for publication.

Contents

Printed in Canada *by* University of Toronto Press